DEVELOPMENT OF A TSUNAMI FORECAST MODEL FOR ATLANTIC CITY, NEW JERSEY

Yong Wei

June, 2011

1. Abstract 1
2. Background and Objectives 2
3. Forecast Methodology 3
4. Model development 3
   4.1 Method 3
   4.2 Forecast area 4
   4.3 Historical events and data 5
   4.4 Model setup 6
      4.4.1 Grid boundary and resolution 6
      4.4.2 Digital Elevation Model of Atlantic City, New Jersey 7
      4.4.3 Development of model grids 7
5. Results and Discussion 8
   5.1 Model validation 8
   5.2 Model stability testing using synthetic scenarios 9
6. Summary and conclusions 12
7. Acknowledgement 14
8. References 14
Tables 21
Appendix A. 22
Appendix B. Propagation database: Atlantic Ocean Unit Sources 23
Appendix C. Short-term Inundation Forecast of Tsunami (SIFT) testing results 31
   C.1 Testing Procedure 32
   C.2 Results 32

1. Abstract

This study addresses the development, validation, and stability tests of the tsunami forecast model for Atlantic City, New Jersey. Based on the Method of Splitting Tsunami (MOST), the tsunami forecast model employs three telescoping grids (A, B, and C) to compute tsunami wave dynamics nearshore, as well as tsunami inundation onshore. The spatial resolutions in the forecast model are 30 arc sec (~ 714 m along longitudinal direction at 39.5°N), 6 arc sec (~ 143 m along the longitudinal direction at 39.5°N), and 2 arc sec (~ 48 m along the longitudinal direction at 39.5°N) in the A, B, and C grids, respectively. The forecast model can complete a 4-hour simulation of the tsunami inundation within 12 minutes of CPU time. A reference inundation model is developed in parallel using finer grids (~ 8 m in the C grid) to provide model reference for the forecast model. The present study conducts sensitivity tests to optimize grid coverage and grid resolution by comparing results between the forecast model and the reference model. Due to a lack of historical tsunami records, the Atlantic City forecast model is evaluated using

the 1755 Lisbon tsunami. Model results show excellent agreement between the forecast model and reference model. Model stability and consistency are also evaluated using eight synthetic scenarios. This study shows the forecast model is an efficient and accurate tool to provide real-time assessment of tsunami impact along the coastline of Atlantic City.

2. Background and Objectives

The National Oceanic and Atmospheric Administration (NOAA) Center for Tsunami, Research (NCTR) at the NOAA Pacific Marine Environmental Laboratory (PMEL) has developed a tsunami forecasting capability for operational use by NOAA's two Tsunami Warning Centers located in Hawaii and Alaska (Titov et al., 2005a). The system is designed to provide a basin-wide warning of approaching tsunami waves accurately and quickly. The system, termed Short-term Inundation Forecast of Tsunamis (SIFT), combines real-time tsunami event data with numerical models to produce estimates of tsunami wave arrival times and amplitudes at a coastal community of interest. The SIFT system integrates several key components: deep-ocean observations of tsunamis in real time, a basin-wide pre-computed propagation database of water level and flow velocities based on potential seismic unit sources, an inversion algorithm to refine the tsunami source based on deep-ocean observations during an event, and high-resolution tsunami forecast models.

Located at the oceanfront of New Jersey, Atlantic City is a major tourist attraction (Figure 1). Aside from 40,000 residents, Atlantic City attracts nearly three million visitors every year, with many vacationing at the oceanfront hotels. Although the threat is minimal compared to the West Coast of the United States, a tsunami generated in the Atlantic Ocean could have potential impact on the shores of Atlantic City. However, this threat is significantly understudied, probably due to the rarity of tsunami activity in the Atlantic as well as a lack of historical tsunami data. Atlantic City did experience tsunami-induced water-level increase during the 2004 Indian Ocean tsunami, generated thousands of miles away in a different ocean basin. A similar earthquake from any seismically active region in the Atlantic, even though the possibility is believed to be low, will pose catastrophic hazards to Atlantic City. The landslide sources along the U.S. Atlantic margin may cause even more severe damage to Atlantic City since these sources are usually much closer to the coastline and afford much less time to prepare. Most of the populated areas of Atlantic City are located on Absecon Island. These areas are connected to the mainland by bridges and highways, bottlenecking evacuation during a tsunami event due to congested traffic through these narrow exits. It is therefore vital to prepare a populated area like Atlantic City for short- and long-term tsunami hazard assessment.

The objective of this present work is to develop an operational forecast model to be used in near real time to protect the community of Atlantic City from the potential impact posed by a tsunami. Titov et al. (2014) employs high-resolution tsunami inundation forecast models to assess the potential tsunami hazards for coastal communities on the U.S. Atlantic Coast due to distant earthquake- and landslide-generated tsunamis in the Atlantic. The development of the Atlantic City tsunami forecast model and high-resolution inundation model is a valuable supplement to this assessment, and more importantly, another essential contribution to the existing NOAA tsunami forecasting system in the Atlantic.

3. Forecast Methodology

Titov et al. (2005a) provides details of NCTR's forecast methodology. The tsunami forecasts are expedited using a basin-wide database of pre-computed water elevations and flow velocities for unit sources covering worldwide subduction zones (Gica et al., 2008). When the tsunami waves propagate across the ocean and successively reach tsunameters employing the Deep-ocean Assessment and Reporting (DART) technology (Meinig et al., 2005), the recorded sea level is ingested into an inversion algorithm (Percival et al., 2011) to produce an improved estimate of the tsunami source in real time. Based on this tsunami source, a linear combination of the pre-computed "unit" tsunami scenarios stored in the database produces synthetic boundary conditions of water elevation and flow velocities to initiate the forecast model computation. The Method of Splitting Tsunami (MOST) is used to develop the tsunami forecast model to provide real-time tsunami forecasts at selected coastal communities. MOST is a suite of numerical simulation codes capable of simulating three processes of tsunami evolution: generation, transoceanic propagation, and inundation of dry land (Titov and González, 1997). It has been extensively tested against a number of laboratory experiments and benchmarks (Synolakis *et al.*, 2008). Forecast models are constructed to operationally provide an estimate of wave arrival time, wave height, and inundation for populous at-risk coastal communities in real time while a tsunami is propagating across the open ocean. The forecast models are designed and tested to perform under stringent time constraints given that time is generally the single limiting factor in saving lives and property. Tang et al. (2009) describes the technical aspects of forecast model development and stability testing. The forecast methodology and models have been successfully used for tsunami model forecast during a number of historical tsunami events since 2003 (Titov et al., 2005b; Titov, 2009; Tang et al., 2008, 2012; Wei et al., 2008, 2013).

4. Model development

4.1 Method

Implementation of high-resolution grids improves modeling accuracy, but also increases the computational time for real-time forecasts. To obtain rapid and accurate model results, a forecast model consists of a set of three telescoping grids, referred to as A, B, and C, with each grid having successively finer spatial resolution into the population and economic center of the community of interest. The offshore area is covered by the A grid, with the lowest resolution typically at a range of 0.5 to 2 arc min (1,000 to 3,700 m). The B grid provides computational results for tsunami wave transition from offshore to nearshore at an intermediate grid resolution of 12 to 18 arc sec (360 to 540 m). In the C grid, the model computes the tsunami inundation at a grid resolution ranging from 1 to 3 arc sec (30 to 90 m). This optimal setup allows the model to finish 4 to 10 hr simulations within 10 min of wall-clock time.

Similarly, a set of three high-resolution, "reference" elevation grids can also be constructed to develop a high-resolution reference model. Typically, a reference model provides inundation computation in its C grid at a grid resolution of 1/3 arc sec (~ 10 m). Compared to a forecast model, a reference model generally provides better accuracy of the inundation computation, but is much more computationally intensive due to much finer grid resolution.

Accurate forecasting of the tsunami impact on a coastal community largely relies on the accuracy of bathymetry and topography used in the numerical model. The forecast model utilizes the high-resolution Digital Elevation Models (DEMs) constructed by the National Geophysical Data Center (NGDC) using available bathymetric, topographic, and shoreline data. The vertical datum of these DEMs is set to Mean High Water, and the horizontal datum is the World Geodetic System 1984 (http://ngdc.noaa.gov/mgg/inundation/tsunami/inundation.html).

4.2 Forecast area

Atlantic City is a coastal city in southern New Jersey with an economy mostly relying on gambling, conventions, and leisure. Today, Atlantic City has a year-round population of 40,517. It is within easy driving distance for a third of the population of the United States and attracts three million visitors each year. The entire city was built on low land, less than 3 m above sea level, between barrier islands and marshlands, making the city particularly vulnerable to tsunamis generated in the Atlantic (Figure 1).

Barrier islands are dynamic landforms, subject to storm-surge flooding and sand transport processes. These coastal features are particularly vulnerable to marine hazards since they are detached from the mainland and are composed entirely of loose sediment (Leatherman, 1982). Historically, the oceanfront of Absecon Island (Figure 1) has been one of the hardest hit of all the New Jersey barrier islands during the coastal storms (http://www.nap.usace.army.mil/Missions/CivilWorks/AbseconIslandStormDamageReduction.aspx). It is well known that barrier islands in the Atlantic Ocean suffer from serious beach erosion in storm season. Along Absecon Island, the predominant transport of sand by waves is to the southwest. Beach nourishments have been conducted periodically, particularly over the past half-century, in order to stabilize the shoreline locations as Ventnor, Margate, and Longport. Figure 2 shows these nourishments have moved the shoreline seaward more than a street block since 1899. Atlantic City has had several large beachfills to maintain the beach along its northern end. A series of groins – a long, narrow structure built out into the water to prevent beach erosion – have been built to help stabilize the shoreline. The low-elevation beaches at Ventnor and Margate are prone to oceanside flooding despite the presence of bulkheads. At Longport, shore protection is provided by concrete seawall and timber bulkhead. However, the bulkhead protection has failed in the past resulting in significant property damage during coastal storms.

The National Ocean Service (NOS) tide station at Atlantic City, established on 5 June 1978, was upgraded on 17 November 1997. This tide station is located on a steel pier (Taj Mahal Pier) on the waterfront of Atlantic City without harbor sheltering (Figure 3). The water depth at the tide gauge location is about 5 m at mean high water level. The local mean tide range is about 0.65 m, and the diurnal range is 0.76 m. Analysis of more than 90 years of tide records indicates the sea level near Atlantic City is increasing at a rate of

3.99±0.18 mm/year
(http://tidesandcurrents.noaa.gov/sltrends/sltrends_station.shtml?stnid=8534720).

4.3 Historical events and data

NGDC's tsunami runup database (http://www.ngdc.noaa.gov/hazard/tsu.shtml) shows that a number of historical tsunamis affected the coasts of Virginia, Maryland, Delaware, New Jersey and New York (Figure 4 and Table 1). The Atlantic City tide station recorded four of these events, including 1918 Puerto Rico, 1929 Grand Banks, a meteorological event in 1931, and 2004 Sumatra.

The 1929 Grand Banks tsunami is notable for a number of reasons. First, this Mw 7.2 earthquake is the most tragic event of its kind in Canadian history, claiming 28 lives (Ruffman, 1996). Second, with a runup of up to 27 m, a tsunami this catastrophic is extremely rare in the Atlantic Ocean. Finally, it was one of the very few transoceanic tsunamis generated by a landslide (Pasad et al., 2009). Natural Resources Canada (2006) reported that "the earthquake triggered a large submarine slump (an estimated volume of 200 cubic kilometers of material was moved on the Laurentian slope), which ruptured 12 transatlantic cables in multiple places and generated a tsunami. The tsunami was recorded along the eastern seaboard as far south as South Carolina and across the Atlantic Ocean in Portugal." Lockridge et al. (2002) reported that the Atlantic City tide gauge recorded a change of approximately 0.68 m. This tsunami was also recorded at Ocean City, Maryland, and Charleston, South Carolina. However, the generation of landslides- or meteo-tsunamis has large uncertainties and is not well suitable for model testing purposes. Also, this version of the forecast system does not include landslide- or meteo-tsunami generated tsunami forecast. Therefore, the 1929 Grand Banks tsunami was not modeled in this study.

Tsunami waves affecting the U.S. East Coast have multiple triggering mechanisms including earthquake, landslide, or meteorological events (Table 1). Historically, some of these earthquakes generated tsunamis affecting coastlines mostly within 200 km of the epicenter. Such earthquakes include 1817 Philadelphia, 1840 Philadelphia, 1871 New York, 1884 New York, and 1895 New Jersey. Earthquakes in the Caribbean Sea were known to have generated tsunamis affecting the U.S. East Coast, such as the 1973 Mona Passage, 4 August 1946 Dominican Republic, and 8 August 1946 Dominican Republic tsunamis. In addtion to the 1929 Grand Banks, another transatlantic tsunami that may have had an impact on Atlantic City is the 1755 Lisbon tsunami caused by an Mw 8.5–9.0 earthquake (Barkan et al., 2009; Roger et al., 2009; Muir-Wood and Mignan, 2009). Runup heights due to the 1755 Lisbon tsunami were documented in the Caribbean, Brazil, and Newfoundland, Canada, but not along the U.S. East Coast (Barkan et al., 2009). A model simulation of the Lisbon tsunami (see section 5.1 of this report) shows that the computed maximum wave amplitudes are about 2 m along the Atlantic City's shoreline and about 1.9 m at the tide gauge. Titov et al. (2005b) studied the global reach of the catastrophic 26 December 2004 Indian tsunami, reporting tsunami water level of 0.11 m at Atlantic City and 0.06 m at Cape May, New Jersey. It is worth noting that large tsunamis can propagate substantial and damaging wave energy to distant coasts, even different oceans, through a combination of source focusing and topographic waveguides. Local resonant effects may also amplify the arriving waves (Titov et al., 2005b).

Tsunami sources and potential impact in the Atlantic and on the Gulf Coast were evaluated by ten Brink et al. (2008). Their report indicates that earthquake sources located west of Gibraltar and in Puerto Rico Trench are capable of generating transoceanic tsunamis. A large earthquake striking in the Puerto Rico Trench could be destructive to many parts of the U.S. East Coast, although the potential of this plate boundary generating large earthquakes is still in debate. It is also speculated that landslides along the U.S. Atlantic margin have the potential to cause tsunamis locally. For instance, the Currituck slide, having occurred 300 km southeast of Atlantic City, was one of the major mass movements on the Atlantic continental margin over the last 100,000 years (Prior et al., 1986) and may have caused a damaging tsunami along the U.S. East Coast. The landslide modeling results of Geist et al. (2009) show that the Currituck slide could have triggered tsunami waves of 3-m amplitude on the shelf offshore of Ocean City, Maryland.

Other than earthquake-generated tsunamis, tsunamis with an unclear generation mechanism have also been recorded at tide gauges along the U.S. East Coast. Some of them are associated with passing hurricanes or meteorological pressure changes, such as the tsunami-like waves observed in Virginia when a category 4 hurricane moved over the area on 3 September 1821. When "heavy tides" up to 3 m were observed in Atlantic City on 10 June 1913, these observations could not be attributed to either storm surge or earthquakes (Lockridge et al., 2002), but more likely were related to abnormal weather events or submarine landslides. These unusual waves were seen along the coast of New Jersey and New York in 1923, 1924, 1931, 1932, 1938, 1944, and 1964.

4.4 Model setup

4.4.1 Grid boundary and resolution

While the wave amplitude of a tsunami is small in deep water, the amplitude increases dramatically as the wave shoals on the continental shelf. The shallow water also intensifies the wave diffusion and dispersion of a progressing tsunami. Although MOST is not a dispersive model, careful model setup makes MOST, to a certain degree, mimic physical diffusion and dispersion through a numerical scheme. Burwell et al. (2007) studies the diffusion and dispersion characterization of the MOST model, and concludes that the nature of the scheme, at all resolvable wave numbers, is diffusive and dispersive for $\beta = (gd)^{1/2}(\Delta t/\Delta x) \neq 1$, where Δt is the temporal step and Δx is the space step. Diffusive effects are stronger for poorly resolved waves (large space step compared to wave length). As β decreases, diffusive effects are reduced and dispersion continues to increase. Numerical dispersion can be an issue closer to shore, but can be controlled through a proper choice of β, or in other words, the ratio between Δt and Δx. The tsunami propagation database (Gica et al., 2008) was developed at a grid spacing of 4 arc min (about 7.2 km at the equator) and saved at 16-arc-minute (about 28.8 km at the equator) resolution. Zhou et al. (2012, 2014) shows that, for tsunami propagation in an ocean basin, MOST with numerical dispersion produces more comparable results than a shallow water model without numerical dispersion does for a dispersive model. However, the same grid resolution may introduce large model diffusion effects if applied directly to the continental shelf, where the water depth is generally less than 100 m. The telescoping grids employed in MOST are critical for wave transformation over the continental shelf and for the inundation modeling at the coastline. Proper adjustment of β at each grid level allows better calibration of numerical diffusion and dispersion in the model.

4.4.2 Digital Elevation Model of Atlantic City, New Jersey

The bathymetry and topography used for forecast model development are based on a digital elevation model provided by NGDC and is an adequate representation of the local topography/bathymetry. As new digital elevation models become available, forecast models will be updated and report updates will be posted at http://nctr.pmel.noaa.gov/forecast_reports/.

Carignan et al. (2009) developed a 1/3-arc-sec (~ 8 m along longitudinal direction at 39.35°N) digital elevation model of Atlantic City. The bathymetry is based on hydrographic survey data from NGDC's NOS Hydrographic Survey Data Base, U.S. Army Corps of Engineers (USACE) hydrographic surveys, shallow water multibeam surveys from NOS, extracted soundings from the Office of Coast Survey electronic navigational chart, and intra-coastal waterway data from NGDC. The topography in NGDC's DEM was based on USGS 1/3-arc-sec National Elevation Dataset (NED) DEM and the Coastal Service Center (CSC) LiDAR survey data. The CSC bathymetric-topographic LiDAR dataset provided full coverage of the entire length of the Atlantic Ocean shoreline. Carignan et al. (2009) provides a detailed description of how these datasets were implemented in the DEM development for Atlantic City. They also speculate that the CSC bathymetric and topographic LiDAR data was not processed to bare earth. The hydrographic and LiDAR surveys for nearshore area, especially in bays, estuaries, and coastal marshes, need to be completed in order to further improve the Atlantic City DEM.

4.4.3 Development of model grids

Atlantic City bathymetric and topographic grids are shown in Figures 5 to 9. Grid dimension extension and additional information are updated as needed and appropriate. A significant portion of the modeled tsunami waves, typically 4 to 10 hr of modeled tsunami time, pass through the model domain without appreciable signal degradation. Table 2 provides details of grid extents and input parameters for both reference and forecast model grids. The model input files are provided in Appendix A.

Figure 5 shows the coverage of A grid with a spatial resolution of 30 arc sec (~ 715 m along longitudinal direction at 39.5°N). This A grid is employed by both forecast and reference models. It is obtained from the General Bathymetric Chart of Oceans (GEBCO) 30-arc-sec global database. The eastern boundary of A grid is specified at 71°W, where the water depth ranges between 1,000 m and 5,000 m. It is recommended that the ocean boundary of A grid be placed at a water depth greater than 1,500 m to allow a smooth transition from the 4-arc-min tsunami propagation database where the waves are assumed to be linear. One can see the abrupt depth change, from 2,000 m to less then 100 m, along the continental slope. The continental shelf extends more than 100 km offshore, with typical water depths of less than 100 m, 60% of which are shallower than 50 m. This grid covers nearly the entire coastline of New Jersey between Delaware Bay to the south and Lower Bay to the north.

Figures 6 and 7 show the bathymetry and topography of B grid for forecast and reference models. These two grids have the same model extent (Table 2) but different grid resolutions, 6 arc sec (~ 140 m along the longitudinal direction at 39.5°N) for the forecast model and 3 arc sec (~ 70 m along the longitudinal direction at 39.5°N) for the reference model. Both grids were obtained from the Atlantic City 1/3-arc-sec DEM developed by NGDC (Carignan et al., 2009). The eastern boundary of the B grid is located about 40 km offshore of Atlantic City with a maximum water depth of 40 m. Atlantic City is placed at the center of B grid to minimize the numerical errors introduced by the connecting boundary between grids A and B. The long and slim barrier islands in the south and central part of New Jersey coastlines are covered by B grid. The B-grid bathymetry clearly shows sand ripples offshore formed by longshore sediment transport. It is worth noting that these dynamic bathymetric features may affect tsunami propagation on the shelf differently season by season.

The C grid of forecast model is developed with a 2-arc-sec spatial resolution (~ 48 m along the longitudinal direction at 39.5°N, Figure 8), while a 1/3-arc-sec (~ 8 m along the longitudinal direction at 39.5°N) resolution is used in the reference model covering the same area (Figure 9). Both C grids cover the entire coastline of Atlantic County, New Jersey, including the most populated area in Atlantic City and four other coastal cities (Longport, Margate, Ventnor, and Brigantine). Both grids are developed from NGDC's Atlantic City 1/3-arc-sec DEM (Carignan et al., 2009), with a maximum water depth of 15 m along the southeastern boundary. As the CSC LiDAR dataset was not processed to bald earth, a stripe of dense building structures can be clearly identified, especially in the reference model grid. Harbor entrances and the marina are artificially enlarged in the C grid of the forecast model. This numerical treatment in the model prevents narrow waterways from forming enclosed water bodies due to the 2-arc-sec spatial resolution of the grid.

5. Results and Discussion

5.1 Model validation

A lack of tsunami measurements in the Atlantic has been a major issue of model validation for the tsunami forecast models developed for the U.S. East Coast and Caribbean. A crude method is to test the model with a historical case, where the tsunami impact is well known at the modeling site or its vicinity, and consider the model validated if it gives no unreasonable results. The 1755 Lisbon tsunami is such a representative case for Atlantic City. As indicated in Table 1, the 1918 Puerto Rico and 2004 Sumartra tsunamis also produced up to 11 cm tsunami wave amplitude at the Atlantic tide gauge. However, they are not used here for model validation because of the uncertainties of their sources, which are usually determined by data inversion process in the forecast system (Titov, 2009). There also lacks of tide gage mareograms at the Atlantic City for the 1918 Puerto Rico event.

The earthquake source of the 1755 Lisbon tsunami is not fully understood. Previous studies have proposed a few source mechanisms that may have produced this basin-wide tsunami. The magnitude of the proposed earthquake ranges from 8.0 to 9.0 (Barkan et al., 2009; Muir-Wood and Mignan, 2009; Titov et al., 2014; Roger et al., 2009), while the rupture area varies between 6,000 km^2 and 480,000 km^2. Titov et al. (2014) has compared model results computed from five different earthquake scenarios and they all indicate minor tsunami impact on the U.S. east coast. These results are supported by historical accounts reporting no catastrophic impact anywhere in the United States. Barkan et al. (2009) obtained similar results for their preferred scenario after comparing the tsunami records at a number of sites in the Atlantic, particularly in the Caribbean (**Figure 10**).

The present report uses the 1755 Lisbon tsunami as a "validation" case study, for which we adopted earthquake rupture parameters from Barkan et al. (2009) with a magnitude 9.0 from Muir-Wood and Mignan (2009). This scenario probably represents a "worst case" for the 1755 Lisbon tsunami, which can explain the tsunami runup heights and overwash observed in the British Virgin Islands and Lesser Antilles (Atwater et al., 2012; Wei et al., 2014). **Figure 11** shows the computed time series at the Atlantic City tide gauge, indicating a maximum wave amplitude of ~ 1.9 m and a corresponding wave period of 15 to 20 minutes. The model results show minor tsunami inundation at the waterfront of Atlantic City and Ventnor City (**Figure 12**), where the associated current speeds are up to 4 m/s (about 8 knots). The tsunami currents in the Absecon Inlet are ~ 1.5 m/s (about 3 knots) in the middle of the inlet, and ~ 3.0 m/s (about 6 knots) on the east bank of the inlet. **Figure 12** also shows high waves and fast currents in the inlet as well as in the marinas connecting to the open ocean. One can also observe quick wave energy decay (in the form of wave amplitude and velocities) after the tsunami passes through the narrow channels and enters the marshy area behind the barrier islands.

The results obtained from both forecast model and reference model show high analogy in wave amplitude, wave period, arrival time, and current speed. The computed time series at the tide gauge (**Figure 11**) are nearly identical. It further confirms the forecast model developed at 2 arc sec is able to achieve the computational accuracy that a reference model can provide, while reducing the computing time by ~ 50 times. This efficiency makes the forecast model a suitable tool for providing rapid and accurate tsunami forecast in real time.

5.2 Model stability testing using synthetic scenarios

Model stability testing using synthetic scenarios provides important case studies to test the robustness, durability, and efficiency of the developed models from different perspectives. Synthetic scenarios:

1. Examine the developed models with mega-tsunamis to guarantee model stability. These model tests ensure the efficiency of the forecast model during a catastrophic event.

2. Examine the developed models with medium tsunamis to guarantee model stability under smaller wave conditions. These model tests ensure the efficiency of the forecast model during a moderate event.

3. Examine the developed models with negligible tsunami waves to guarantee that the numerical noise is also negligible.

4. Are selected in a way that at least one from each potential tsunami source zone is tested. These cases are used to examine the reliability of the developed models in response to tsunami waves with variable directionality.

Table 3 summarizes all the synthetic scenarios (plotted in Figure 13) used in the present model testing. Except for the 1755 Lisbon (used as a model validation in section 5.1), other scenarios are artificially constructed from a combination of the unit sources, shown as black boxes. Table 3 gives the details of unit source and the coefficients for a total of eight scenarios, six with Mw 9.3, one with Mw 7.5 and one with small tsunami. Five of the Mw 9.3 scenarios are generated in the Puerto Rico Trench and Hispaniola Trench, the most dangerous tsunamigenic earthquake zones in the Atlantic (ten Brink et al., 2008). The earthquake zones between the Caribbean plate and South America are relatively inactive. Tsunami waves generated there have minor impacts on the U.S. East Coast (Titov, 2009, Chapter 2), and no synthetic scenarios are selected from this area. The Mw 9.3 scenario from the South Sandwich source zone is useful for model stability test of tsunami directionality.

The synthetic scenario ATSZ 48-57, generated by a M_w 9.3 earthquake in the Puerto Rico Trench, poses catastrophic impacts along the coastline of Atlantic City and its vicinity. The modeling results in Figure 14 show that such an event, if coinciding with high tide, would wipe out most of the waterfront on Absecon Island, Ventor, Margate, and Longport, with water level as high as 6.8 m. Flooding water would penetrate inland as far as 2 km from the shoreline with strong current speeding up to 7 m/s (~ 14 knots). Similarly, severe flooding will also occur on 9-km-long Brigantine Island. The waves entering the Absecon Inlet would reach 4 to 5 m above mean high water, flooding the west and east banks of the inlet. Located on the west bank of the Absecon Inlet, the harbor of Atlantic City would have water levels up to 2 m in the basin, along with up to 5 m/s currents in the channels. These hazardous waves and currents need to be seriously accounted for when local emergency management plans for harbor evacuation during a tsunami event. The time series in Figure 15 indicates a dominant first wave up to 5 m (above mean high water) at the tide gauge, followed by a series of smaller waves with a maximum trough of 3 m. The time series obtained from the reference model and forecast model are nearly identical, indicating the forecast model is an efficient tool to provide high-quality model results. The 24-hour run of the forecast model shows no instability, an indication of excellent robustness of the forecast model in predicting large waves. The only difference between the forecast model and the reference model probably lies in the water elevation and flow velocities over the barrier islands during tsunami flooding – the forecast model gives slightly smaller values than those in the reference model. This is probably attributed to differing grid resolutions in the two models, where the reference model describes the structures at the oceanfront better than the forecast model does. Fine coastal features are smoothed out, creating a leveled land topography in the forecast model. It is worth noting that this difference does not affect the computed inundation limit, and the flooding areas are nearly identical in both models.

The synthetic scenario ATSZ 38-47 causes minor flooding along the coastline of Atlantic City with maximum wave amplitude of ~ 3 m. Flooding also occurs in the Atlantic City harbor, with a current speed at the narrow entrance of up to 4 m/s (~ 8 knots). Waves entering the Absecon Inlet reach ~ 2 m above mean high water. The current speed is ~ 2.5 m/s (5 knots) on the west of the channel, and is ~ 4 m/s (8 knots) on the east of the channel (Figure 16). Two model results are in excellent agreement at the tide gauge (Figure 17) with a maximum wave amplitude of 2.5 m (4 m in wave height).

With similar fault orientation and location, the synthetic scenarios ATSZ 58-67 and ATSZ 82-91 give analogous computational results at Atlantic City (Figures 18 to 21). Both scenarios showed no inundation on Absecon Island and Brigantine Island. The color pattern in Figures 18 and 20 show that, in both scenarios, waves are ~ 1.3 m in amplitude with current speed up to 0.5 m/s (1 knot) along the coastline of Atlantic City. The currents are expedited to ~ 1 m/s (2 knots) at the narrow entrance of the inlet, and ~ 2 m/s (about 4 knots) inside the harbor channel, making them hazardous to the harbor facilities and berthing boats. A notable feature of the time series at the tide gauge, in both scenarios (Figures 19 and 21), is the leading depression N-waves (Tadepalli and Synolakis, 1994). Unlike the Puerto Rico Trench and the Hispaniola Trench, where the North America plate subducts southwesterly beneath the Caribbean plate, scenarios ATSZ 58-67 and ATSZ 82-91 feature submarine troughs — Cayman Trough for ATSZ 58-67 and Los Muertos Trough for ATSZ 82-91. Cayman Trough is a complex transform fault zone bounded by strike-slip faults, while Los Muertos trough indicates a northerly dipping Caribbean Plate and associated seismic zones, in contrast to the south-dipping Puerto Rico–Lesser Antilles subduction zone (LaForge and McCann, 2005). The northerly dipping of the Los Muertos Trough results in an uplift at its southern extent but a subsidence at the north that corresponds to the leading depression when the tsunami waves propagate. It is worth noting that the unit sources in scenario ATSZ 58-67 use a pure subducting mechanism, instead of a strike-slip mechanism, to give a conservative estimate of the tsunami waves.

The synthetic scenario of ATSZ 68-77 is a special case that highlights two important characteristics of tsunami waves: wave period and late wave amplification. The computed time series at the Atlantic City tide gauge shows that the wave period is one and half hours to two hours, much longer than a typical tsunami wave. The maximum wave amplitude occurs almost six hours after the first wave arrives, stressing the necessity of retaining a tsunami warning for more than 24 hours along the coastline of Atlantic City during a tsunami event. The forecast and reference models have excellent agreement in maximum wave amplitude, maximum current speed, and waveform at the tide gauge (Figures 22 and 23**)**.

The synthetic scenario SSSZ 1-10, generated by a Mw 9.3 earthquake in the South Sandwich source zone, also shows excellent agreement between the forecast model and reference model (Figures 24 and 25). Model results show the tsunami impact along the coastline is limited with a maximum water elevation ~ 1.2 m. The maximum current speed is at ~ 1 m/s (2 knots) in the inlet and at ~ 3 m/s (6 knots) in the Atlantic City harbor. The maximum wave amplitude at the tide gage is ~ 0.7 m. with limited impact along the coastline. The largest wave, probably reflected from Africa, does not occur until five hours after the arrival of the first wave.

The synthetic scenario ATSZ b52, generated from a Mw 7.5 earthquake source, brings minor impact to the Atlantic City. The maximum wave amplitude is only ~ 0.15 m along the coastline and 0.12 m at the tide gauge. Results from the forecast and the reference models show good consistency in maximum wave amplitude, maximum current speed and the time series at the tide gauge (Figures 26 and 27). The micro-scenario ATSZ b11 is employed to test model stability in terms of negligible wave (Figures 28 and 29). Figure 29 shows that the computed time series from both models have excellent agreement even though the water elevation is only on the order of 10^{-4} m. The two models show difference mostly in the marshy area and narrow marinas, where the reference model contains more bathymetric and topographic features than the forecast model does. While intensifying the wave interaction, these small features may also introduce numerical noise on the same order as the computational results (~ 10^{-4} m) in this case.

6. Summary and conclusions

Atlantic City, New Jersey, is a coastal community built on barrier islands in the Atlantic. Drawing tourists from all over the world, Atlantic City is known for its vulnerability to potential coastal hazards such as beach erosion, sea level change, storm surge, as well as tsunamis. These natural hazards pose challenging, yet long-standing, questions for the coastal communities on how to protect lives and properties. Atlantic City has developed methodologies and procedures to protect their coastline from beach erosion, sea level change, and storm surge. Tsunami forecast and hazard assessment for Atlantic City, however, remains significantly understudied, possibly due to the rare occurrence of tsunamis in the Atlantic.

The present study develops a tsunami forecast model for Atlantic City. The developed model is implemented into NOAA's Short-term Inundation Forecast of Tsunamis (SIFT) to provide real-time modeling forecasts of tsunami wave characteristics, runup, and inundation along the coastline of Atlantic City. This report provides details in bathymetry and topography, model setup, and model parameters. The forecast model employs a spatial resolution of 2 arc sec (~ 48 m along the longitudinal direction at 39.5°N) in C grid. The forecast model is able to accomplish a four-hour simulation of tsunami inundation in 12 minutes of CPU time. In parallel, this study develops a reference model to provide model reference for the forecast model, using a spatial resolution of 1/3 arc sec (~ 8 m along the longitudinal direction at 39.5°N) in the C grid.

Due to a lack of historical record, the 1755 Lisbon tsunami is used to validate the Atlantic City forecast model. Based on Barkan et al. (2009) and Muir-Wood and Mignan (2009), this study constructs a Mw 9.0 earthquake source, possibly a worst-case scenario, for the 1755 Lisbon tsunami. The modeling results show the maximum wave amplitude is ~ 2.9 m along the coastline of Atlantic City and ~ 1.9 m at the tide gauge. Only minor tsunami inundation occurs at the waterfront of Atlantic City. The maximum current speed is ~ 4 m/s along the coastline of Atlantic City, and ranges from 1.5 m/s to 3 m/s in the Absecon Inlet. These rapid currents may pose threats to ship navigation in the inlet and in the harbor. It is worth noting that the modeling of 1755 Lisbon tsunami is based on modern bathymetry and topography, and may not represent how the coastline looked like back then. The results from both the forecast model and the reference model show excellent agreement in arrival time, wave amplitude, wave period, and current speed.

A total of eight synthetic scenarios, including six Mw 9.3, one Mw 7.5, and one micro-tsunami, is used to examine the stability of the forecast model and the reference model for Atlantic City. These scenarios represent tsunamis generated by earthquakes in the Puerto Rico Trench, Hispaniola Trench, and South Sandwich source zone. The computational results are highly consistent between the forecast model and reference model. The forecast model is robust for a 24-hour run for all synthetic scenarios.

The synthetic scenarios also show interesting wave characteristics for tsunamis generated from the Caribbean and South Sandwich source zones.

1. A Mw 9.3 earthquake in Puerto Rico Trench (e.g., scenario ATSZ 48-57) may generate a catastrophic tsunami for communities along the U.S. East Coast. Modeling results show such a tsunami would cause intensive flooding at Atlantic City, with ~ 7 m wave amplitude along the coastline and ~ 7 m/s tsunami current on land.

2. Large tsunamis generated in the Hispaniola Trench (e.g., scenario ATSZ 38-47) would cause minor flooding on the waterfront of Atlantic City, with current speed of ~ 4 m/s along the coastline and in the Absecon Inlet.

3. When compared to the above, large tsunamis generated in other parts of the Caribbean Subduction Zone are less threatening, but may cause damage to the harbor facilities and boats, due to rapid currents in the Absecon Inlet and Atlantic City Harbor.

4. Tsunamis generated in Los Muertos Trough (ATSZ 82-91) or Cayman Trough (ATSZ 58-67) would result in a leading depression for waves propagating in the Atlantic.

5. Model simulations show large late waves for tsunamis generated in the west of the Caribbean source zone (ATSZ 68-77) or in the South Sandwich source zone (SSSZ 1-10). These waves also have long wave period up to one and half hours. Local emergency management may need to retain a tsunami warning for more than 24 hours during a real tsunami event.

All model validation and stability tests demonstrate that the tsunami forecast model and the reference model for Atlantic City are robust and efficient tools for real-time tsunami forecast and long-term tsunami hazards assessment. The forecast model can provide a four-hour forecast of tsunami arrival, wave amplitude, and inundation within 12 minutes. However, it is worth noting that the model requires further validation by real events.

7. Acknowledgement

The author wishes to thank Edison Gica and Jean Newman for their work on the propagation database, Burak Uslu for providing propagation database tabular unit source information and graphics, and the entire modeling group of NCTR for helpful suggestions and discussion. The author acknowledges Michael Dunlap and Sandra Bigley for providing editorial review. Collaborative contributions of the National Weather Service, the National Geophysical Data Center, and the National Data Buoy Center were invaluable.

Funding for this publication and all work leading to development of a tsunami forecast model for Atlantic City was provided by the National Oceanic and Atmospheric Administration (NOAA). This publication was partially funded by the Joint Institute for the Study of the Atmosphere and Ocean (JISAO) under NOAA Cooperative Agreement NO. NA10OARJ4320148, JISAO Contribution No. ****. This is PMEL Contribution No. 3393.

8. References

Atwater, B.F., U.S. ten Brink, M. Buckley, R.S. Halley, B. Jaffe, A.M. López-Venegas, E.G. Reinhardt, M.P. Tuttle, S. Watt, and Y. Wei (2012): Geomorphic and stratigraphic evidence for an unusual tsunami or storm a few centuries ago at Anegada, British Virgin Islands. Nat. Hazards, 63(1), doi: 10.1007/s11069-010-9622-6, 51–84.

Barkan, R., U.S. ten Brink, and J. Lin (2009), Far filed tsunami simulations of the 1755 Lisbon earthquake: implications for tsunami hazards to the U.S. East Coast and the Caribbean, *Marine Geology*, 264, 109-122, doi: 10.1016/j/margeo.2008.10.010.

Burwell, D., E. Tolkova, and A. Chawla (2007), Diffusion and dispersion characterization of a numerical tsunami model, *Ocean Modeling*, 19, 10-30.

Carignan, K.S., L.A. Taylor, B.W. Eakins, R.R. Warnken, T. Sazonova, and D.C. Schoolcraft, 2009. Digital Elevation Model of Atlantic City, New Jersey: Procedures, Data Sources and Analysis, NOAA Technical Memorandum NESDIS NGDC-18, Dept. of Commerce, Boulder, CO, 29 pp.

Geist, E.L., P.J. Lynett and J.D. Chayton (2009), Hydrodynamic modeling of tsunamis from the Currituck landslide, *Marine Geology*, 264, 41-52.

Gica, E., M. Spillane, V.V. Titov, C. Chamberlin, and J.C. Newman (2008), Development of the forecast propagation database for NOAA's Short-term Inundation Forecast for Tsunamis (SIFT). NOAA Tech. Memo. OAR PMEL-139, 89 pp.

LaForge, R.C., and W.R. McCann (2005). A seismic source model for Puerto Rico, for use in probabilistic ground motion hazard analyses, Active Tectonics and Seismic Hazards of Puerto Rico, the Virgin Islands, and Offshore Areas, edited by P. Mann, The Geological Society of America special Paper 385, 223-248.

Leatherman, S.P. (1982). Barrier island handbook. College Park, Md.: University of Maryland, 109pp.

Lockridge, P.A., L.S. Whiteside, J.F. Lander (2002), Tsunamis and tsunami-like waves of the eastern United States, *Science of Tsunami Hazards*, 20(3), 120-157.

Meinig, C., S.E. Stalin, A.I. Nakamura, F. González, and H.G. Milburn (2005): Technology Developments in Real-Time Tsunami Measuring, Monitoring and Forecasting. In Oceans 2005 MTS/IEEE, 19–23 September 2005, Washington, D.C.

Muir-Wood, R. and A. Mignan (2009), A phenomenological reconstruction of the Mw9 Novermber 1st 1755 earthquake source, *The 1755 Lisbon Earthquake: Revisited, Geotechnical, Geological, and Earthquake Engineering*, 7, Part III, 121-146, doi: 10.1007/978-1-4020-8609-0_8.

Natural Resources Canada (2006), Earthquakes Canada; Canadian Hazard Information Service. Historic Earthquakes Web Pages, http://earthquakescanada.nrcan.gc.ca/

Pasad, R., E. Cunningham, and G. Bagchi (2009), Tsunami hazard assessment at nuclear power plant sites in the United States of America – Final Report, United States Nuclear Regulatory Commission, NUREG/CR-6966 and PNNL-17397, NRC Job Code J3301, Office of New Reactors, p84.

Percival, D.B., D.W. Denbo, M.C. Eble, E. Gica, H.O. Mofjeld, M.C. Spillane, L. Tang, and V.V. Titov (2011): Extraction of tsunami source coefficients via inversion of DART® buoy data. *Nat. Hazards*, *58*(1), doi: 10.1007/s11069-010-9688-1, 567–590.

Prior, D.P., Doyle, E.H., and Neurauter, T. (1986), The Currituck Slide, Mid Atlantic continental slope-revisited, *Marine Geology*, V73, p25-4.

Roger, J., S. Allgeyer, H. Hebert, M.A. Baptista, A. Loevenbruck, F. Schindele (2009), The 1755 Lisbon tsunami in guadeloup Archipelago: source sensitivity and investigation of resonance effects, *The Open Oceanography Journal*, 3, 1-13.

Ruffman, A. (1996). Tsunami runup mapping as an emergency preparedness planning tool: the 1929 tsunami in St. Lawrance, Newfoundland. *Geomarine Associates Ltd.*, Contract Report for Emergency Preparedness Canada (EPC), Office of the Senior Scientific Advisor, Ottawa, Ontario, V1 – Report, 107 pp.; V2 – Appendices and Enclosures, 281 pp.

Synolakis, C.E., E.N. Bernard, V.V. Titov, U. Kânoğlu, and F.I. González (2008): Validation and verification of tsunami numerical models. *Pure Appl. Geophys.*, *165*(11–12), 2197–2228.

Tadepalli, S., and C.E. Synolakis (1994). The run-up of N-waves on sloping beaches. Proc. R. Soc. A 445, 99-112.

Tang, L., V.V. Titov, E. Bernard, Y. Wei, C. Chamberlin, J.C. Newman, H. Mofjeld, D. Arcas, M. Eble, C. Moore, B. Uslu, C. Pells, M.C. Spillane, L.M. Wright, and E. Gica (2012): Direct energy estimation of the 2011 Japan tsunami using deep-ocean pressure measurements. J. Geophys. Res., 117, C08008, doi: 10.1029/2011JC007635.

Tang, L., V. V. Titov, and C. D. Chamberlin (2009), Development, testing, and applications of site-specific tsunami inundation models for real-time forecasting, *J. Geophys. Res.*, 114, C12025, doi:10.1029/2009JC005476.

Tang, L., V.V. Titov, Y. Wei, H.O. Mofjeld, M. Spillane, D. Arcas, E.N. Bernard, C. Chamberlin, E. Gica, and J. Newman (2008): Tsunami forecast analysis for the May 2006 Tonga tsunami. *J. Geophys. Res.*, *113*, C12015, doi: 10.1029/2008JC004922.

ten Brink, U., D. Twichell, E. Geist, J. Chaytor, J. Locat, H. Lee, B. Buczkowski, R. Barkan, A. Solow, B. Andrews, T. Parsons, P. Lynett, J. Lin, and M. Sansoucy (2008): Evaluation of tsunami sources with the potential to impact the U.S. Atlantic and Gulf coasts, *USGS Administrative report to the Nuclear Regulatory Commission*, 300pp.

Titov, V.V. (2009): Tsunami forecasting. Chapter 12 in *The Sea, Volume 15: Tsunamis*, Harvard University Press, Cambridge, MA and London, England, 371–400.

Titov, V.V, E. Gica, M. Spillane, Y. Wei, C. Moore, H. Zhou and R. Weiss (2014), Tsunami hazard assessment for the U.S. East Coast based on generation, propagation and inundation modeling, *NCTR Letter Report to the Nuclear Regulatory Commission*, in revision.

Titov, V., and F.I. González (1997): Implementation and testing of the Method of Splitting Tsunami (MOST) model. NOAA Tech. Memo. ERL PMEL-112 (PB98-122773), NOAA/Pacific Marine Environmental Laboratory, Seattle, WA, 11 pp.

Titov, V.V., F.I. González, E.N. Bernard, M.C. Eble, H.O. Mofjeld, J.C. Newman, and A.J. Venturato (2005a): Real-time tsunami forecasting: Challenges and solutions. Nat. Hazards, 35(1), Special Issue, U.S. National Tsunami Hazard Mitigation Program, 41–58.

Titov, V.V., A.B. Rabinovich, H.O. Mofjeld, R.E. Thomson, and F.I. González (2005b), The global reach of the 26 December 2004 Sumatra Tsunami. *Science*. doi: 10.1126/science.1114576.

Wei, Y., E. Bernard, L. Tang, R. Weiss, V. Titov, C. Moore, M. Spillane, M. Hopkins, and U. Kânoğlu (2008): Real-time experimental forecast of the Peruvian tsunami of August 2007 for U.S. coastlines. *Geophys. Res. Lett.*, *35*, L04609, doi: 10.1029/2007GL032250.

Wei, Y., C. Chamberlin, V. Titov, L. Tang, and E.N. Bernard (2013): Modeling of the 2011 Japan tsunami - Lessons for near-field forecast. Pure Appl. Geophys., 170(6–8), doi: 10.1007/s00024-012-0519-z, 1309–1331.

Wei, Y., U.S. ten Brink, and B. Atwater (2014): Tsunami sources that might explain the catastrophic overwash of Anegada, British Virgin Islands, between 1650 and 1800. *Journal of Geophysical Research*, in preparation.

Zhou, H., Y. Wei, L. Wright, and V. Titov (2014): Waves and currents in Hawaiian waters induced by the dispersive 2011 Tohoku tsunami. Published online, Pure Appl. Geophys., doi: 10.1007/s00024-014-0781-3.

Zhou, H., Y. Wei, and V.V. Titov (2012): Dispersive modeling of the 2009 Samoa tsunami. Geophys. Res. Lett., 39(16), L16603, doi: 1029/2012GL053068.

Figures

Figure 1. (a) Aerial view of the coastline of Atlantic City from the north. (b) Aerial view of the coastline of Atlantic City from the south.

Figure 2. Historical shoreline changes at Ventnor City, New Jersey (Courtesy of United States Army Corps of Engineers).

Figure 3. Location of NOS Atlantic City tide station. (a) Google aerial view of Absecon Island, Absecon Inlet, and Brigantine Island; (b) location of the pier (Taj Mahal Pier) that hosts the tide station; (c) closer view of Taj Mahal Pier and the location of the tide station; (d) outside appearance of the tide station (photo courtesy of http://tideandcurrents.noaa.gov).

Figure 4. Historical tsunami events that have affected the U.S. East Coast, where ● indicates the earthquake location and M represents meteorological tsunamis. The black boxes are the tsunami propagation unit sources (Gica et al., 2008).

Figure 5. A-grid bathymetry and topography for both the forecast model and the reference model, where the black boxes indicate coverage of B grid (outermost) and C grid (innermost) and the red circle indicates the location of Atlantic City tide station.

Figure 6. B-grid bathymetry and topography for the forecast model, where the black box indicates coverage of C grid in the forecast model and the red circle indicates the location of Atlantic City tide station.

Figure 7. B-grid bathymetry and topography for the reference model, where the black box indicates coverage of C grid in forecast model and the red circle indicates the location of Atlantic City tide station.

Figure 8. C-grid bathymetry and topography for the forecast model, where the red circle indicates the location of Atlantic City tide station.

Figure 9. C-grid bathymetry and topography for the reference model, where the red circle indicates the location of Atlantic City tide station.

Figure 10. Tsunami energy projection (or computed maximum wave amplitude) of the 1755 Lisbon tsunami (Mw 9.0 scenario) in the Atlantic.

Figure 11. Comparison of computed time series between forecast model and reference model at the Atlantic City tide station for 1755 Lisbon tsunami. The upper panel shows an 8-hour segment (hour 8 to 16) of the 24-hour model run (lower panel).

Figure 12. Computed maximum wave amplitude and maximum current speed in C grid for the 1755 Lisbon tsunami (Mw 9.0 scenario). (a) Maximum wave amplitude in C grid computed with the reference model; (b) maximum current speed in C grid computed with the reference model; (c) maximum wave amplitude in C grid computed with the forecast model; (d) maximum current speed in C grid computed with the forecast model.

Figure 13. Model scenarios used in model validation and model stability testing. See Table 3 for model details.

Figure 14. Computed maximum wave amplitude and maximum current speed in C grid for ATSZ 48-57 scenario. (a) Maximum wave amplitude in C grid computed with the reference model; (b) maximum current speed in C grid computed with the reference model; (c) maximum wave amplitude in C grid computed with the forecast model; (d) maximum current speed in C grid computed with the forecast model.

Figure 15. Comparison of computed time series between forecast model and reference model at the Atlantic City tide station for ATSZ 48-57 scenario. The upper panel shows an 8-hour segment (hour 4 to 12) of the 24-hour model run (lower panel).

Figure 16. Computed maximum wave amplitude and maximum current speed in C grid for ATSZ 38-47 scenario. (a) Maximum wave amplitude in C grid computed with the reference model; (b) maximum current speed in C grid computed with the reference model; (c) maximum wave amplitude in C grid computed with the forecast model; (d) maximum current speed in C grid computed with the forecast model.

Figure 17. Comparison of computed time series between forecast model and reference model at the Atlantic City tide station for ATSZ 38-47 scenario. The upper panel shows an 8-hour segment (hour 4 to 12) of the 24-hour model run (lower panel).

Figure 18. Computed maximum wave amplitude and maximum current speed in C grid for ATSZ 58-67 scenario. (a) Maximum wave amplitude in C grid computed with the reference model; (b) maximum current speed in C grid computed with the reference model; (c) maximum wave amplitude in C grid computed with the forecast model; (d) maximum current speed in C grid computed with the forecast model.

Figure 19. Comparison of computed time series between forecast model and reference model at the Atlantic City tide station for ATSZ 58-67 scenario. The upper panel shows an 8-hour segment (hour 4 to 12) of the 24-hour model run (lower panel).

Figure 20. Computed maximum wave amplitude and maximum current speed in C grid for ATSZ 82-91 scenario. (a) Maximum wave amplitude in C grid computed with the reference model; (b) maximum current speed in C grid computed with the reference model; (c) maximum wave amplitude in C grid computed with the forecast model; (d) maximum current speed in C grid computed with the forecast model.

Figure 21. Comparison of computed time series between forecast model and reference model at the Atlantic City tide station for ATSZ 82-91 scenario. The upper panel shows an 8-hour segment (hour 4 to 12) of the 24-hour model run (lower panel).

Figure 22. Computed maximum wave amplitude and maximum current speed in C grid for ATSZ 68-77 scenario. (a) Maximum wave amplitude in C grid computed with the reference model; (b) maximum current speed in C grid computed with the reference model; (c) maximum wave amplitude in C grid computed with the forecast model; (d) maximum current speed in C grid computed with the forecast model.

Figure 23. Comparison of computed time series between forecast model and reference model at the Atlantic City tide station for ATSZ 68-77 scenario. The upper panel shows an 8-hour segment (hour 4 to 12) of the 24-hour model run (lower panel).

Figure 24. Computed maximum wave amplitude and maximum current speed in C grid for SSSZ 01-10 scenario. (a) Maximum wave amplitude in C grid computed with the reference model; (b) maximum current speed in C grid computed with the reference model; (c) maximum wave amplitude in C grid computed with the forecast model; (d) maximum current speed in C grid computed with the forecast model.

Figure 25. Comparison of computed time series between forecast model and reference model at the Atlantic City tide station for SSSZ 01-10 scenario. The upper panel shows an 8-hour segment (hour 17 to 25) of the 24-hour model run (lower panel).

Figure 26. Computed maximum wave amplitude and maximum current speed in C grid for ATSZ b52 scenario. (a) Maximum wave amplitude in C grid computed with the reference model; (b) maximum current speed in C grid computed with the reference model; (c) maximum wave amplitude in C grid computed with the forecast model; (d) maximum current speed in C grid computed with the forecast model.

Figure 27. Comparison of computed time series between forecast model and reference model at the Atlantic City tide station for ATSZ b52 scenario. The upper panel shows an 8-hour segment (hour 4 to 12) of the 24-hour model run (lower panel).

Figure 28. Computed maximum wave amplitude and maximum current speed in C grid for SSSZ b11scenario. (a) Maximum wave amplitude in C grid computed with the reference model; (b) maximum current speed in C grid computed with the reference model; (c) maximum wave amplitude in C grid computed with the forecast model; (d) maximum current speed in C grid computed with the forecast model.

Figure 29. Comparison of computed time series between forecast model and reference model at the Atlantic City tide station for SSSZ b11 scenario. The upper panel shows an 8-hour segment (hour 22 to 30) of the 24-hour model run (lower panel).

Tables

Table 1: Historical tsunami events that have affected central north of U.S. East Coast, including Atlantic City, New Jersey.

Table 2: Model parameters for reference and forecast models for Atlantic City, New Jersey.

Table 3: Synthetic tsunami scenarios in the Atlantic Ocean used in this study.

Appendix A.

Development of the Atlantic City tsunami forecast model occurred prior to parameters changes that were made to reflect modification to the MOST model code. As a result, the input file for running both the optimized tsunami forecast model and the high-resolution reference inundation model in MOST have been updated accordingly. Appendix A1 and A2 provide the updated files for Atlantic City models.

A1. Reference model *.in file for Atlantic City, New Jersey

```
1.0E-4 Minimum amplitude of input offshore wave (m)
1.0  Input minimum depth for offshore (m)
0.1   Input "dry land" depth for inundation (m)
0.0009 Input friction coefficient (n**2)
1     let a and b run up
300.0 blowup limit
0.45   input time step (sec)
96000 input amount of steps
7     Compute "A" arrays every n-th time step, n=
6     Compute "B" arrays every n-th time step, n=
168   Input number of steps between snapshots
0    ...Starting from
1    ...saving grid every n-th node, n=
```

A2. Forecast model *.in file for Atlantic City, New Jersey

```
1.0E-4 Minimum amplitude of input offshore wave (m)
1.0  Input minimum depth for offshore (m)
0.1   Input "dry land" depth for inundation (m)
0.0009 Input friction coefficient (n**2)
1     let a and b run up
300.0 blowup limit
3.0   input time step (sec)
14400 input amount of steps
1     Compute "A" arrays every n-th time step, n=
2     Compute "B" arrays every n-th time step, n=
10   Input number of steps between snapshots
0    ...Starting from
1    ...saving grid every n-th node, n=
```

Appendix B. Propagation database: Atlantic Ocean Unit Sources

This section lists the earthquake parameters of each unit source in the Atlantic Ocean which covers the Caribbean and South Sandwich sources.

These propagation source details reflect the database as of January 2010, and there may have been updates in the earthquake source parameters after this date.

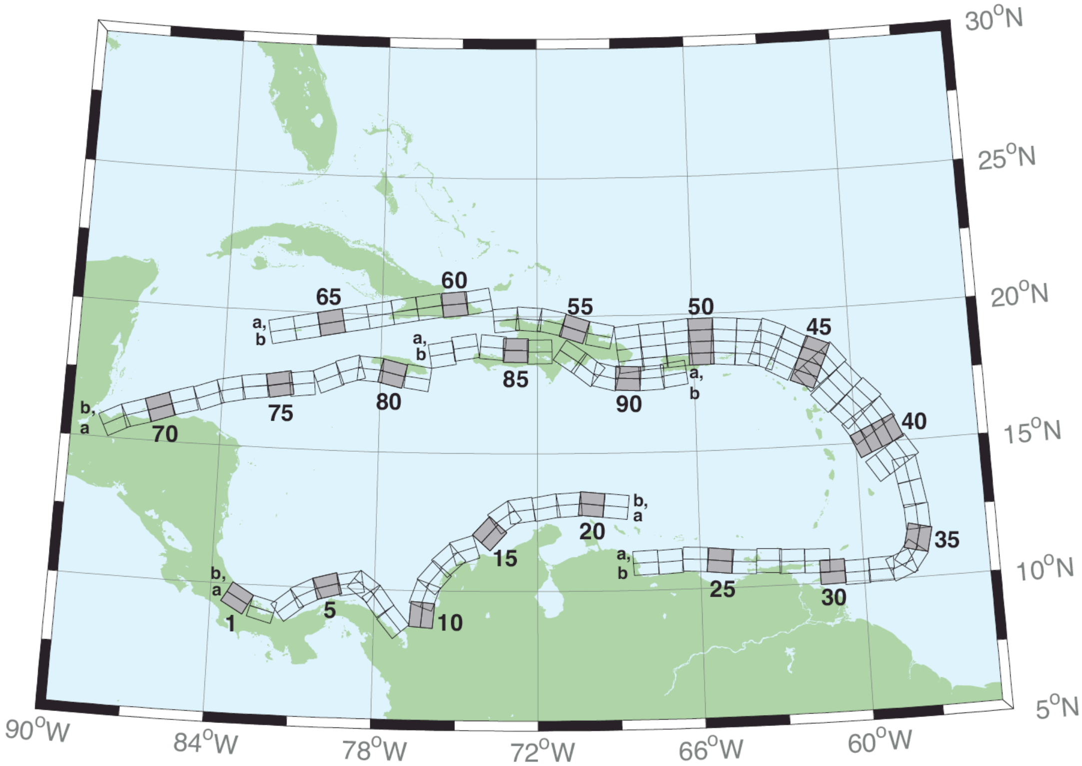

Figure B1. Atlantic Source Zone unit sources

Table B1. Earthquake parameter for unit sources in Atlantic.

Unit Source	Description	Lon (°)	Lat (°)	Strike (°)	Dip (°)	Depth (km)
atsz-01a	Atlantic Source Zone	-83.2020	9.1449	27.50	120.00	28.09
atsz-01b	Atlantic Source Zone	-83.0000	9.4899	27.50	120.00	5.00
atsz-02a	Atlantic Source Zone	-82.1932	8.7408	27.50	105.11	28.09
atsz-02b	Atlantic Source Zone	-82.0880	9.1254	27.50	105.11	5.00
atsz-03a	Atlantic Source Zone	-80.9172	9.0103	30.00	51.31	30.00
atsz-03b	Atlantic Source Zone	-81.1636	9.3139	30.00	51.31	5.00
atsz-04a	Atlantic Source Zone	-80.3265	9.4308	30.00	63.49	30.00
atsz-04b	Atlantic Source Zone	-80.5027	9.7789	30.00	63.49	5.00
atsz-05a	Atlantic Source Zone	-79.6247	9.6961	30.00	74.44	30.00
atsz-05b	Atlantic Source Zone	-79.7307	10.0708	30.00	74.44	5.00

atsz-06a	Atlantic Source Zone	-78.8069	9.8083	30.00	79.71	30.00
atsz-06b	Atlantic Source Zone	-78.8775	10.1910	30.00	79.71	5.00
atsz-07a	Atlantic Source Zone	-78.6237	9.7963	30.00	127.25	30.00
atsz-07b	Atlantic Source Zone	-78.3845	10.1059	30.00	127.25	5.00
atsz-08a	Atlantic Source Zone	-78.1693	9.3544	30.00	143.76	30.00
atsz-08b	Atlantic Source Zone	-77.8511	9.5844	30.00	143.76	5.00
atsz-09a	Atlantic Source Zone	-77.5913	8.5989	30.00	139.93	30.00
atsz-09b	Atlantic Source Zone	-77.2900	8.8493	30.00	139.93	5.00
atsz-10a	Atlantic Source Zone	-75.8109	9.0881	17.00	4.67	19.62
atsz-10b	Atlantic Source Zone	-76.2445	9.1231	17.00	4.67	5.00
atsz-11a	Atlantic Source Zone	-75.7406	9.6929	17.00	19.67	19.62
atsz-11b	Atlantic Source Zone	-76.1511	9.8375	17.00	19.67	5.00
atsz-12a	Atlantic Source Zone	-75.4763	10.2042	17.00	40.40	19.62
atsz-12b	Atlantic Source Zone	-75.8089	10.4826	17.00	40.40	5.00
atsz-13a	Atlantic Source Zone	-74.9914	10.7914	17.00	47.17	19.62
atsz-13b	Atlantic Source Zone	-75.2890	11.1064	17.00	47.17	5.00
atsz-14a	Atlantic Source Zone	-74.5666	11.0708	17.00	71.68	19.62
atsz-14b	Atlantic Source Zone	-74.7043	11.4786	17.00	71.68	5.00
atsz-15a	Atlantic Source Zone	-73.4576	11.8012	17.00	42.69	19.62
atsz-15b	Atlantic Source Zone	-73.7805	12.0924	17.00	42.69	5.00
atsz-16a	Atlantic Source Zone	-72.9788	12.3365	17.00	54.75	19.62
atsz-16b	Atlantic Source Zone	-73.2329	12.6873	17.00	54.75	5.00
atsz-17a	Atlantic Source Zone	-72.5454	12.5061	17.00	81.96	19.62
atsz-17b	Atlantic Source Zone	-72.6071	12.9314	17.00	81.96	5.00
atsz-18a	Atlantic Source Zone	-71.6045	12.6174	17.00	79.63	19.62
atsz-18b	Atlantic Source Zone	-71.6839	13.0399	17.00	79.63	5.00
atsz-19a	Atlantic Source Zone	-70.7970	12.7078	17.00	86.32	19.62
atsz-19b	Atlantic Source Zone	-70.8253	13.1364	17.00	86.32	5.00
atsz-20a	Atlantic Source Zone	-70.0246	12.7185	17.00	95.94	19.62
atsz-20b	Atlantic Source Zone	-69.9789	13.1457	17.00	95.94	5.00
atsz-21a	Atlantic Source Zone	-69.1244	12.6320	17.00	95.94	19.62
atsz-21b	Atlantic Source Zone	-69.0788	13.0592	17.00	95.94	5.00
atsz-22a	Atlantic Source Zone	-68.0338	11.4286	15.00	266.94	17.94
atsz-22b	Atlantic Source Zone	-68.0102	10.9954	15.00	266.94	5.00
atsz-23a	Atlantic Source Zone	-67.1246	11.4487	15.00	266.94	17.94
atsz-23b	Atlantic Source Zone	-67.1010	11.0155	15.00	266.94	5.00
atsz-24a	Atlantic Source Zone	-66.1656	11.5055	15.00	273.30	17.94
atsz-24b	Atlantic Source Zone	-66.1911	11.0724	15.00	273.30	5.00
atsz-25a	Atlantic Source Zone	-65.2126	11.4246	15.00	276.36	17.94
atsz-25b	Atlantic Source Zone	-65.2616	10.9934	15.00	276.36	5.00
atsz-26a	Atlantic Source Zone	-64.3641	11.3516	15.00	272.87	17.94
atsz-26b	Atlantic Source Zone	-64.3862	10.9183	15.00	272.87	5.00
atsz-27a	Atlantic Source Zone	-63.4472	11.3516	15.00	272.93	17.94

atsz-27b	Atlantic Source Zone	-63.4698	10.9183	15.00	272.93	5.00
atsz-28a	Atlantic Source Zone	-62.6104	11.2831	15.00	271.11	17.94
atsz-28b	Atlantic Source Zone	-62.6189	10.8493	15.00	271.11	5.00
atsz-29a	Atlantic Source Zone	-61.6826	11.2518	15.00	271.57	17.94
atsz-29b	Atlantic Source Zone	-61.6947	10.8181	15.00	271.57	5.00
atsz-30a	Atlantic Source Zone	-61.1569	10.8303	15.00	269.01	17.94
atsz-30b	Atlantic Source Zone	-61.1493	10.3965	15.00	269.01	5.00
atsz-31a	Atlantic Source Zone	-60.2529	10.7739	15.00	269.01	17.94
atsz-31b	Atlantic Source Zone	-60.2453	10.3401	15.00	269.01	5.00
atsz-32a	Atlantic Source Zone	-59.3510	10.8123	15.00	269.01	17.94
atsz-32b	Atlantic Source Zone	-59.3734	10.3785	15.00	269.01	5.00
atsz-33a	Atlantic Source Zone	-58.7592	10.8785	15.00	248.62	17.94
atsz-33b	Atlantic Source Zone	-58.5984	10.4745	15.00	248.62	5.00
atsz-34a	Atlantic Source Zone	-58.5699	11.0330	15.00	217.15	17.94
atsz-34b	Atlantic Source Zone	-58.2179	10.7710	15.00	217.15	5.00
atsz-35a	Atlantic Source Zone	-58.3549	11.5300	15.00	193.68	17.94
atsz-35b	Atlantic Source Zone	-57.9248	11.4274	15.00	193.68	5.00
atsz-36a	Atlantic Source Zone	-58.3432	12.1858	15.00	177.65	17.94
atsz-36b	Atlantic Source Zone	-57.8997	12.2036	15.00	177.65	5.00
atsz-37a	Atlantic Source Zone	-58.4490	12.9725	15.00	170.73	17.94
atsz-37b	Atlantic Source Zone	-58.0095	13.0424	15.00	170.73	5.00
atsz-38a	Atlantic Source Zone	-58.6079	13.8503	15.00	170.22	17.94
atsz-38b	Atlantic Source Zone	-58.1674	13.9240	15.00	170.22	5.00
atsz-39a	Atlantic Source Zone	-58.6667	14.3915	15.00	146.85	17.94
atsz-39b	Atlantic Source Zone	-58.2913	14.6287	15.00	146.85	5.00
atsz-39y	Atlantic Source Zone	-59.4168	13.9171	15.00	146.85	43.82
atsz-39z	Atlantic Source Zone	-59.0415	14.1543	15.00	146.85	30.88
atsz-40a	Atlantic Source Zone	-59.1899	15.2143	15.00	156.23	17.94
atsz-40b	Atlantic Source Zone	-58.7781	15.3892	15.00	156.23	5.00
atsz-40y	Atlantic Source Zone	-60.0131	14.8646	15.00	156.23	43.82
atsz-40z	Atlantic Source Zone	-59.6012	15.0395	15.00	156.23	30.88
atsz-41a	Atlantic Source Zone	-59.4723	15.7987	15.00	146.33	17.94
atsz-41b	Atlantic Source Zone	-59.0966	16.0392	15.00	146.33	5.00
atsz-41y	Atlantic Source Zone	-60.2229	15.3177	15.00	146.33	43.82
atsz-41z	Atlantic Source Zone	-59.8473	15.5582	15.00	146.33	30.88
atsz-42a	Atlantic Source Zone	-59.9029	16.4535	15.00	136.99	17.94
atsz-42b	Atlantic Source Zone	-59.5716	16.7494	15.00	136.99	5.00
atsz-42y	Atlantic Source Zone	-60.5645	15.8616	15.00	136.99	43.82
atsz-42z	Atlantic Source Zone	-60.2334	16.1575	15.00	136.99	30.88
atsz-43a	Atlantic Source Zone	-60.5996	17.0903	15.00	138.71	17.94
atsz-43b	Atlantic Source Zone	-60.2580	17.3766	15.00	138.71	5.00
atsz-43y	Atlantic Source Zone	-61.2818	16.5177	15.00	138.71	43.82
atsz-43z	Atlantic Source Zone	-60.9404	16.8040	15.00	138.71	30.88

atsz-44a	Atlantic Source Zone	-61.1559	17.8560	15.00	141.07	17.94
atsz-44b	Atlantic Source Zone	-60.8008	18.1286	15.00	141.07	5.00
atsz-44y	Atlantic Source Zone	-61.8651	17.3108	15.00	141.07	43.82
atsz-44z	Atlantic Source Zone	-61.5102	17.5834	15.00	141.07	30.88
atsz-45a	Atlantic Source Zone	-61.5491	18.0566	15.00	112.84	17.94
atsz-45b	Atlantic Source Zone	-61.3716	18.4564	15.00	112.84	5.00
atsz-45y	Atlantic Source Zone	-61.9037	17.2569	15.00	112.84	43.82
atsz-45z	Atlantic Source Zone	-61.7260	17.6567	15.00	112.84	30.88
atsz-46a	Atlantic Source Zone	-62.4217	18.4149	15.00	117.86	17.94
atsz-46b	Atlantic Source Zone	-62.2075	18.7985	15.00	117.86	5.00
atsz-46y	Atlantic Source Zone	-62.8493	17.6477	15.00	117.86	43.82
atsz-46z	Atlantic Source Zone	-62.6352	18.0313	15.00	117.86	30.88
atsz-47a	Atlantic Source Zone	-63.1649	18.7844	20.00	110.46	22.10
atsz-47b	Atlantic Source Zone	-63.0087	19.1798	20.00	110.46	5.00
atsz-47y	Atlantic Source Zone	-63.4770	17.9936	20.00	110.46	56.30
atsz-47z	Atlantic Source Zone	-63.3205	18.3890	20.00	110.46	39.20
atsz-48a	Atlantic Source Zone	-63.8800	18.8870	20.00	95.37	22.10
atsz-48b	Atlantic Source Zone	-63.8382	19.3072	20.00	95.37	5.00
atsz-48y	Atlantic Source Zone	-63.9643	18.0465	20.00	95.37	56.30
atsz-48z	Atlantic Source Zone	-63.9216	18.4667	20.00	95.37	39.20
atsz-49a	Atlantic Source Zone	-64.8153	18.9650	20.00	94.34	22.10
atsz-49b	Atlantic Source Zone	-64.7814	19.3859	20.00	94.34	5.00
atsz-49y	Atlantic Source Zone	-64.8840	18.1233	20.00	94.34	56.30
atsz-49z	Atlantic Source Zone	-64.8492	18.5442	20.00	94.34	39.20
atsz-50a	Atlantic Source Zone	-65.6921	18.9848	20.00	89.59	22.10
atsz-50b	Atlantic Source Zone	-65.6953	19.4069	20.00	89.59	5.00
atsz-50y	Atlantic Source Zone	-65.6874	18.1407	20.00	89.59	56.30
atsz-50z	Atlantic Source Zone	-65.6887	18.5628	20.00	89.59	39.20
atsz-51a	Atlantic Source Zone	-66.5742	18.9484	20.00	84.98	22.10
atsz-51b	Atlantic Source Zone	-66.6133	19.3688	20.00	84.98	5.00
atsz-51y	Atlantic Source Zone	-66.4977	18.1076	20.00	84.98	56.30
atsz-51z	Atlantic Source Zone	-66.5353	18.5280	20.00	84.98	39.20
atsz-52a	Atlantic Source Zone	-67.5412	18.8738	20.00	85.87	22.10
atsz-52b	Atlantic Source Zone	-67.5734	19.2948	20.00	85.87	5.00
atsz-52y	Atlantic Source Zone	-67.4781	18.0319	20.00	85.87	56.30
atsz-52z	Atlantic Source Zone	-67.5090	18.4529	20.00	85.87	39.20
atsz-53a	Atlantic Source Zone	-68.4547	18.7853	20.00	83.64	22.10
atsz-53b	Atlantic Source Zone	-68.5042	19.2048	20.00	83.64	5.00
atsz-53y	Atlantic Source Zone	-68.3575	17.9463	20.00	83.64	56.30
atsz-53z	Atlantic Source Zone	-68.4055	18.3658	20.00	83.64	39.20
atsz-54a	Atlantic Source Zone	-69.6740	18.8841	20.00	101.54	22.10
atsz-54b	Atlantic Source Zone	-69.5846	19.2976	20.00	101.54	5.00
atsz-55a	Atlantic Source Zone	-70.7045	19.1376	20.00	108.19	22.10

atsz-55b	Atlantic Source Zone	-70.5647	19.5386	20.00	108.19	5.00
atsz-56a	Atlantic Source Zone	-71.5368	19.3853	20.00	102.64	22.10
atsz-56b	Atlantic Source Zone	-71.4386	19.7971	20.00	102.64	5.00
atsz-57a	Atlantic Source Zone	-72.3535	19.4838	20.00	94.20	22.10
atsz-57b	Atlantic Source Zone	-72.3206	19.9047	20.00	94.20	5.00
atsz-58a	Atlantic Source Zone	-73.1580	19.4498	20.00	84.34	22.10
atsz-58b	Atlantic Source Zone	-73.2022	19.8698	20.00	84.34	5.00
atsz-59a	Atlantic Source Zone	-74.3567	20.9620	20.00	259.74	22.10
atsz-59b	Atlantic Source Zone	-74.2764	20.5467	20.00	259.74	5.00
atsz-60a	Atlantic Source Zone	-75.2386	20.8622	15.00	264.18	17.94
atsz-60b	Atlantic Source Zone	-75.1917	20.4306	15.00	264.18	5.00
atsz-61a	Atlantic Source Zone	-76.2383	20.7425	15.00	260.70	17.94
atsz-61b	Atlantic Source Zone	-76.1635	20.3144	15.00	260.70	5.00
atsz-62a	Atlantic Source Zone	-77.2021	20.5910	15.00	259.95	17.94
atsz-62b	Atlantic Source Zone	-77.1214	20.1638	15.00	259.95	5.00
atsz-63a	Atlantic Source Zone	-78.1540	20.4189	15.00	259.03	17.94
atsz-63b	Atlantic Source Zone	-78.0661	19.9930	15.00	259.03	5.00
atsz-64a	Atlantic Source Zone	-79.0959	20.2498	15.00	259.24	17.94
atsz-64b	Atlantic Source Zone	-79.0098	19.8236	15.00	259.24	5.00
atsz-65a	Atlantic Source Zone	-80.0393	20.0773	15.00	258.85	17.94
atsz-65b	Atlantic Source Zone	-79.9502	19.6516	15.00	258.85	5.00
atsz-66a	Atlantic Source Zone	-80.9675	19.8993	15.00	258.60	17.94
atsz-66b	Atlantic Source Zone	-80.8766	19.4740	15.00	258.60	5.00
atsz-67a	Atlantic Source Zone	-81.9065	19.7214	15.00	258.51	17.94
atsz-67b	Atlantic Source Zone	-81.8149	19.2962	15.00	258.51	5.00
atsz-68a	Atlantic Source Zone	-87.8003	15.2509	15.00	62.69	17.94
atsz-68b	Atlantic Source Zone	-88.0070	15.6364	15.00	62.69	5.00
atsz-69a	Atlantic Source Zone	-87.0824	15.5331	15.00	72.73	17.94
atsz-69b	Atlantic Source Zone	-87.2163	15.9474	15.00	72.73	5.00
atsz-70a	Atlantic Source Zone	-86.1622	15.8274	15.00	70.64	17.94
atsz-70b	Atlantic Source Zone	-86.3120	16.2367	15.00	70.64	5.00
atsz-71a	Atlantic Source Zone	-85.3117	16.1052	15.00	73.70	17.94
atsz-71b	Atlantic Source Zone	-85.4387	16.5216	15.00	73.70	5.00
atsz-72a	Atlantic Source Zone	-84.3470	16.3820	15.00	69.66	17.94
atsz-72b	Atlantic Source Zone	-84.5045	16.7888	15.00	69.66	5.00
atsz-73a	Atlantic Source Zone	-83.5657	16.6196	15.00	77.36	17.94
atsz-73b	Atlantic Source Zone	-83.6650	17.0429	15.00	77.36	5.00
atsz-74a	Atlantic Source Zone	-82.7104	16.7695	15.00	82.35	17.94
atsz-74b	Atlantic Source Zone	-82.7709	17.1995	15.00	82.35	5.00
atsz-75a	Atlantic Source Zone	-81.7297	16.9003	15.00	79.86	17.94
atsz-75b	Atlantic Source Zone	-81.8097	17.3274	15.00	79.86	5.00
atsz-76a	Atlantic Source Zone	-80.9196	16.9495	15.00	82.95	17.94
atsz-76b	Atlantic Source Zone	-80.9754	17.3801	15.00	82.95	5.00

atsz-77a	Atlantic Source Zone	-79.8086	17.2357	15.00	67.95	17.94
atsz-77b	Atlantic Source Zone	-79.9795	17.6378	15.00	67.95	5.00
atsz-78a	Atlantic Source Zone	-79.0245	17.5415	15.00	73.61	17.94
atsz-78b	Atlantic Source Zone	-79.1532	17.9577	15.00	73.61	5.00
atsz-79a	Atlantic Source Zone	-78.4122	17.5689	15.00	94.07	17.94
atsz-79b	Atlantic Source Zone	-78.3798	18.0017	15.00	94.07	5.00
atsz-80a	Atlantic Source Zone	-77.6403	17.4391	15.00	103.33	17.94
atsz-80b	Atlantic Source Zone	-77.5352	17.8613	15.00	103.33	5.00
atsz-81a	Atlantic Source Zone	-76.6376	17.2984	15.00	98.21	17.94
atsz-81b	Atlantic Source Zone	-76.5726	17.7278	15.00	98.21	5.00
atsz-82a	Atlantic Source Zone	-75.7299	19.0217	15.00	260.15	17.94
atsz-82b	Atlantic Source Zone	-75.6516	18.5942	15.00	260.15	5.00
atsz-83a	Atlantic Source Zone	-74.8351	19.2911	15.00	260.83	17.94
atsz-83b	Atlantic Source Zone	-74.7621	18.8628	15.00	260.83	5.00
atsz-84a	Atlantic Source Zone	-73.6639	19.2991	15.00	274.84	17.94
atsz-84b	Atlantic Source Zone	-73.7026	18.8668	15.00	274.84	5.00
atsz-85a	Atlantic Source Zone	-72.8198	19.2019	15.00	270.60	17.94
atsz-85b	Atlantic Source Zone	-72.8246	18.7681	15.00	270.60	5.00
atsz-86a	Atlantic Source Zone	-71.9143	19.1477	15.00	269.06	17.94
atsz-86b	Atlantic Source Zone	-71.9068	18.7139	15.00	269.06	5.00
atsz-87a	Atlantic Source Zone	-70.4738	18.8821	15.00	304.49	17.94
atsz-87b	Atlantic Source Zone	-70.7329	18.5245	15.00	304.49	5.00
atsz-88a	Atlantic Source Zone	-69.7710	18.3902	15.00	308.94	17.94
atsz-88b	Atlantic Source Zone	-70.0547	18.0504	15.00	308.44	5.00
atsz-89a	Atlantic Source Zone	-69.2635	18.2099	15.00	283.88	17.94
atsz-89b	Atlantic Source Zone	-69.3728	17.7887	15.00	283.88	5.00
atsz-90a	Atlantic Source Zone	-68.5059	18.1443	15.00	272.93	17.94
atsz-90b	Atlantic Source Zone	-68.5284	17.7110	15.00	272.93	5.00
atsz-91a	Atlantic Source Zone	-67.6428	18.1438	15.00	267.84	17.94
atsz-91b	Atlantic Source Zone	-67.6256	17.7103	15.00	267.84	5.00
atsz-92a	Atlantic Source Zone	-66.8261	18.2536	15.00	262.00	17.94
atsz-92b	Atlantic Source Zone	-66.7627	17.8240	15.00	262.00	5.00

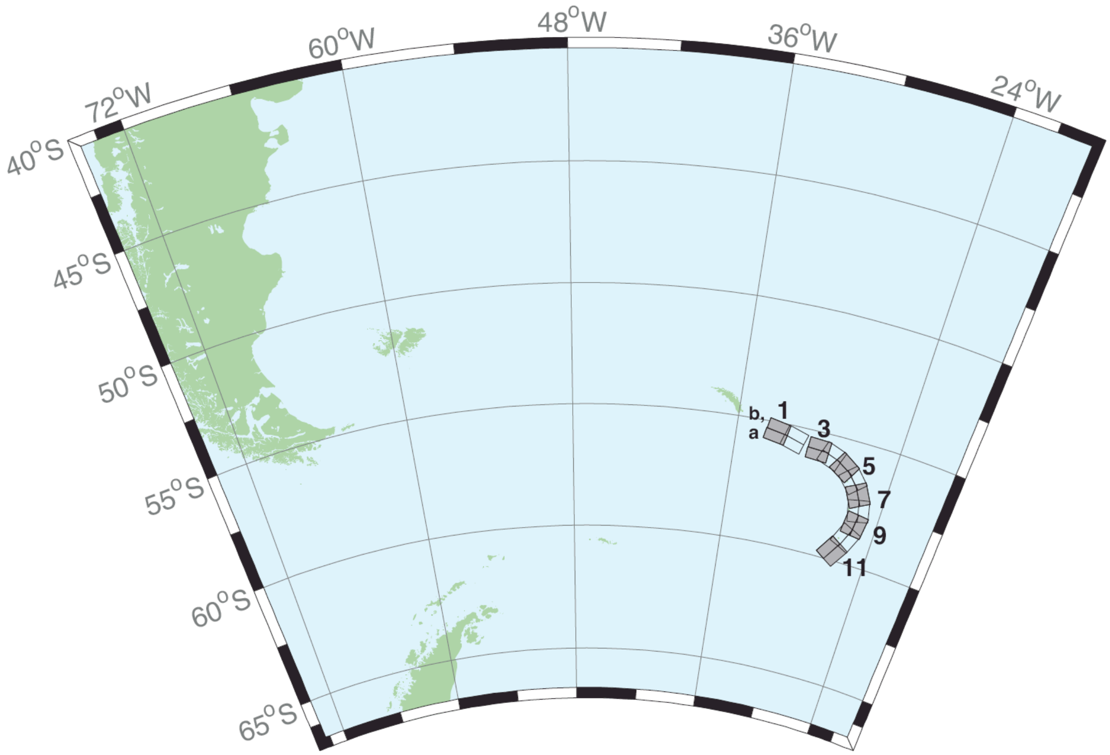

Figure B2. South Sandwich Source Zone unit sources

Table B2. Earthquake parameters for unit sources in South Sandwich source zone.

Unit Source	Description	Lon (°)	Lat (°)	Strike (°)	Dip (°)	Depth (km)
sssz-01a	South Sandwich Source Zone	-32.3713	-55.4655	28.528	104.6905	17.511
sssz-01b	South Sandwich Source Zone	-32.1953	-55.0832	9.957	104.6905	8.866
sssz-01z	South Sandwich Source Zone	-32.5091	-55.7624	46.989	104.6905	41.391
sssz-2a	South Sandwich Source Zone	-30.8028	-55.6842	28.528	102.4495	17.511
sssz-02b	South Sandwich Source Zone	-30.6524	-55.2982	9.957	102.4495	8.866
sssz-02z	South Sandwich Source Zone	-30.9207	-55.9839	46.989	102.4495	41.391
sssz-03a	South Sandwich Source Zone	-29.0824	-55.8403	28.528	95.5322	17.511
sssz-03b	South Sandwich Source Zone	-29.0149	-55.4469	9.957	95.5322	8.866
sssz-03z	South Sandwich Source Zone	-29.1354	-56.1458	46.989	95.5322	41.391
sssz-04a	South Sandwich Source Zone	-27.8128	-55.9796	28.528	106.1387	17.511
sssz-04b	South Sandwich Source Zone	-27.6174	-55.5999	9.957	106.1387	8.866
sssz-04z	South Sandwich Source Zone	-27.9659	-56.2744	46.989	106.1387	41.391
sssz-05a	South Sandwich Source Zone	-26.7928	-56.2481	28.528	123.1030	17.511
sssz-05b	South Sandwich Source Zone	-26.4059	-55.9170	9.957	123.1030	8.866
sssz-05z	South Sandwich Source Zone	-27.0955	-56.5052	46.989	123.1030	41.391
sssz-06a	South Sandwich Source Zone	-26.1317	-56.6466	23.277	145.6243	16.110
sssz-06b	South Sandwich Source Zone	-25.5131	-56.4133	9.090	145.6243	8.228

sssz-06z	South Sandwich Source Zone	-26.5920	-56.8194	47.151	145.6243	35.869
sssz-07a	South Sandwich Source Zone	-25.6787	-57.2162	21.210	162.9420	14.235
sssz-07b	South Sandwich Source Zone	-24.9394	-57.0932	7.596	162.9420	7.626
sssz-07z	South Sandwich Source Zone	-26.2493	-57.3109	44.159	162.9420	32.324
sssz-08a	South Sandwich Source Zone	-25.5161	-57.8712	20.328	178.2111	15.908
sssz-08b	South Sandwich Source Zone	-24.7233	-57.8580	8.449	178.2111	8.562
sssz-08z	South Sandwich Source Zone	-26.1280	-57.8813	43.649	178.2111	33.278
sssz-09a	South Sandwich Source Zone	-25.6657	-58.5053	25.759	195.3813	15.715
sssz-09b	South Sandwich Source Zone	-24.9168	-58.6128	8.254	195.3813	8.537
sssz-09z	South Sandwich Source Zone	-26.1799	-58.4313	51.691	195.3813	37.444
sssz-10a	South Sandwich Source Zone	-26.1563	-59.1048	32.821	212.5129	15.649
sssz-10b	South Sandwich Source Zone	-25.5335	-59.3080	10.449	212.5129	6.581
sssz-10z	South Sandwich Source Zone	-26.5817	-58.9653	54.773	212.5129	42.750
sssz-11a	South Sandwich Source Zone	-27.0794	-59.6799	33.667	224.2397	15.746
sssz-11b	South Sandwich Source Zone	-26.5460	-59.9412	11.325	224.2397	5.927
sssz-11z	South Sandwich Source Zone	-27.4245	-59.5098	57.190	224.2397	43.464

Appendix C. Short-term Inundation Forecast of Tsunami (SIFT) testing results

Jean Newman, Yong Wei

Forecast models are tested with synthetic tsunami events covering a range of tsunami source locations. Testing is also done with selected historical tsunami events when available.

The purpose of forecast model testing is three-fold. The first objective is to assure that the results obtained with NOAA's tsunami forecast system, which has been released to the Tsunami Warning Centers for operational use, are identical to those obtained by the researcher during the development of the forecast model. The second objective is to test the forecast model for consistency, accuracy, time efficiency, and quality of results over a range of possible tsunami locations and magnitudes. The third objective is to identify bugs and issues in need of resolution by the researcher who developed the Forecast Model or by the forecast software development team before the next version release to NOAA's two Tsunami Warning Centers.

Local hardware and software applications, and tools familiar to the researcher(s), are used to run the Method of Splitting Tsunamis (MOST) model during the forecast model development. The test results presented in this report lend confidence that the model performs as developed and produces the same results when initiated within the forecast application in an operational setting as those produced by the researcher during the forecast model development. The test results assure those who rely on the Atlantic City tsunami forecast model that consistent results are produced irrespective of system.

C.1 Testing Procedure

The general procedure for forecast model testing is to run a set of synthetic tsunami scenarios through the forecast system application and compare the results with those obtained by the researcher during the forecast model development and presented in the Tsunami Forecast Model Report. Specific steps taken to test the model include:

1. Identification of testing scenarios, including the standard set of synthetic events and customized synthetic scenarios that may have been used by the researcher(s) in developing the forecast model.
2. Creation of new events to represent customized synthetic scenarios used by the researcher(s) in developing the forecast model, if any.
3. Submission of test model runs with the forecast system, and export of the results from A, B, and C grids, along with time series.
4. Recording applicable metadata, including the specific version of the forecast system used for testing.
5. Examination of forecast model results from the forecast system for instabilities in both time series and plot results.
6. Comparison of forecast model results obtained through the forecast system with those obtained during the forecast model development.
7. Summarization of results with specific mention of quality, consistency, and time efficiency.
8. Reporting of issues identified to modeler and forecast software development team.
9. Retesting the forecast models in the forecast system when reported issues have been addressed or explained.

Synthetic model runs were tested on a DELL PowerEdge R510 computer equipped with two Xeon E5670 processors at 2.93 Ghz, each with 12 MBytes of cache and 32GB memory. The processors are hex core and support hyperthreading, resulting in the computer performing as a 24 processor core machine. Additionally, the testing computer supports 10 Gigabit Ethernet for fast network connections. This computer configuration is similar or the same as the configurations of the computers installed at the Tsunami Warning Centers so the compute times should only vary slightly.

C.2 Results

The Atlantic City forecast model was tested with SIFT version 3.2 using MOST v2.

The Atlantic City, New Jersey forecast model was tested with three synthetic scenarios. Test results from the forecast system and comparisons with the results obtained during the forecast model development are shown numerically in **Table C1** and graphically in **Figures C1** to **C3**. The results show that the forecast model is stable and robust, with consistent and high quality results across geographically distributed tsunami sources and mega-event tsunami magnitudes.   The model run time (wall clock time) was under 38 minutes for 12 hours of simulation time, and under 13 minutes for 4 hours. This run time is just over the 10 minute run time for 4 hours of simulation time that satisfies time efficiency requirements.

Three synthetic events were run on the Atlantic City forecast model. The modeled scenarios were stable for all cases tested, with no instabilities or ringing (**Figures C4 to C12**). Results show that the largest modeled height was 489.88 cm and originated in the Caribbean (ATSZ 48-57) source. Amplitudes greater than 100 cm were recorded for the two test sources. The smallest signal of 48.92 cm was recorded for the far field South Sandwich Islands (SSSZ 1-10) source. Direct comparisons, of output from the forecast tool with results from available development synthetic events, demonstrated that the wave pattern is similar in shape, pattern and amplitude but does not match by eye. These discrepancies are mainly caused by different propagation databases used to provide the boundary conditions for model runs. Developed in April 2011, the forecast model report shows the Atlantic City model results based on an old tsunami propagation database, while the SIFT testing results in Appendix C reflect the tsunami propagation database that were updated in December of 2011. It is known that the new propagation database will lead to improvement of the model results.

Source Zone	Tsunami Source	α [m]	SIFT Max (cm)	Development Max (cm)	SIFT Min (cm)	Development Min (cm)
ATSZ	A38-A47, B38-B47	25	271.005	241.7	-171.153	-164.2
ATSZ	A48-A57, B48-B57	25	489.880	486.7	-314.680	-322.7
SSSZ	A1-A10, B1-B10	25	48.919	67.9	-47.050	-60.13

Table C1. Table of maximum and minimum amplitudes (cm) at the Atlantic City, New Jersey warning point for synthetic and historical events tested using SIFT 3.2 and obtained during development.

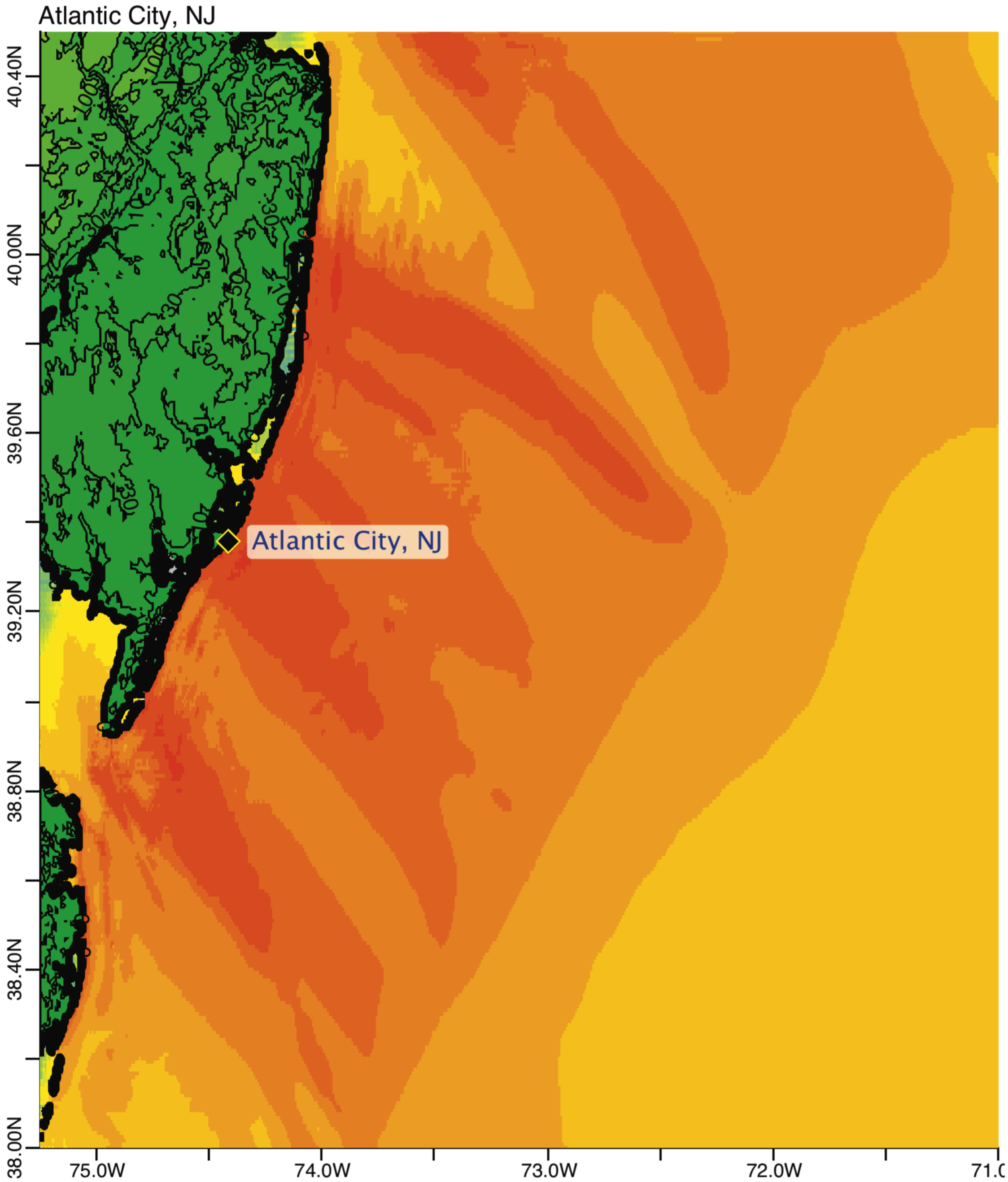

Figure C1. Max computed wave amplitude of A grid, Atlantic City, for synthetic event ATSZ 38-47.

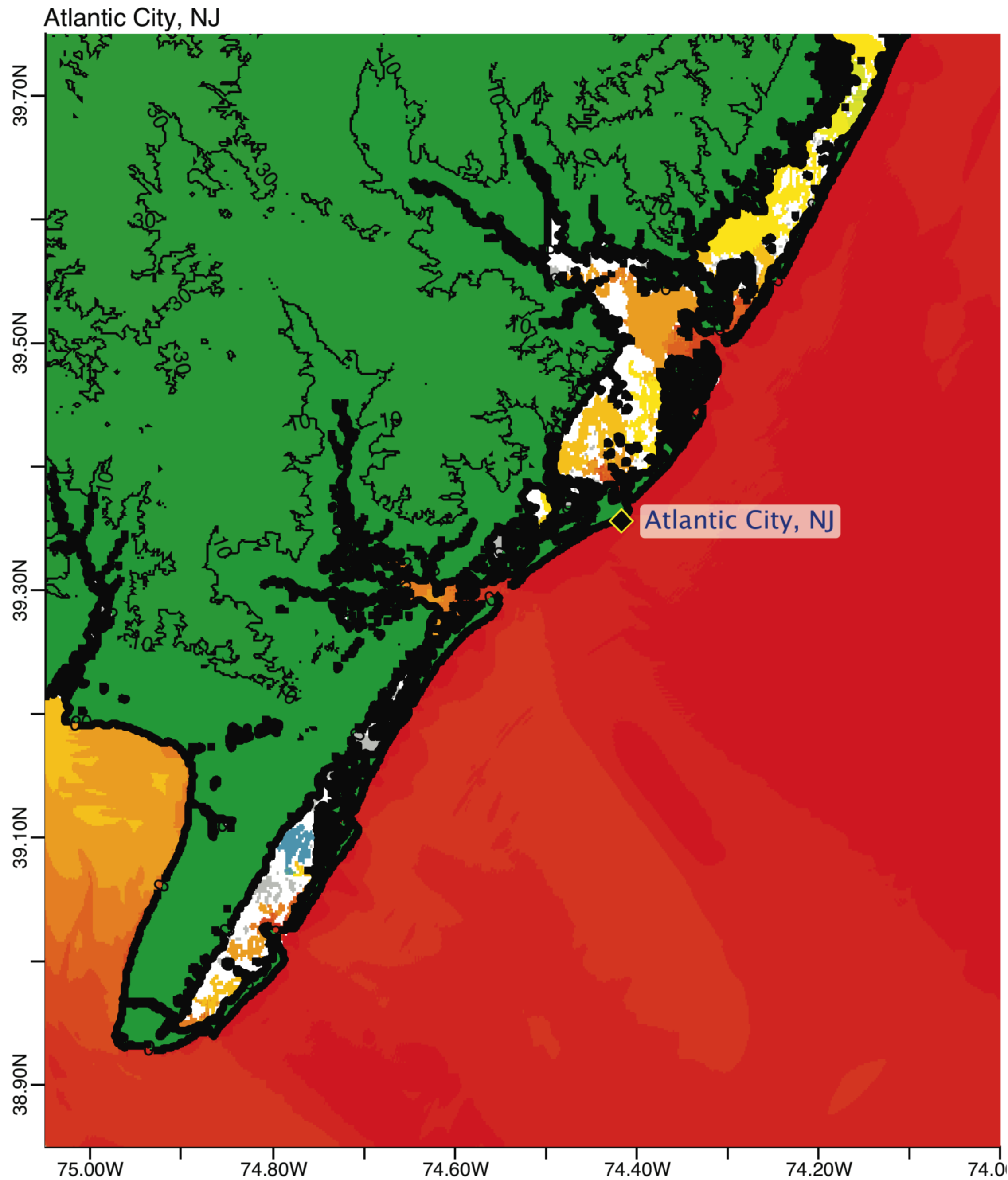

Figure C2. Max computed wave amplitude of B grid, Atlantic City, for synthetic event ATSZ 38-47.

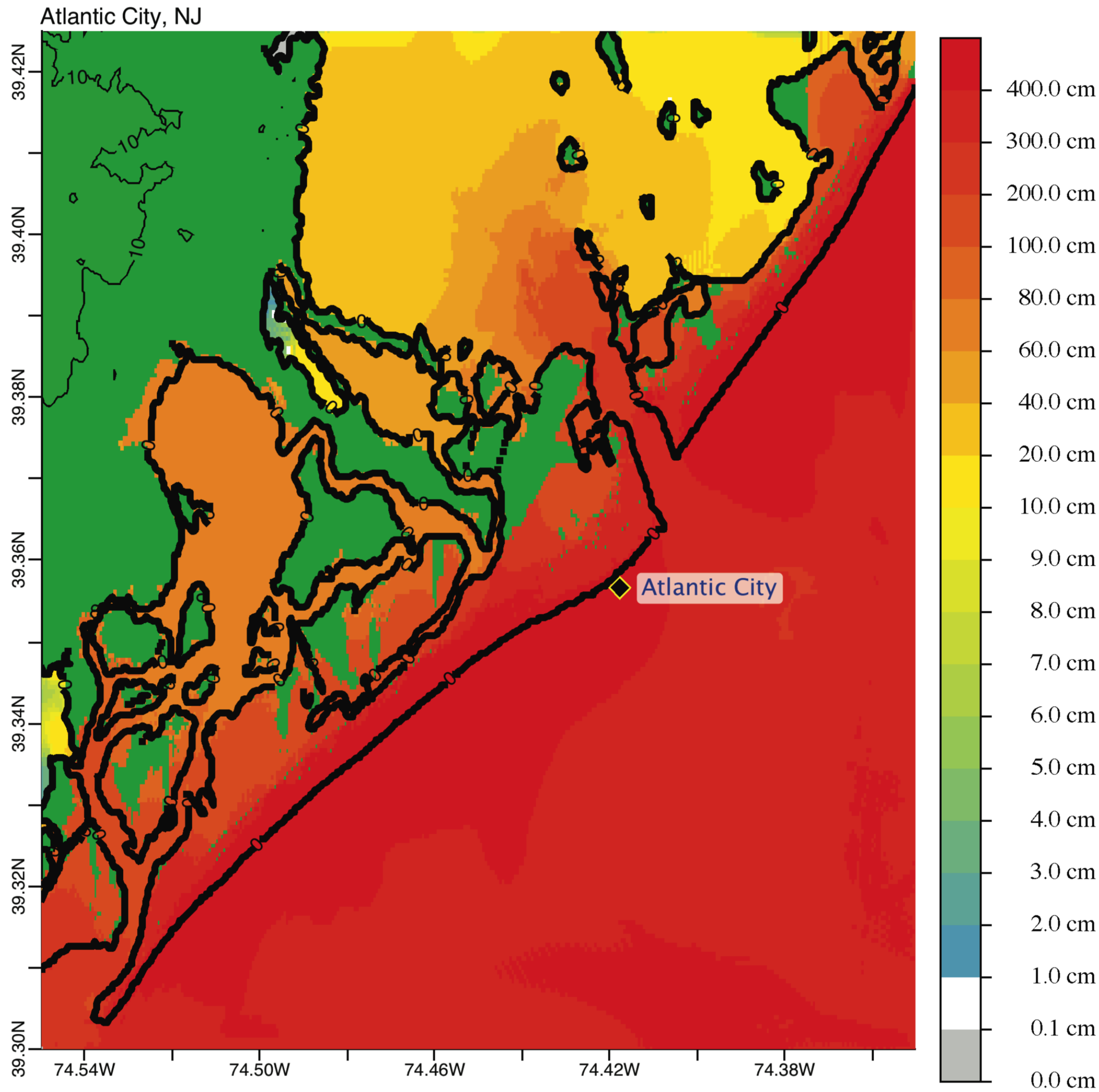

Figure C3. Max computed wave amplitude of C grid, Atlantic City, for synthetic event ATSZ 38-47.

(a)

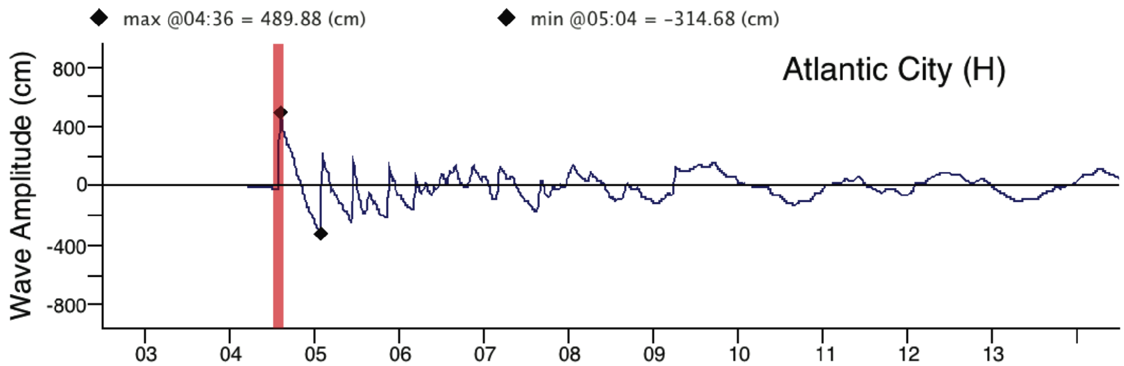

(b)

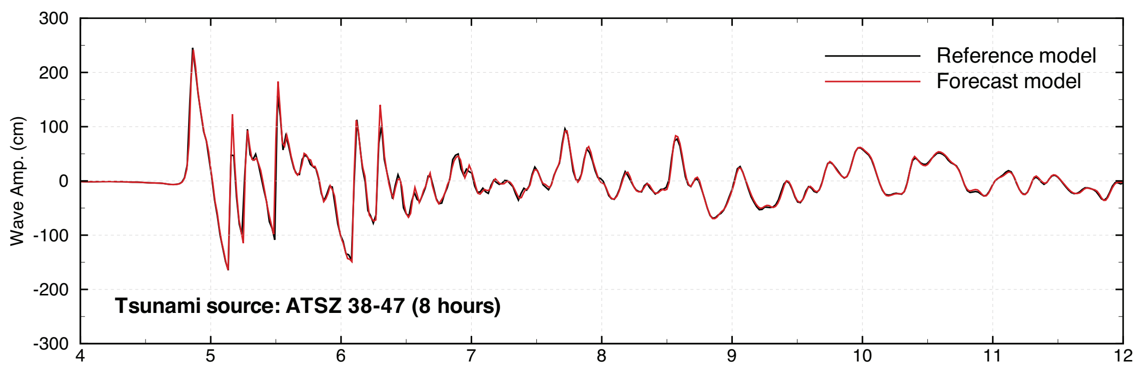

Figure C4. Computed time series at Atlantic City tide gage, for synthetic event ATSZ 38-47: (a) time series computed in the forecast system; (b) time series shown in the forecast model report.

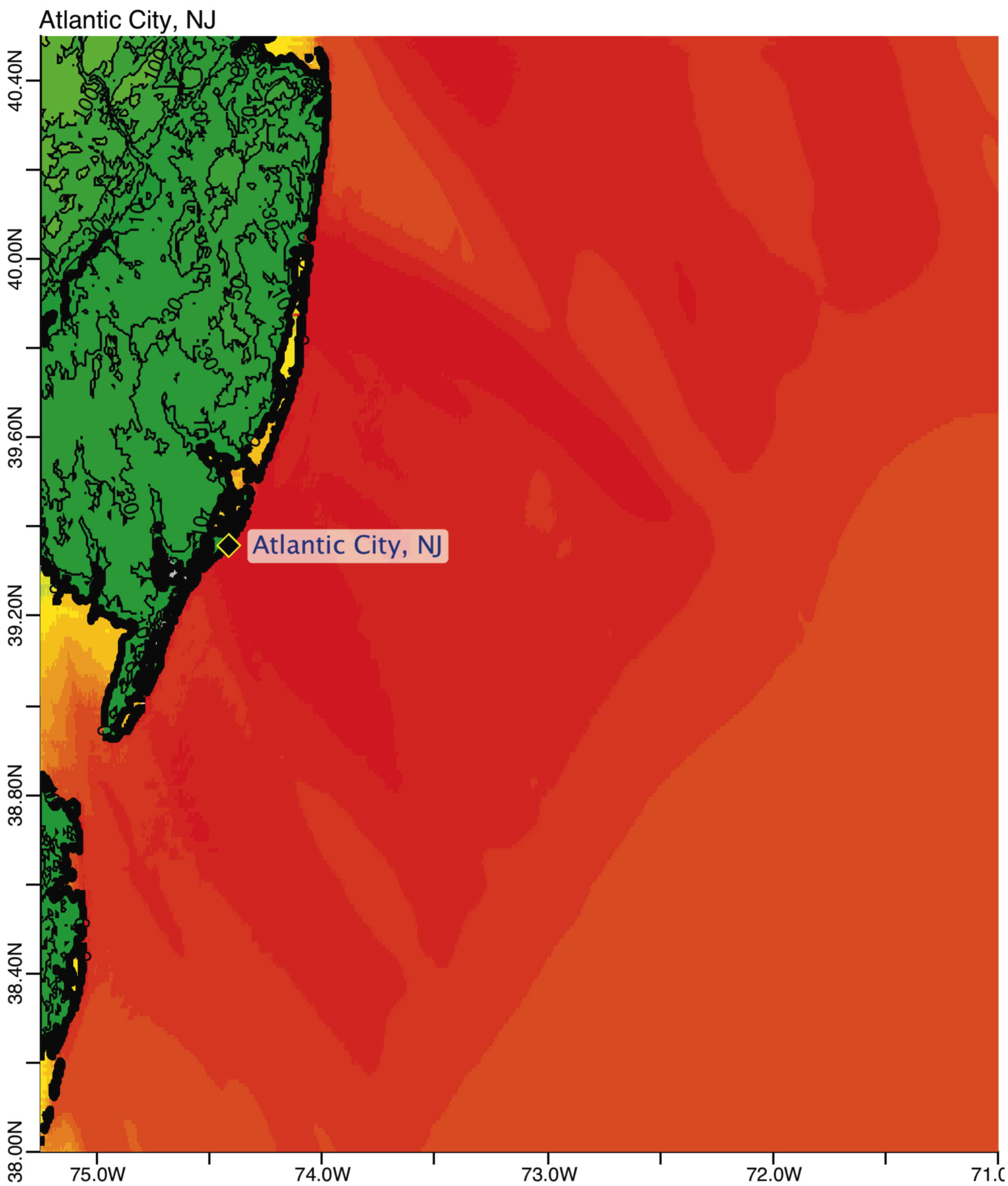

Figure C5. Max computed wave amplitude of A grid, Atlantic City, for synthetic event ATSZ 48-57.

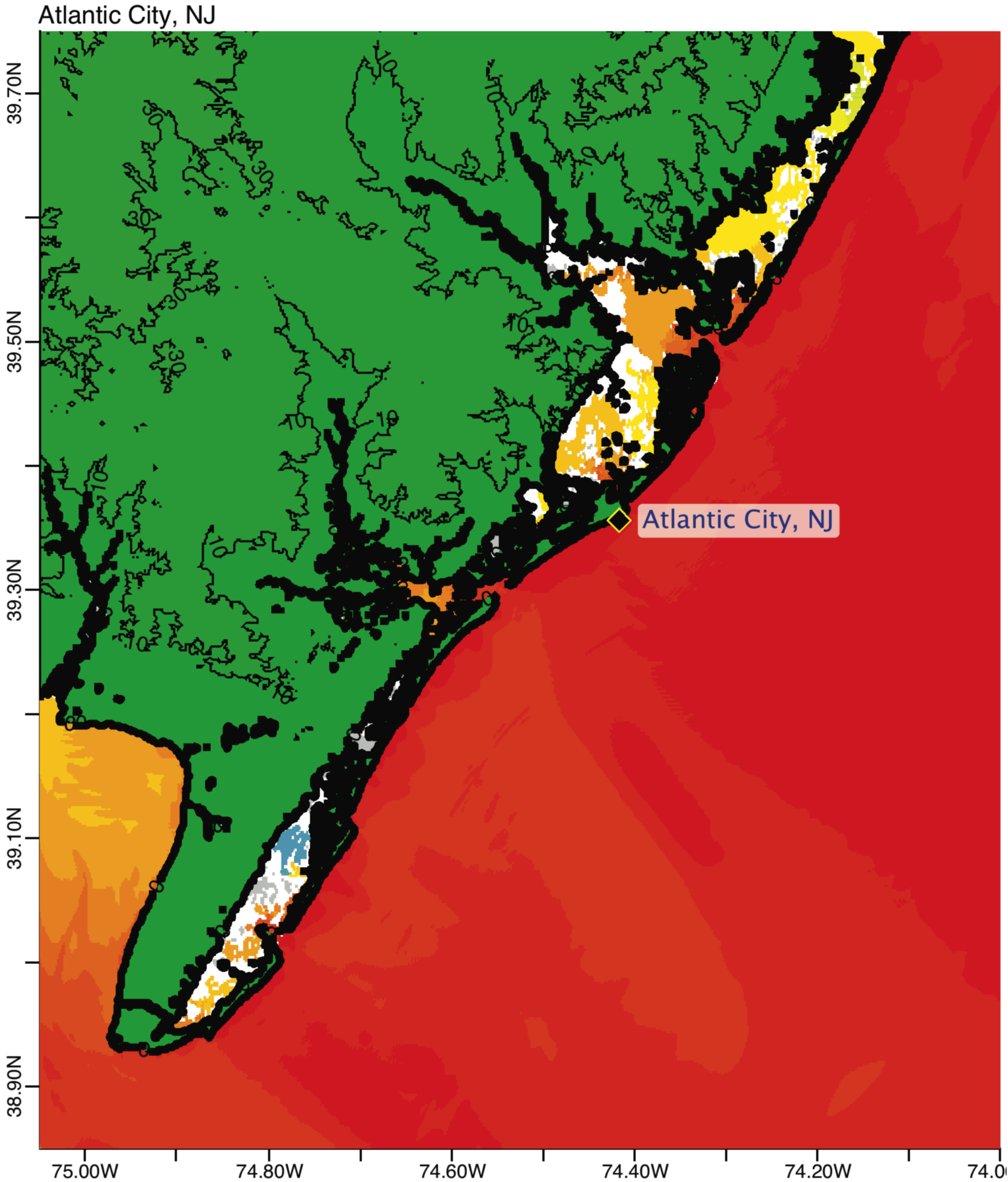

Figure C6. Max computed wave amplitude of B grid, Atlantic City, for synthetic event ATSZ 48-57.

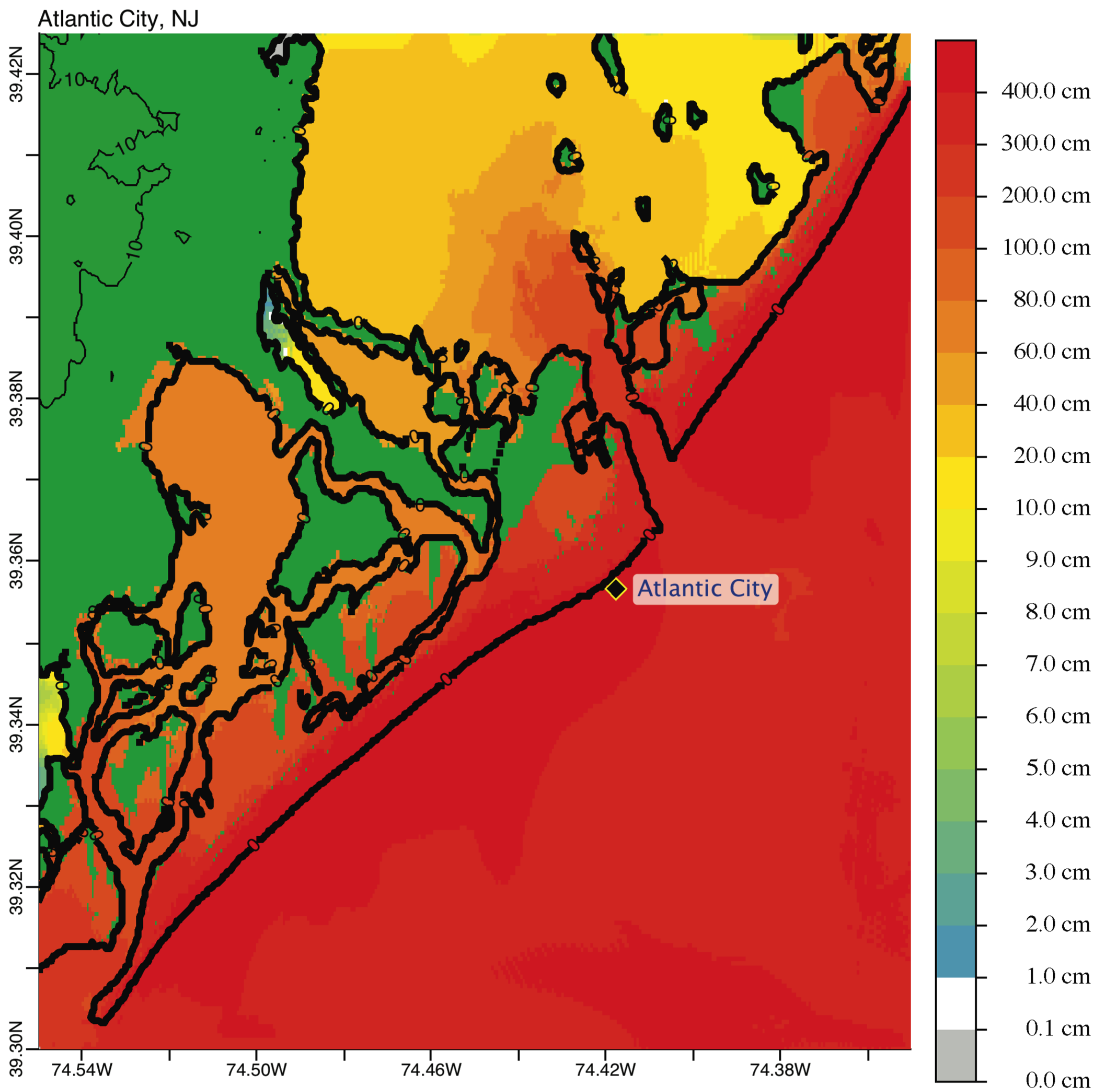

Figure C7. Max computed wave amplitude of C grid, Atlantic City, for synthetic event ATSZ 48-57.

(a)

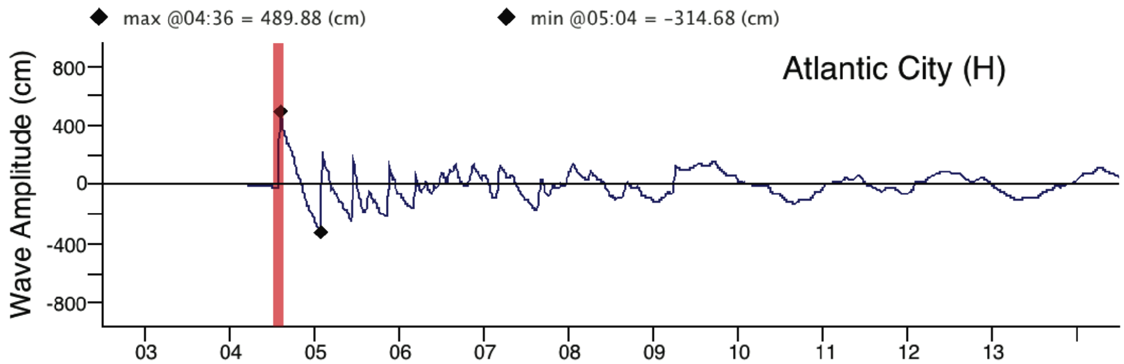

(b)

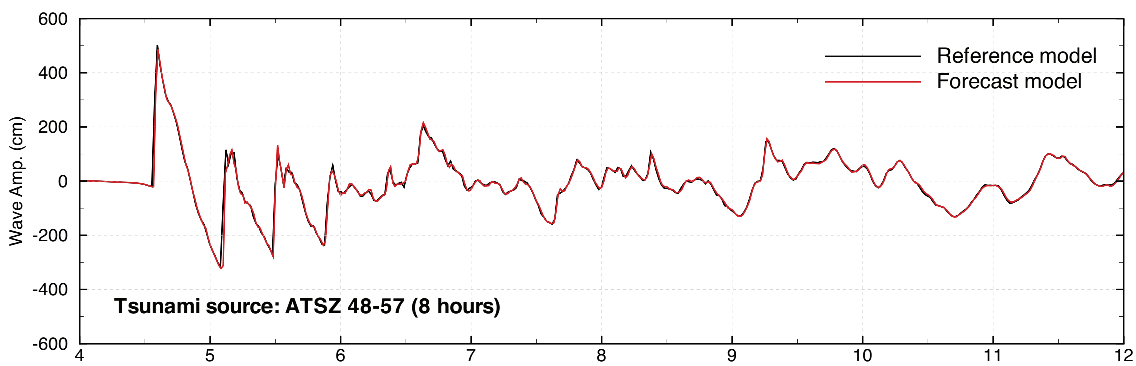

Figure C8. Computed time series at Atlantic City tide gage, for synthetic event ATSZ 48-57: (a) time series computed in the forecast system; (b) time series shown in the forecast model report.

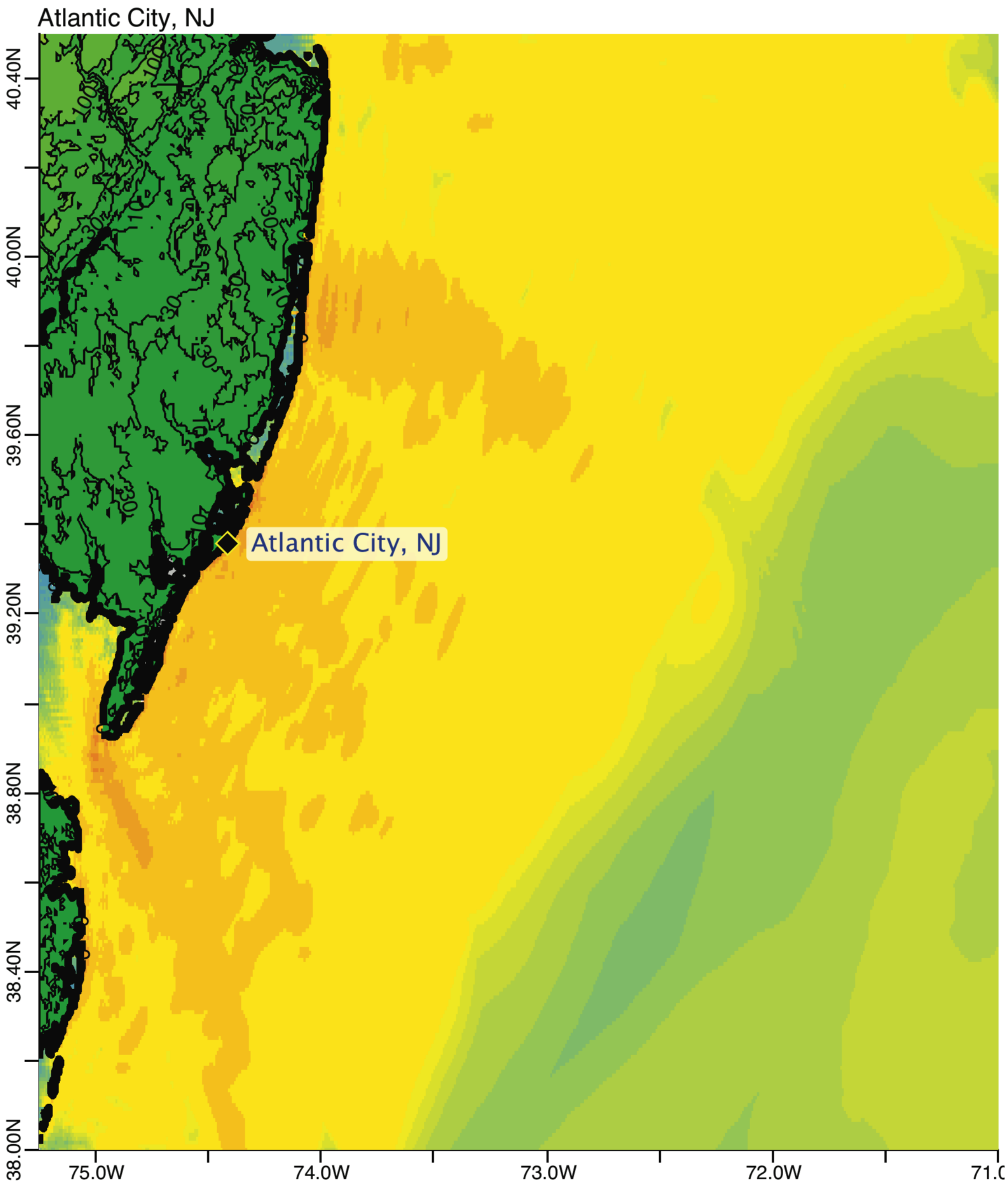

Figure C9. Max computed wave amplitude of A grid, Atlantic City, for synthetic event SSSZ 1-10.

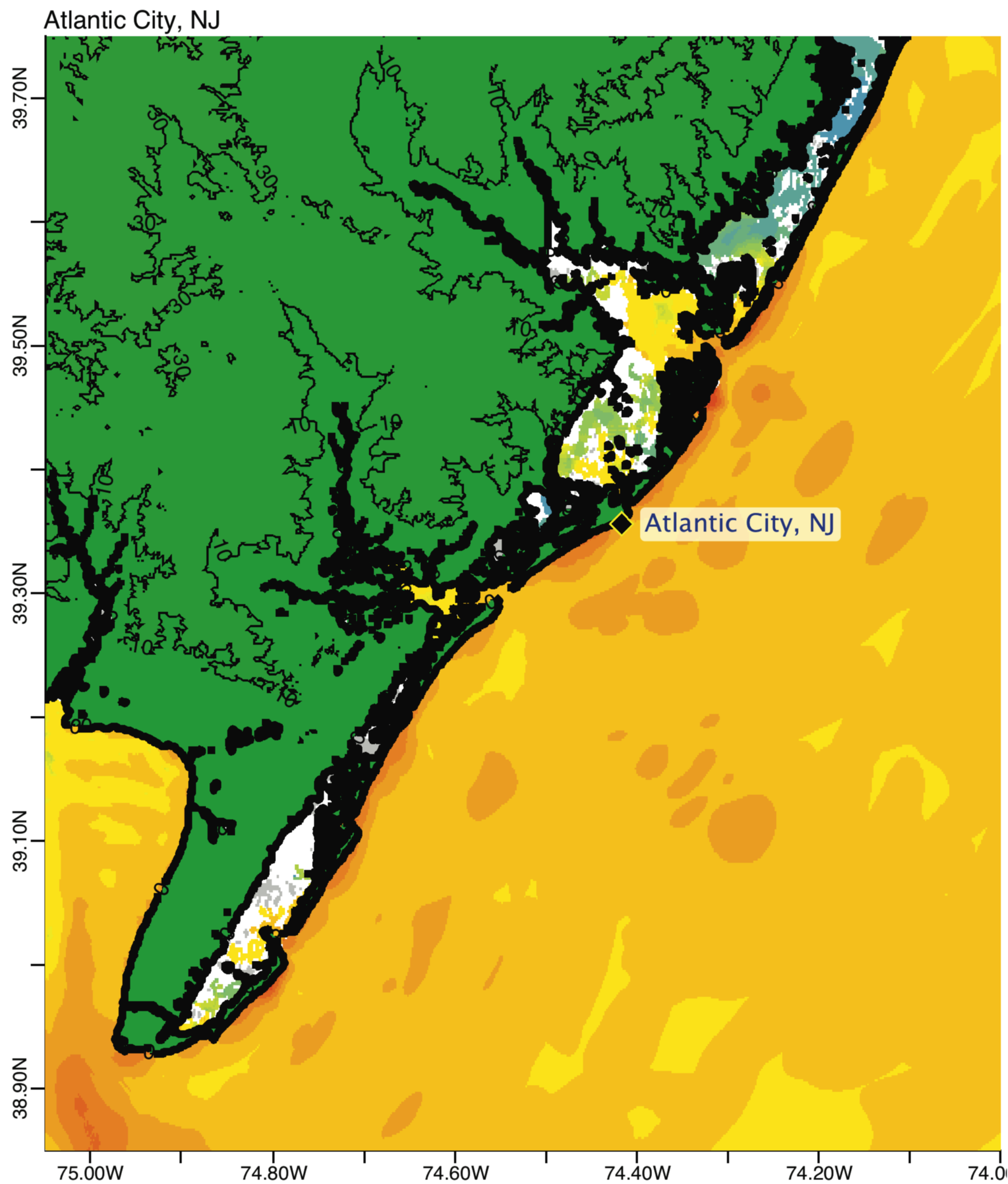

Figure C10. Max computed wave amplitude of B grid, Atlantic City, for synthetic event SSSZ 1-10.

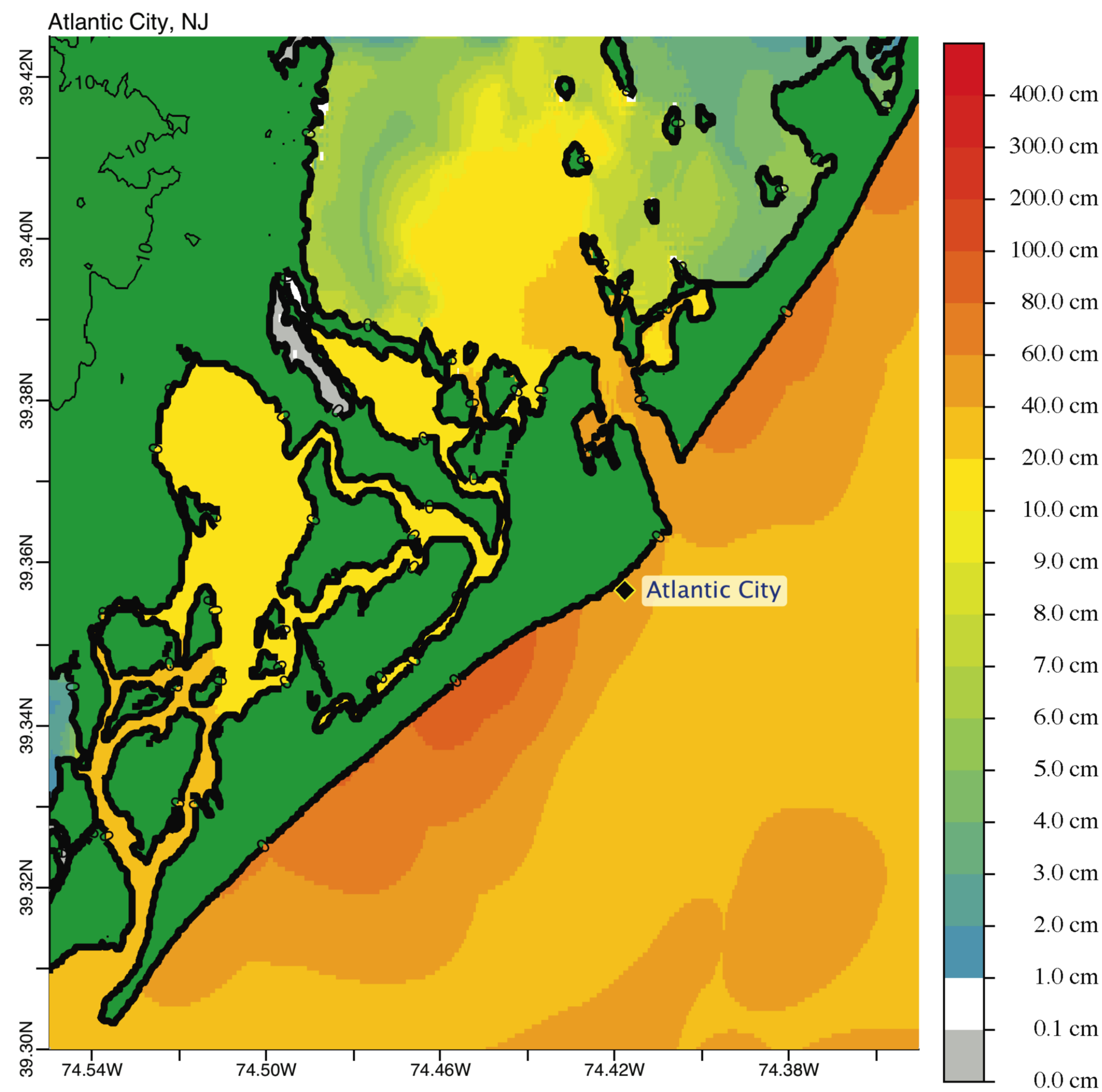

Figure C11. Max computed wave amplitude of C grid, Atlantic City, for synthetic event SSSZ 1-10.

(a)

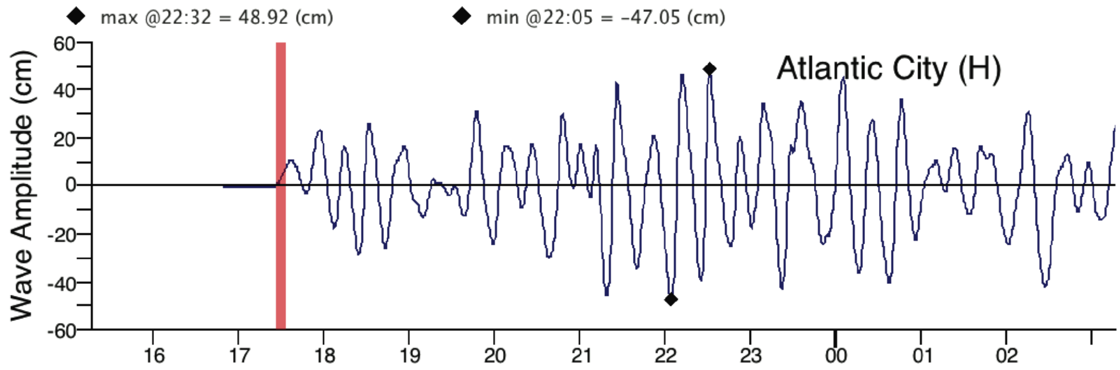

(b)

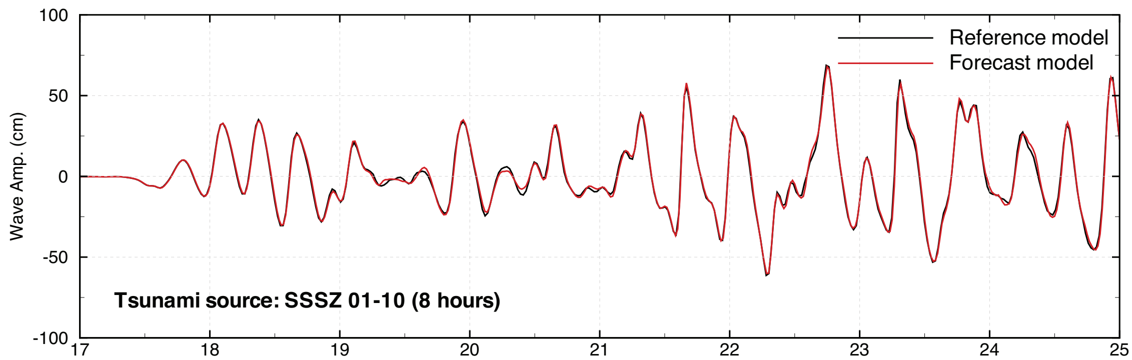

Figure C12. Computed time series at Atlantic City tide gage, for synthetic event SSSZ 1-10: (a) time series computed in the forecast system; (b) time series shown in the forecast model report.

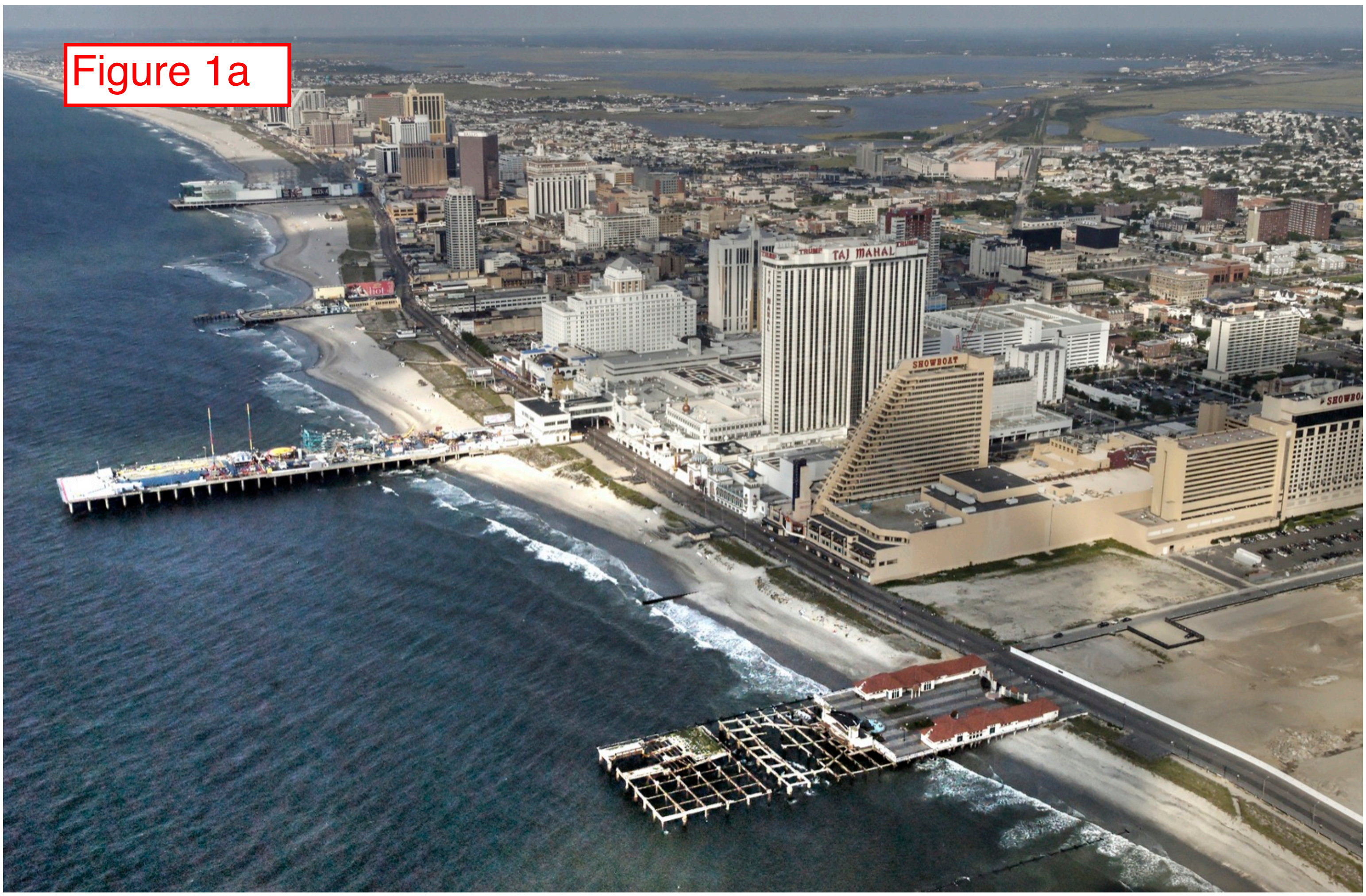

Figure 1a

Figure 1b
© www.AerialPhotosofNJ.com

Figure 2

ABSECON ISLAND
HISTORICAL SHORELINES
VENTNOR, NEW JERSEY


Brigantine
Brigantine Island
Atlantic City
Absecon
Inlet
Detail in (b)
Ventnor
Margate
Absecon Island
Longport
(a)
Absecon
Inlet
Atlantic City
Detail in (c)
(b)
Atlantic CIty
Tide Gage
Taj Mahal
Pier
(c)
(d)

Figure 3

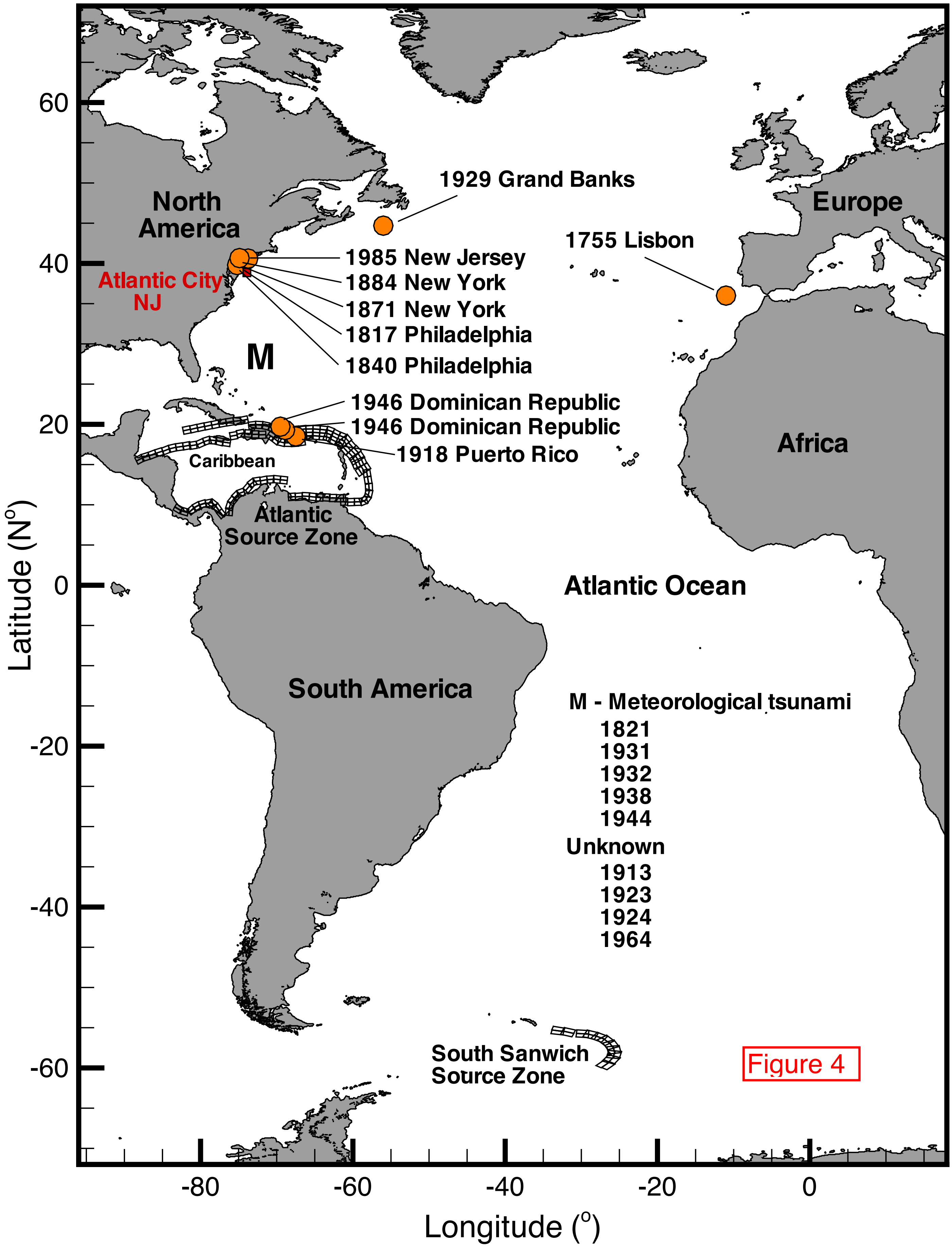

60
40
20
0
-20
-40
-60
-80
-60
-40
-20
0
Latitude (N°)
Longitude (°)
North America
Atlantic City
NJ
M
1929 Grand Banks
1985 New Jersey
1884 New York
1871 New York
1817 Philadelphia
1840 Philadelphia
Europe
1755 Lisbon
1946 Dominican Republic
1946 Dominican Republic
1918 Puerto Rico
Caribbean
Atlantic
Source Zone
Africa
Atlantic Ocean
South America
M - Meteorological tsunami
1821
1931
1932
1938
1944
Unknown
1913
1923
1924
1964
South Sanwich
Source Zone

Figure 4

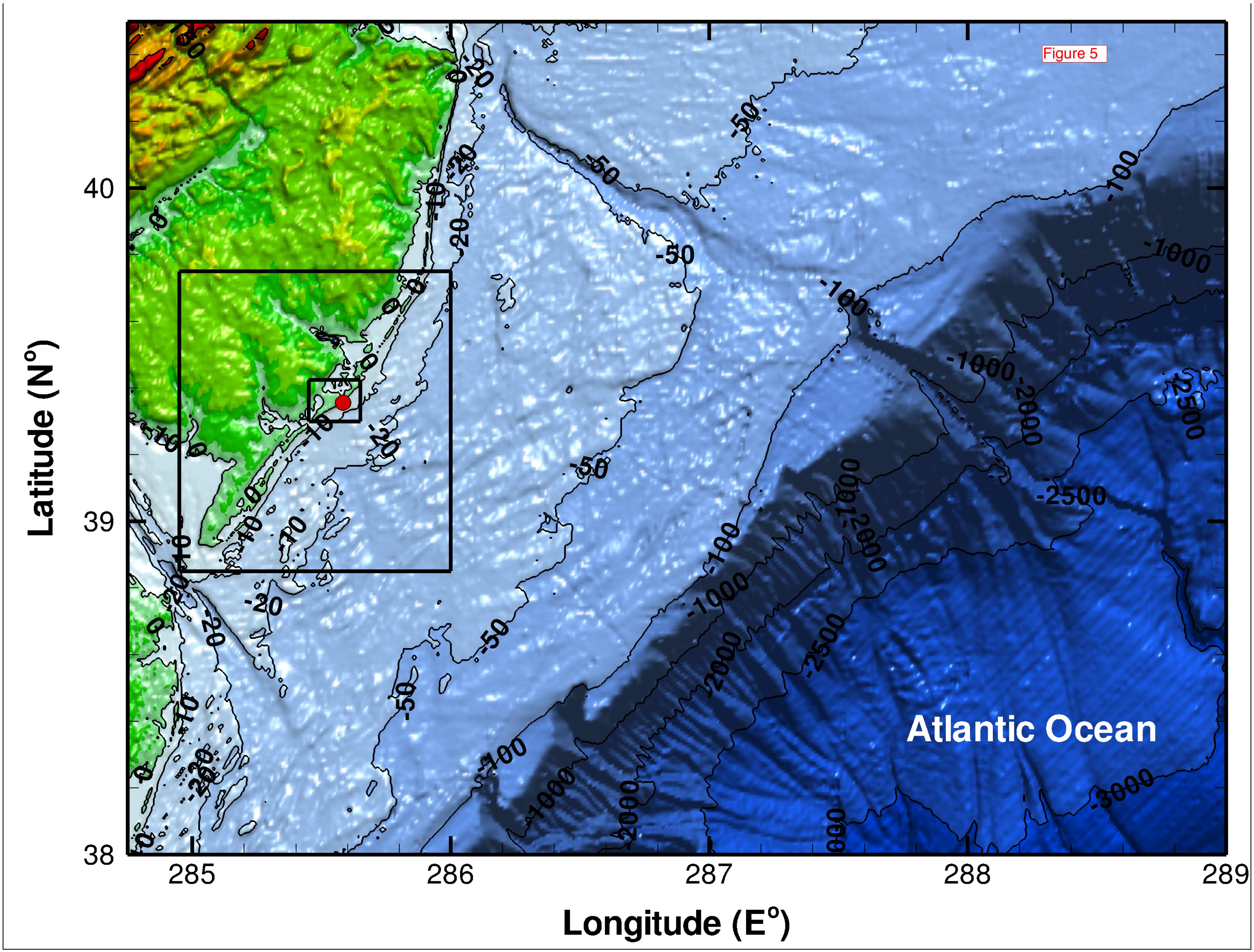

Figure 5
Latitude (N°)
Longitude (E°)
Atlantic Ocean
38
39
40
285
286
287
288
289

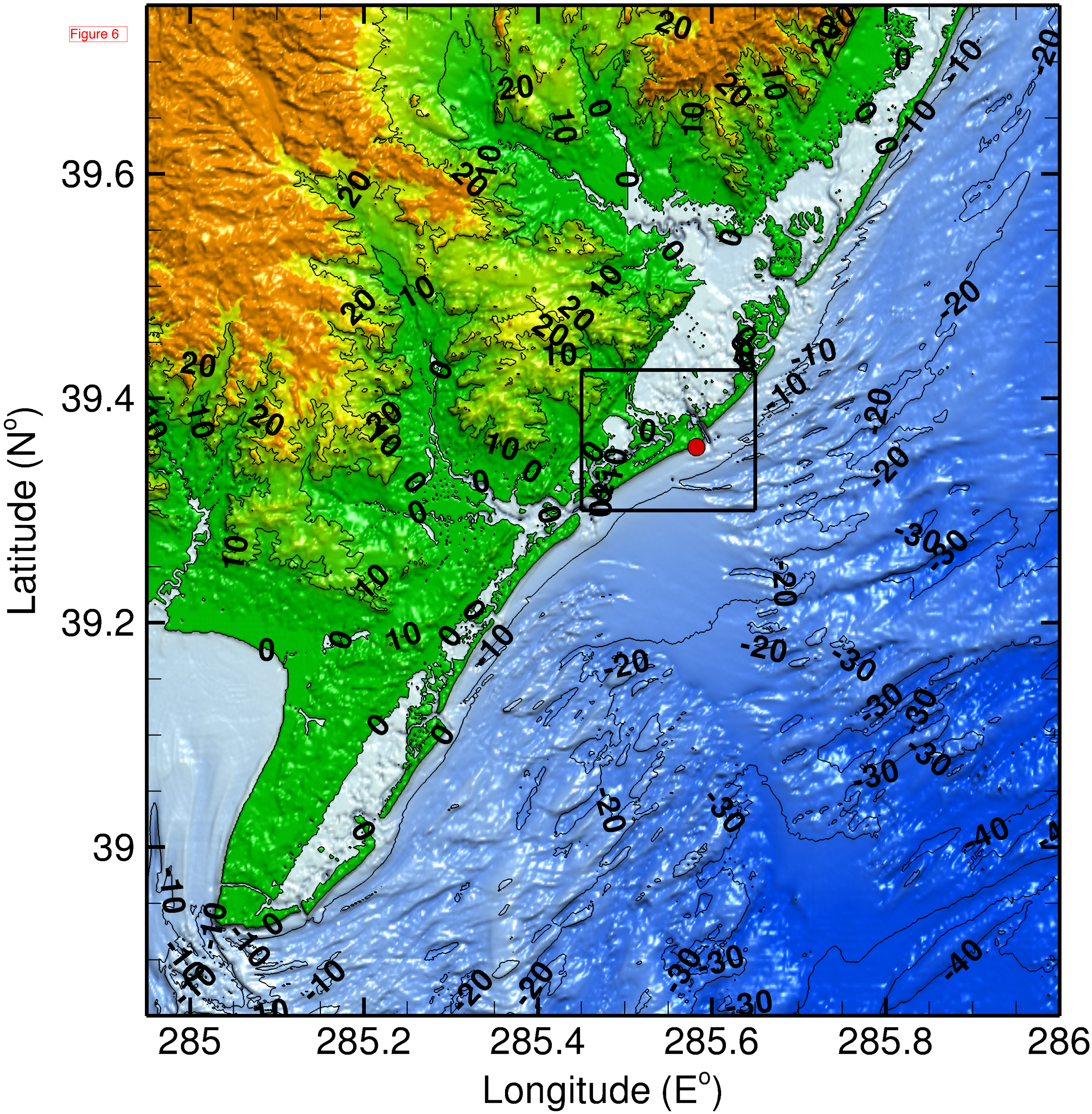

Figure 6
39.6
39.4
39.2
39
Latitude (N°)
285
285.2
285.4
285.6
285.8
286
Longitude (E°)

Figure 7

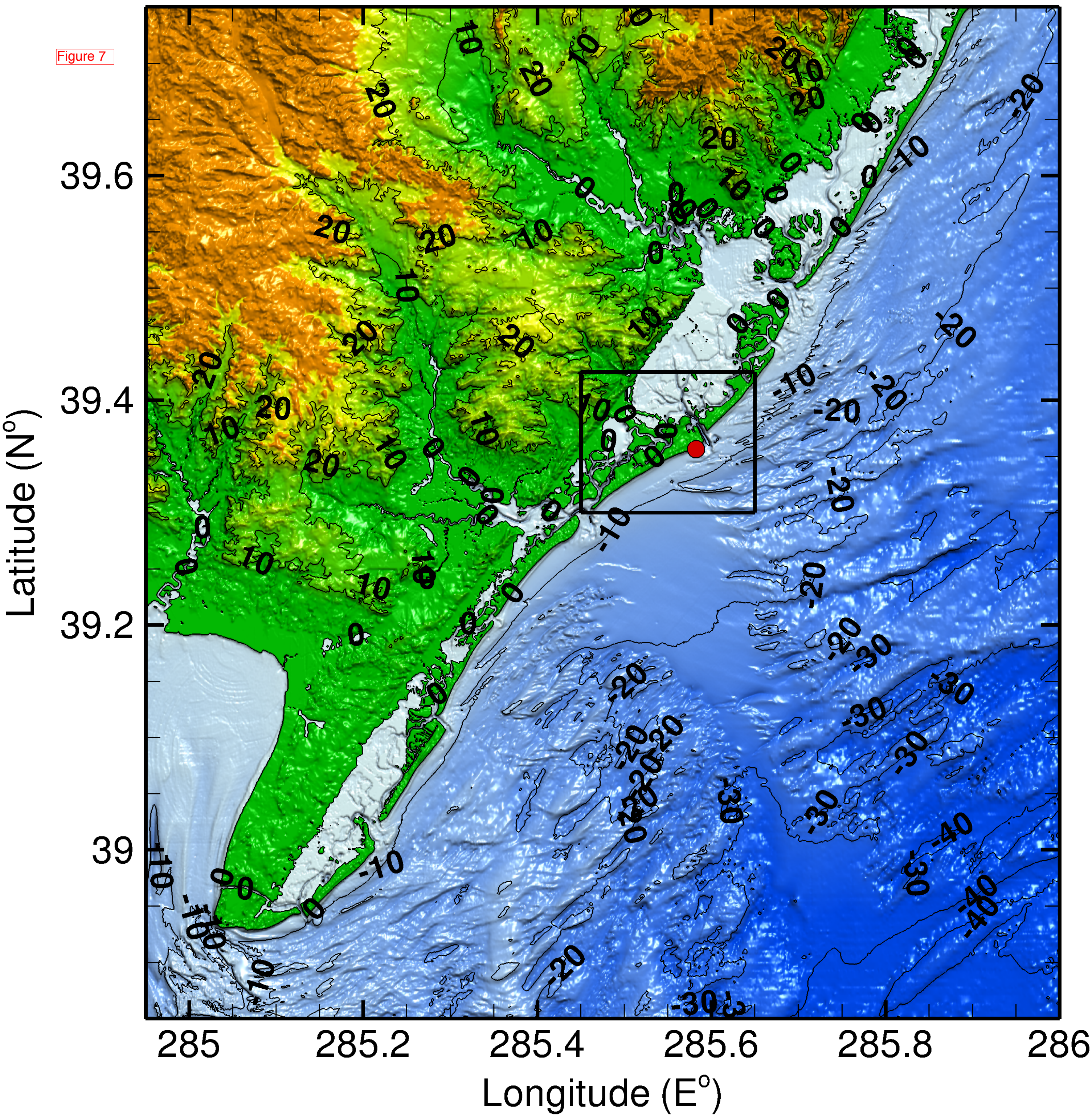
Latitude (N°)
Longitude (E°)
39.6
39.4
39.2
39
285
285.2
285.4
285.6
285.8
286

Figure 8

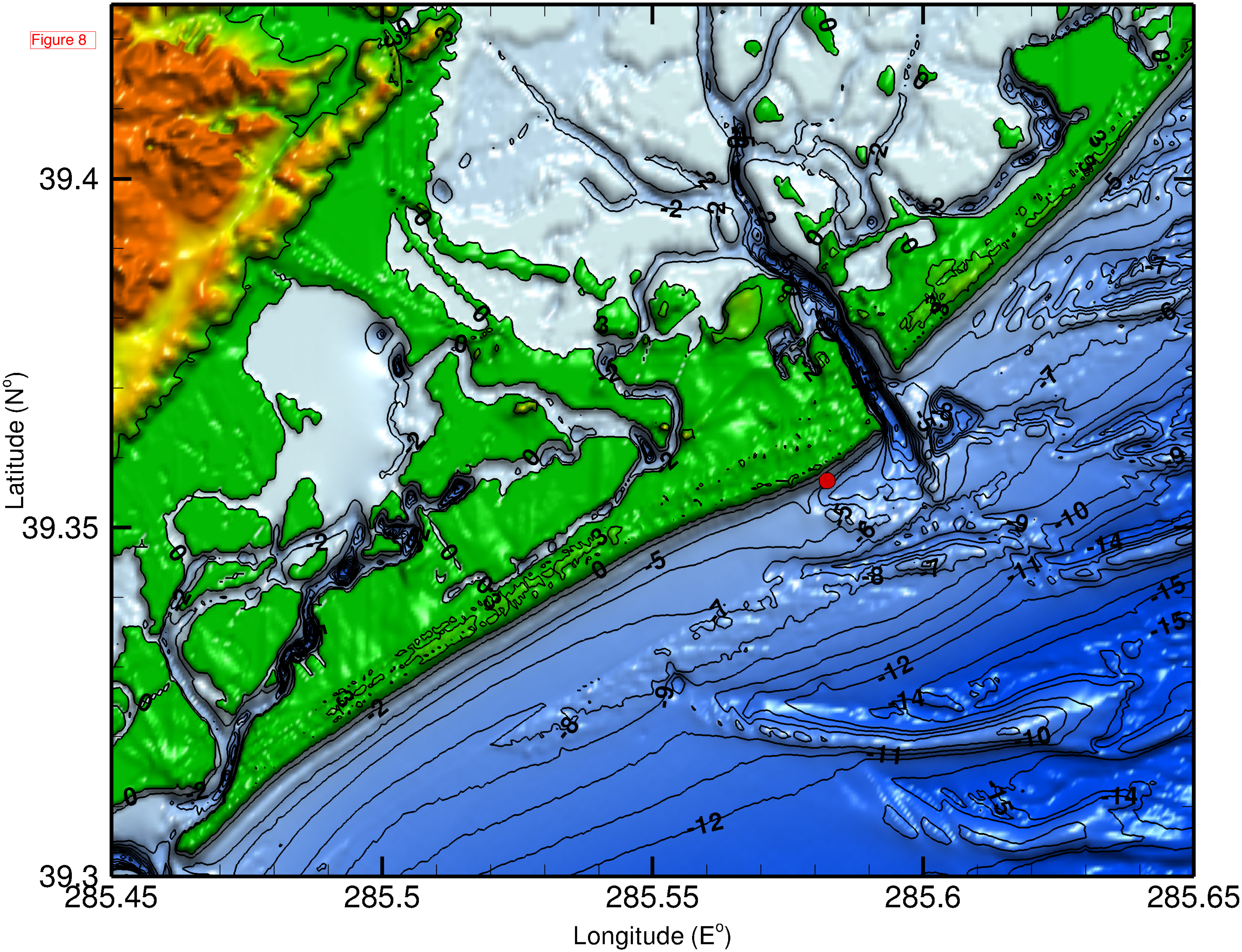
Latitude (N°)
39.4
39.35
39.3
285.45
285.5
285.55
285.6
285.65
Longitude (E°)

Figure 9

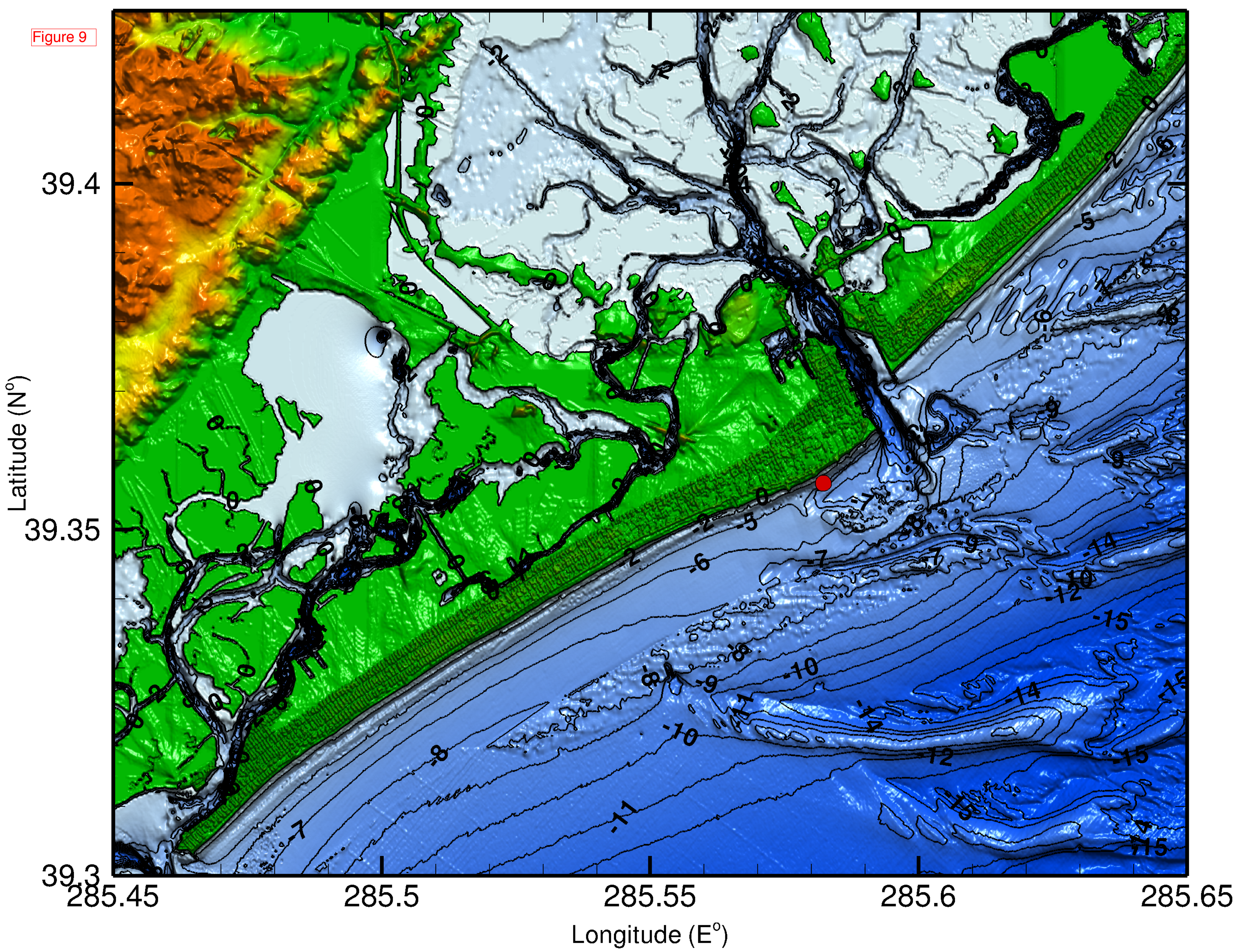
Latitude (N°)
39.4
39.35
39.3
285.45
285.5
285.55
285.6
285.65
Longitude (E°)

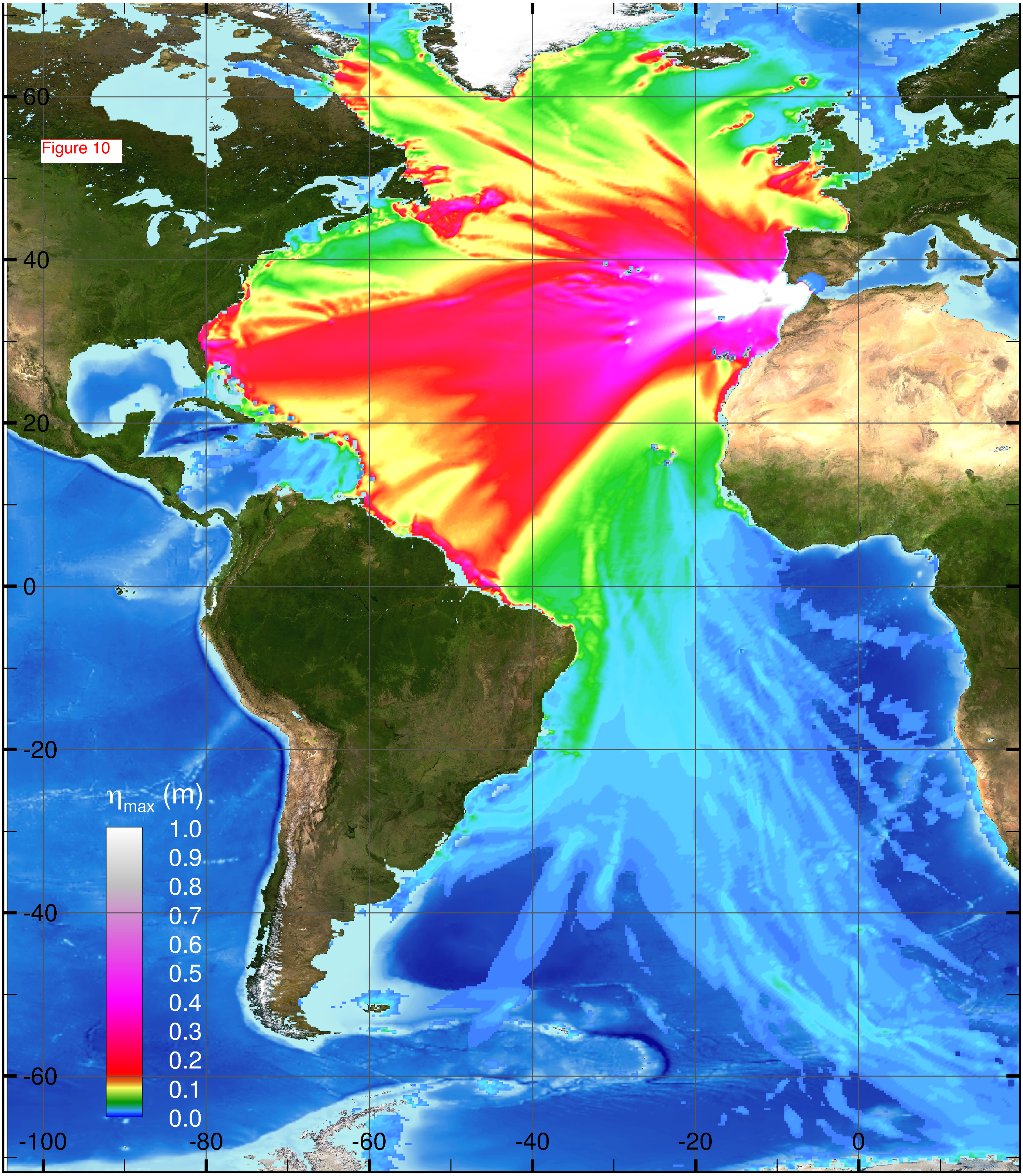
Figure 10
η_{max} (m)
1.0
0.9
0.8
0.7
0.6
0.5
0.4
0.3
0.2
0.1
0.0
60
40
20
0
-20
-40
-60
-100
-80
-60
-40
-20
0

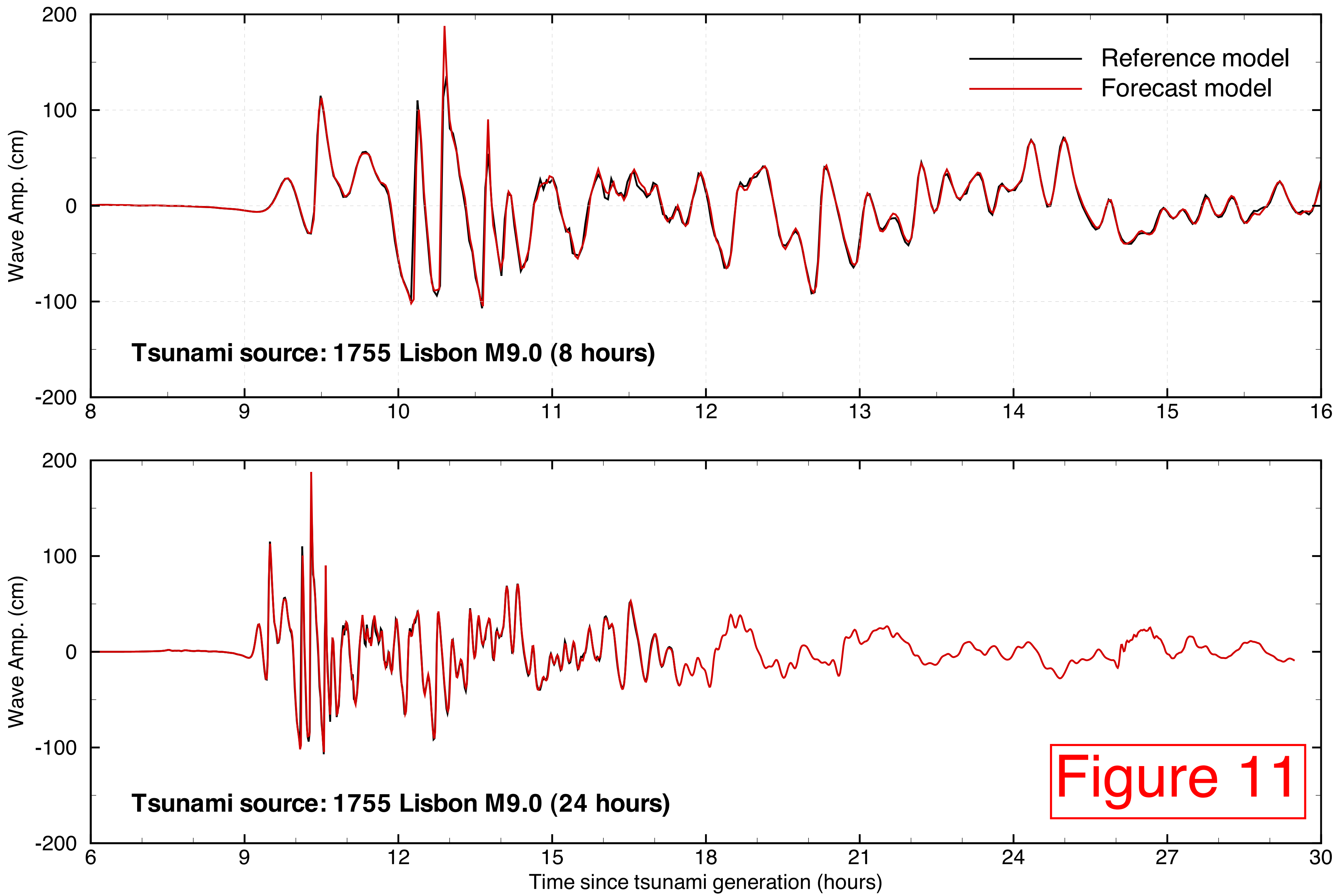

Wave Amp. (cm)
200
100
0
-100
-200
8
9
10
11
12
13
14
15
16
Reference model
Forecast model
Tsunami source: 1755 Lisbon M9.0 (8 hours)
Wave Amp. (cm)
6
9
12
15
18
21
24
27
30
Tsunami source: 1755 Lisbon M9.0 (24 hours)
Time since tsunami generation (hours)

Figure 11

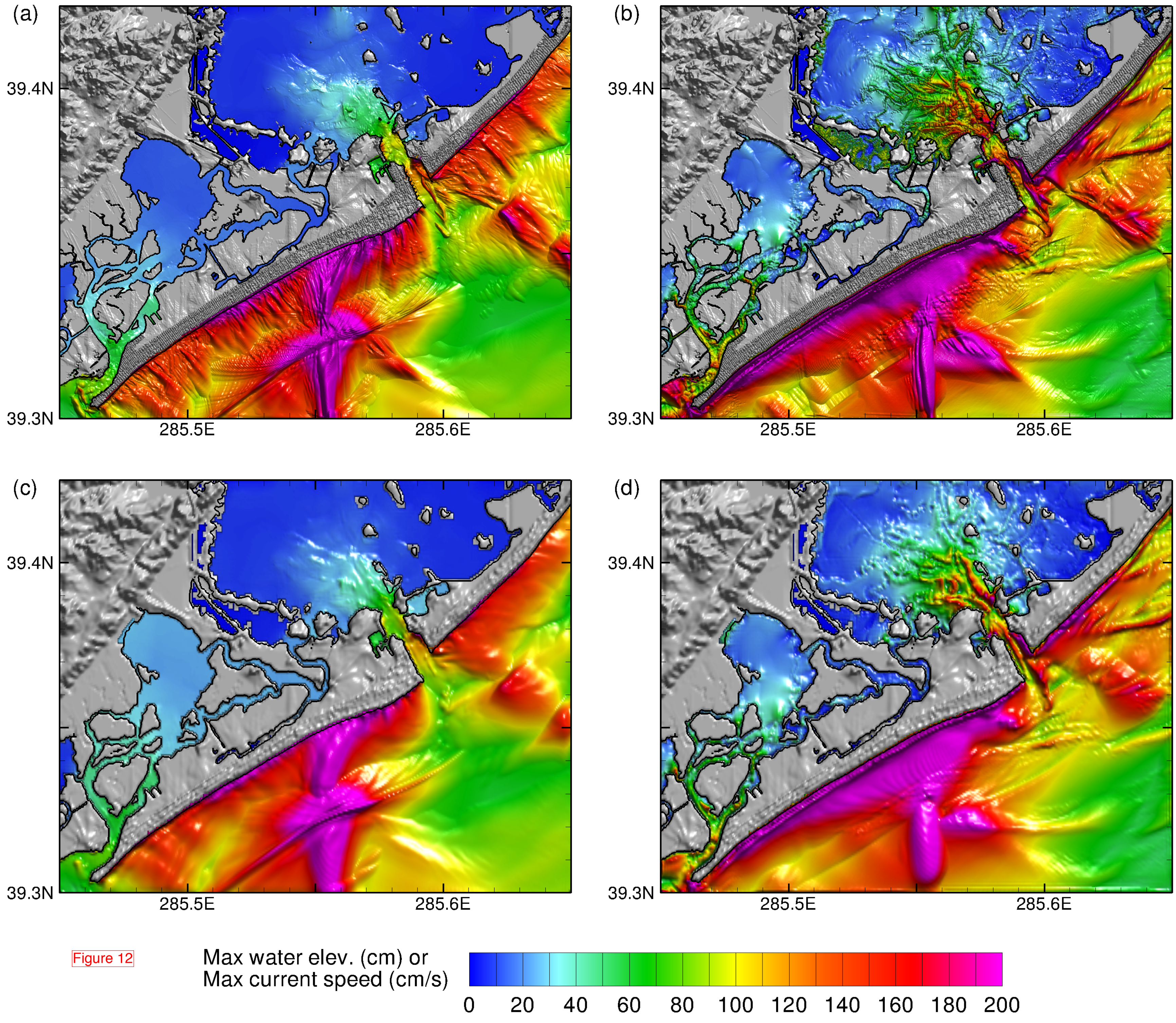

(a)
(b)
(c)
(d)
39.4N
39.3N
285.5E
285.6E
Max water elev. (cm) or
Max current speed (cm/s)
0 20 40 60 80 100 120 140 160 180 200

Figure 12

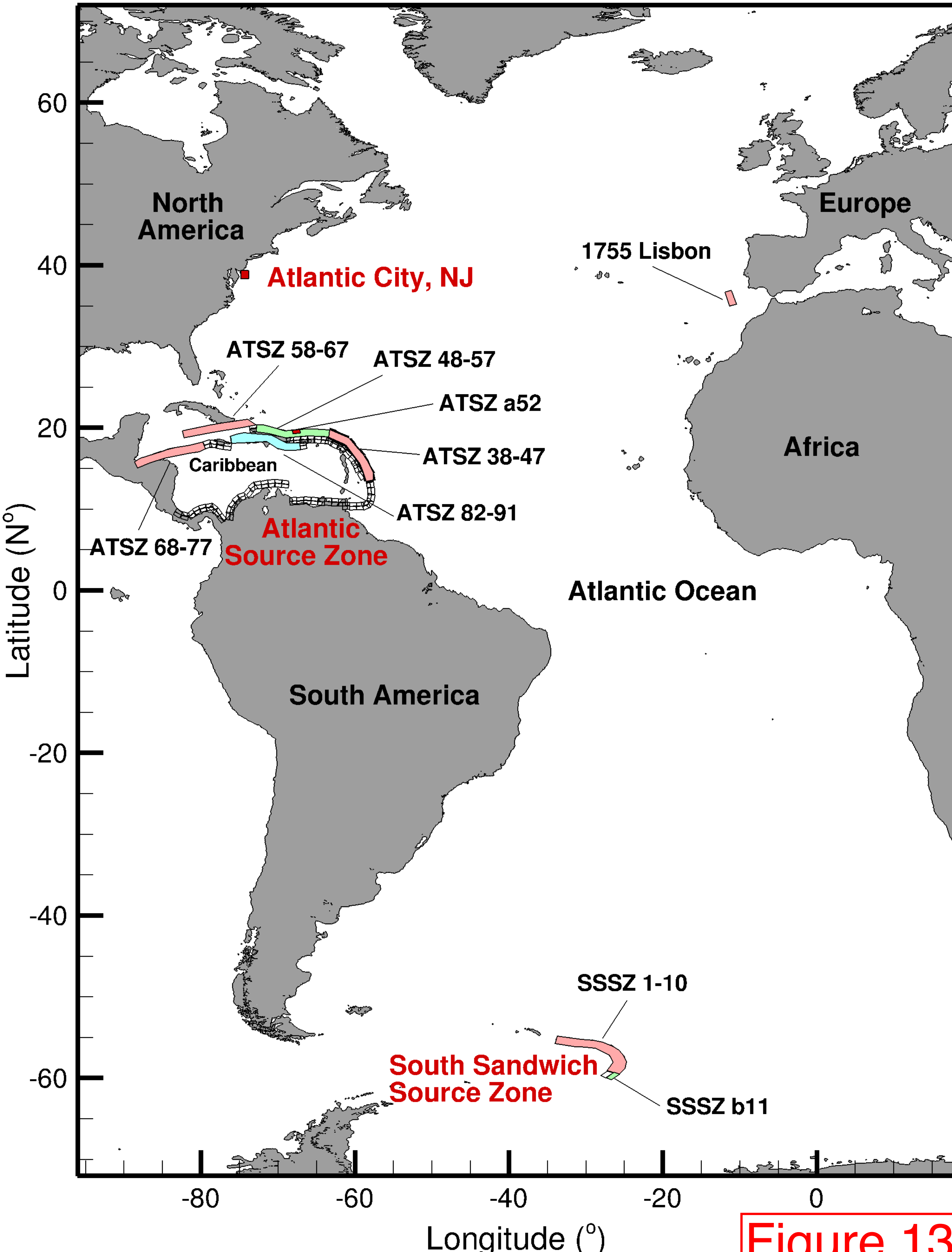
North America
Europe
Atlantic City, NJ
1755 Lisbon
ATSZ 58-67
ATSZ 48-57
ATSZ a52
ATSZ 38-47
Caribbean
Africa
ATSZ 82-91
Atlantic Source Zone
ATSZ 68-77
Atlantic Ocean
South America
SSSZ 1-10
South Sandwich Source Zone
SSSZ b11
60
40
20
0
-20
-40
-60
Latitude (N°)
-80
-60
-40
-20
0
Longitude (°)

Figure 13

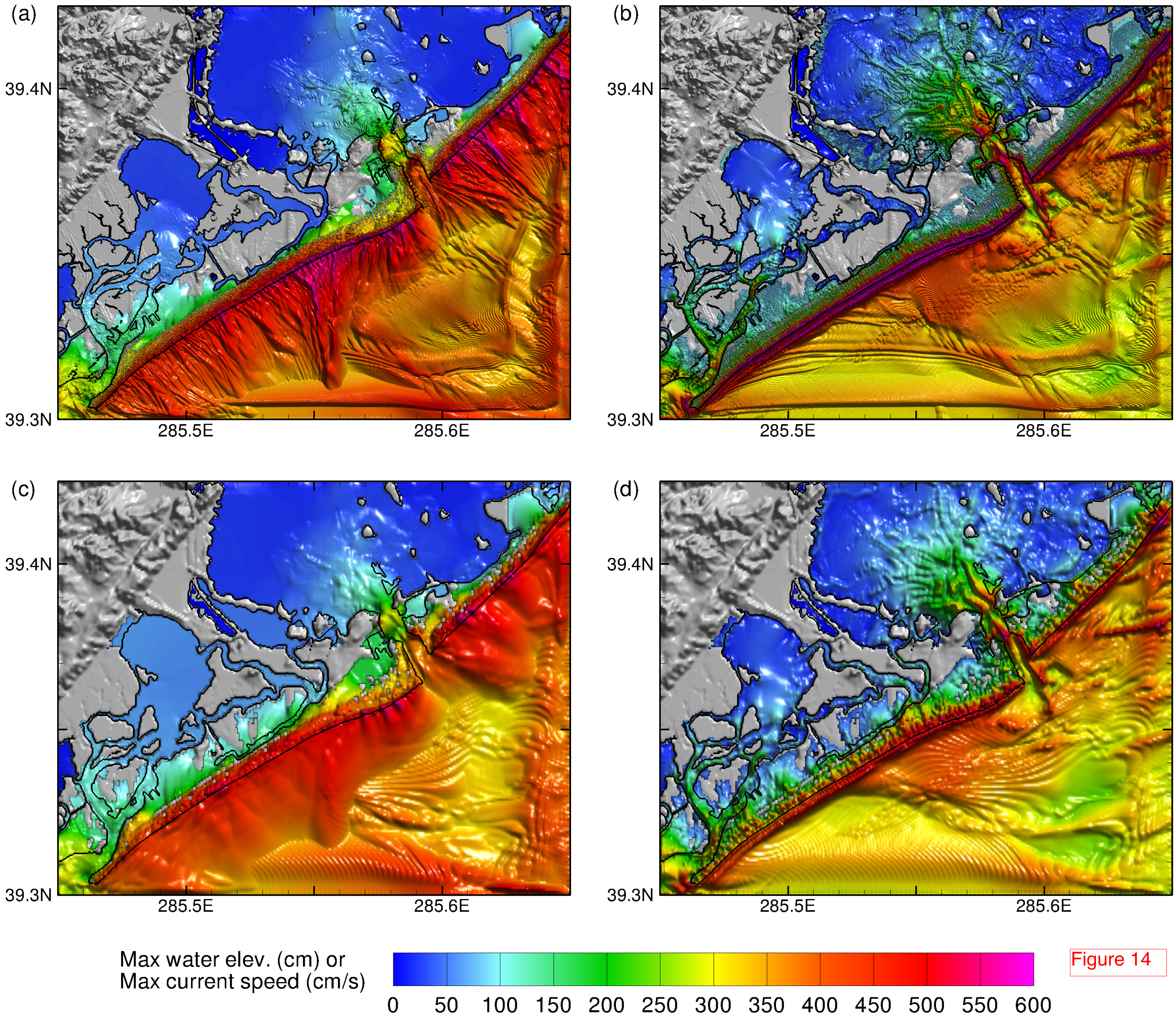
(a)
(b)
(c)
(d)
39.4N
39.3N
285.5E
285.6E
Max water elev. (cm) or
Max current speed (cm/s)
0 50 100 150 200 250 300 350 400 450 500 550 600

Figure 14

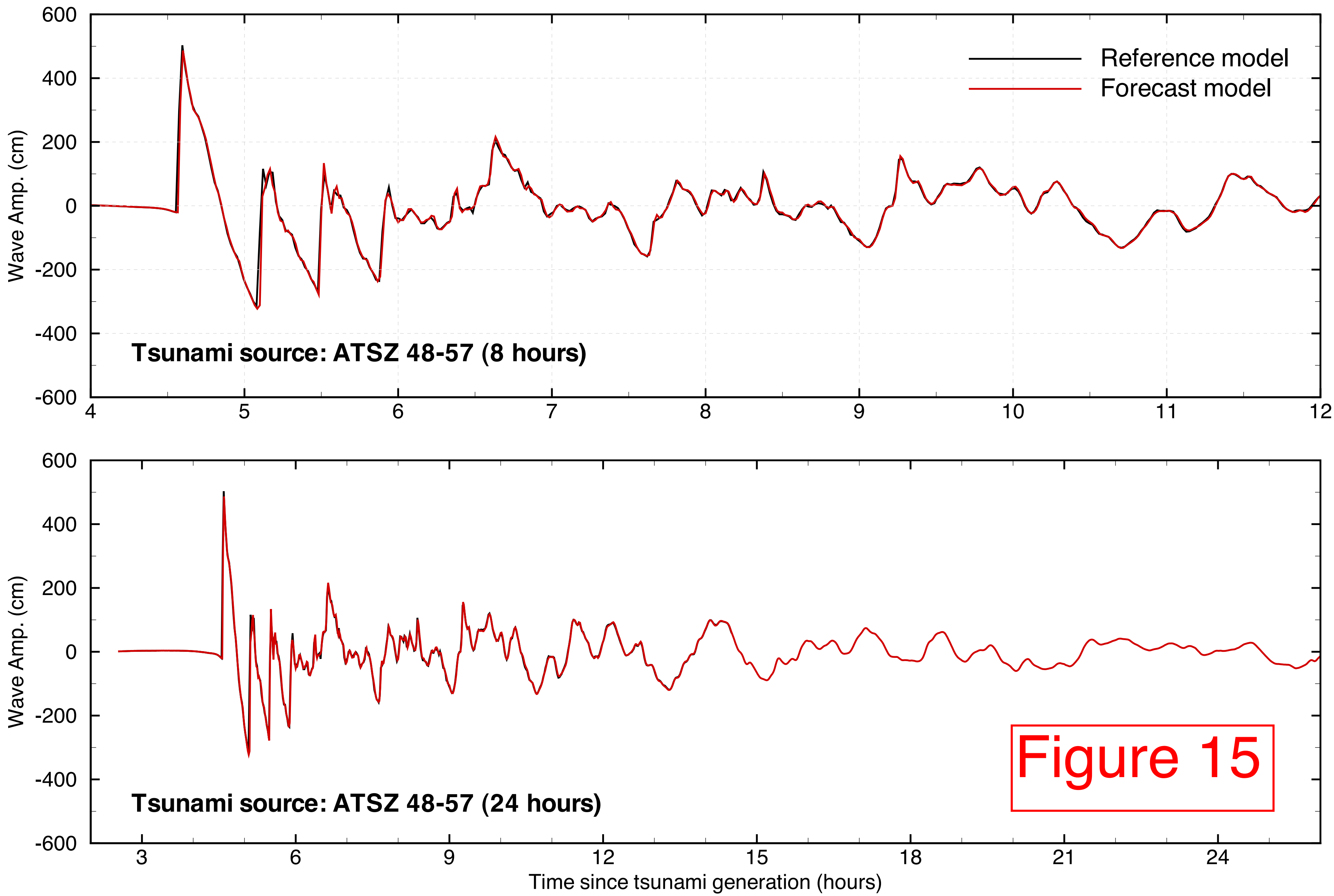
Wave Amp. (cm)
600
400
200
0
-200
-400
-600
4
5
6
7
8
9
10
11
12
Reference model
Forecast model
Tsunami source: ATSZ 48-57 (8 hours)
Wave Amp. (cm)
3
6
9
12
15
18
21
24
Tsunami source: ATSZ 48-57 (24 hours)
Time since tsunami generation (hours)

Figure 15

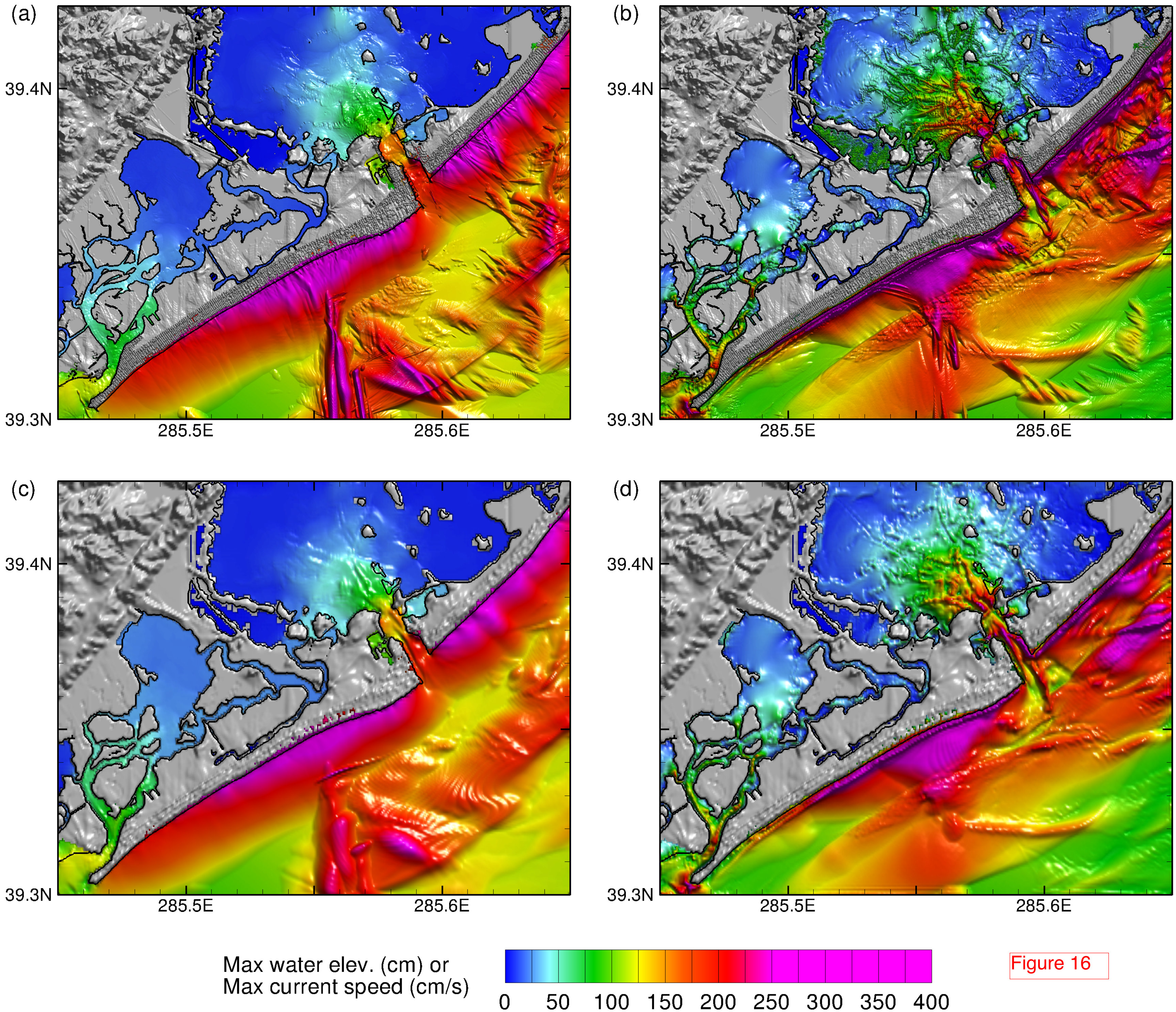
(a)
(b)
(c)
(d)
39.4N
39.3N
285.5E
285.6E
Max water elev. (cm) or
Max current speed (cm/s)
0 50 100 150 200 250 300 350 400

Figure 16

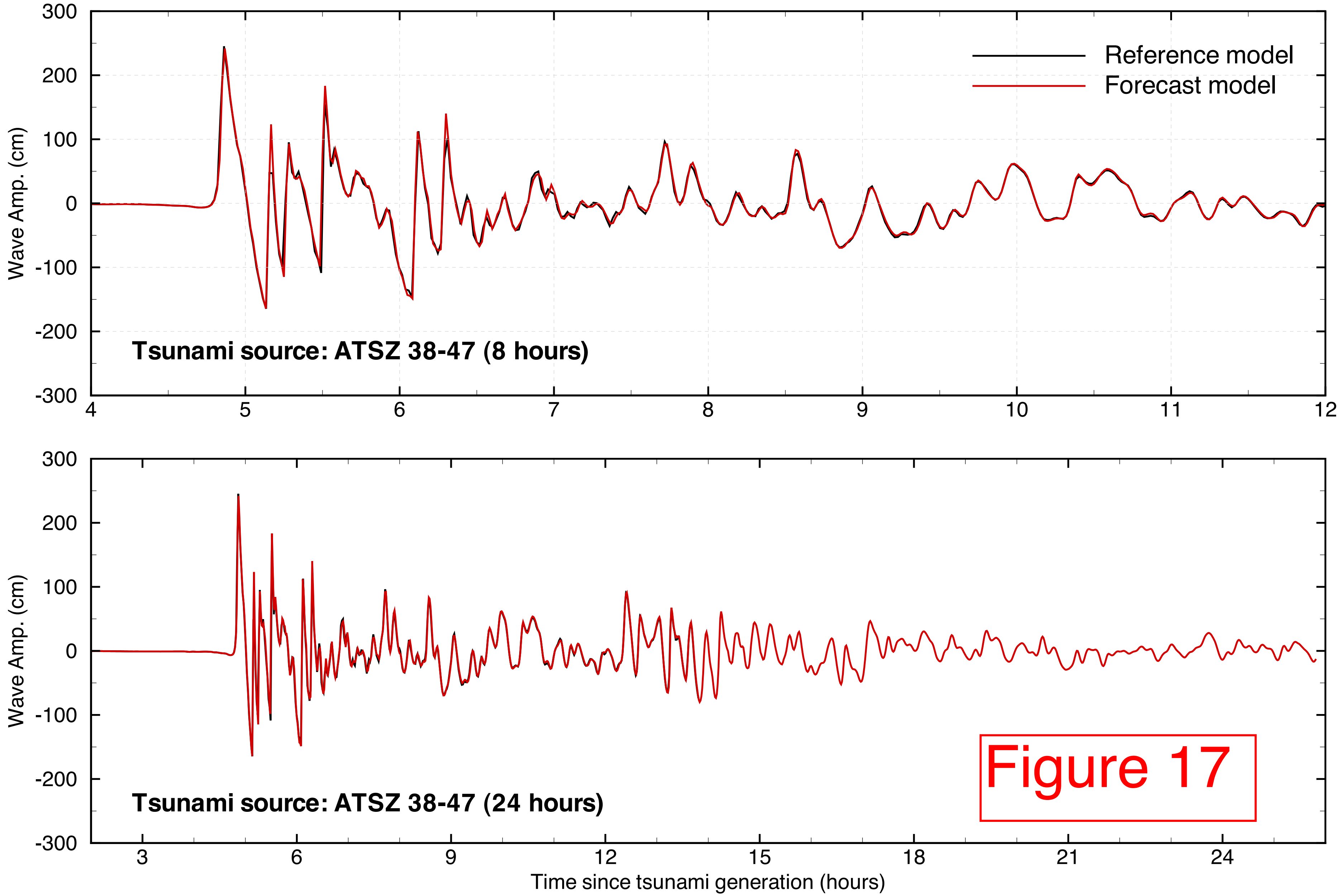
Wave Amp. (cm)
Reference model
Forecast model
Tsunami source: ATSZ 38-47 (8 hours)
Tsunami source: ATSZ 38-47 (24 hours)
Time since tsunami generation (hours)

Figure 17

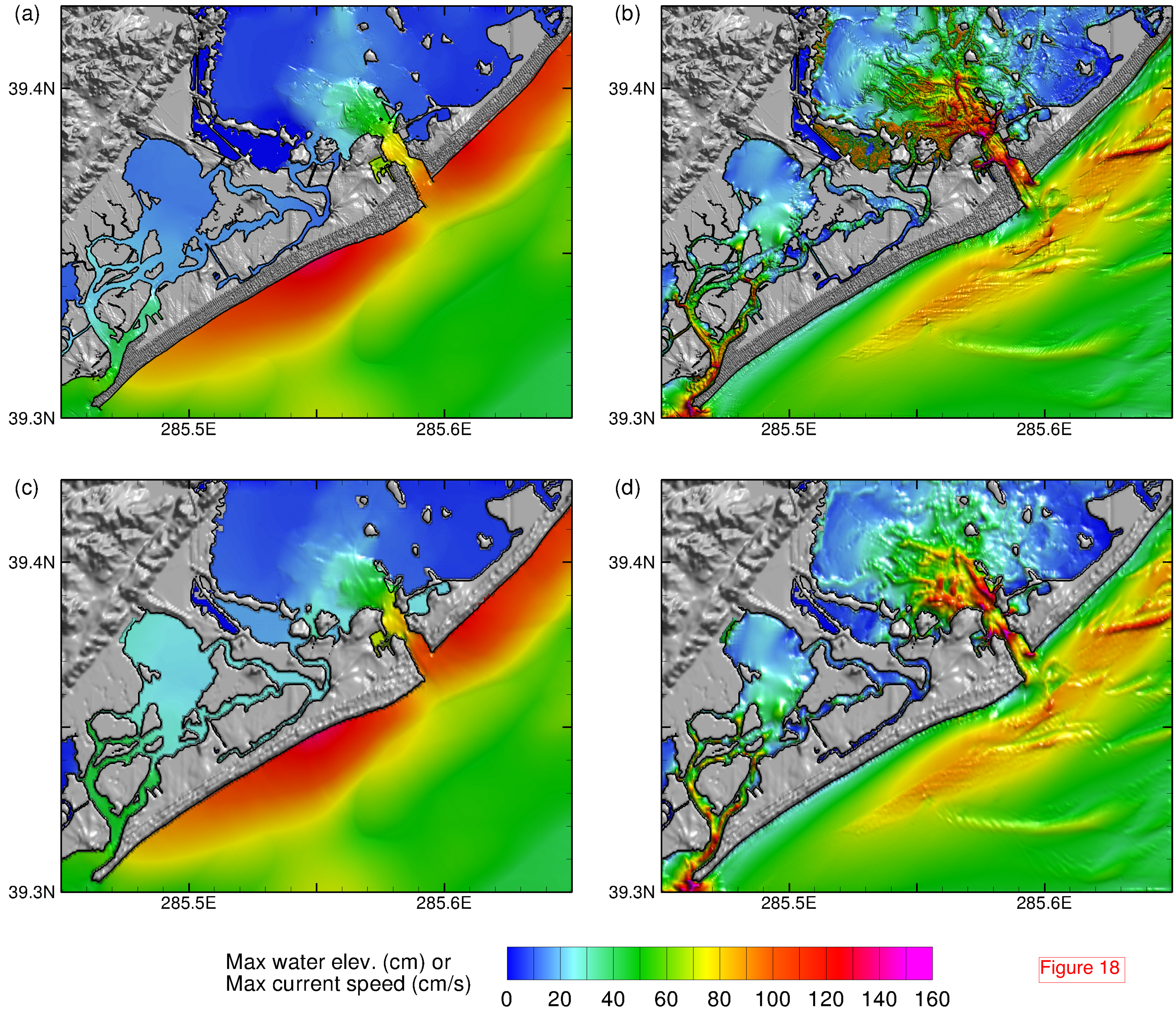
(a)
(b)
(c)
(d)
39.4N
39.3N
285.5E
285.6E
Max water elev. (cm) or
Max current speed (cm/s)
0 20 40 60 80 100 120 140 160

Figure 18

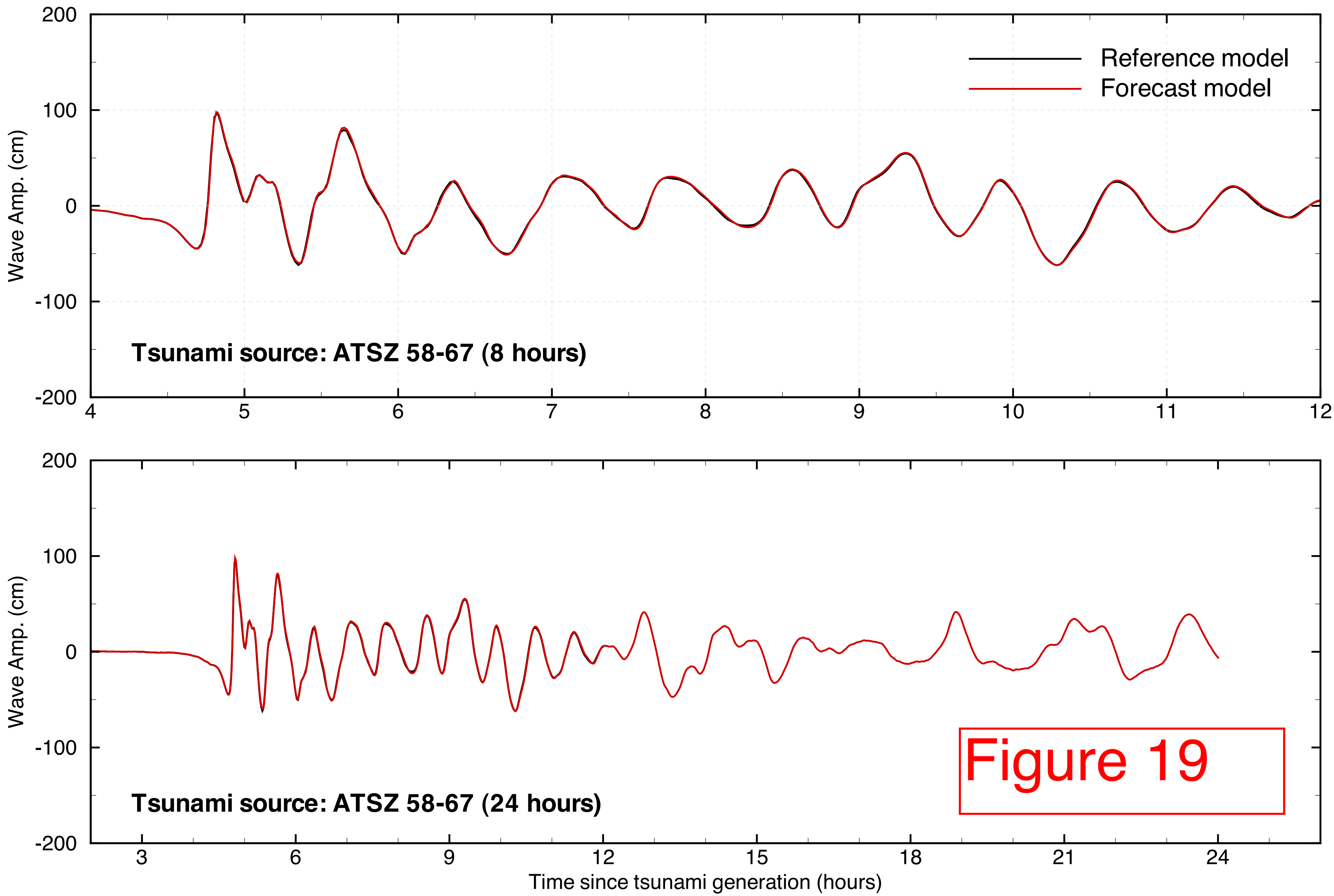
Wave Amp. (cm)
200
100
0
-100
-200
4
5
6
7
8
9
10
11
12
Reference model
Forecast model
Tsunami source: ATSZ 58-67 (8 hours)
Wave Amp. (cm)
200
100
0
-100
-200
3
6
9
12
15
18
21
24
Tsunami source: ATSZ 58-67 (24 hours)
Time since tsunami generation (hours)

Figure 19

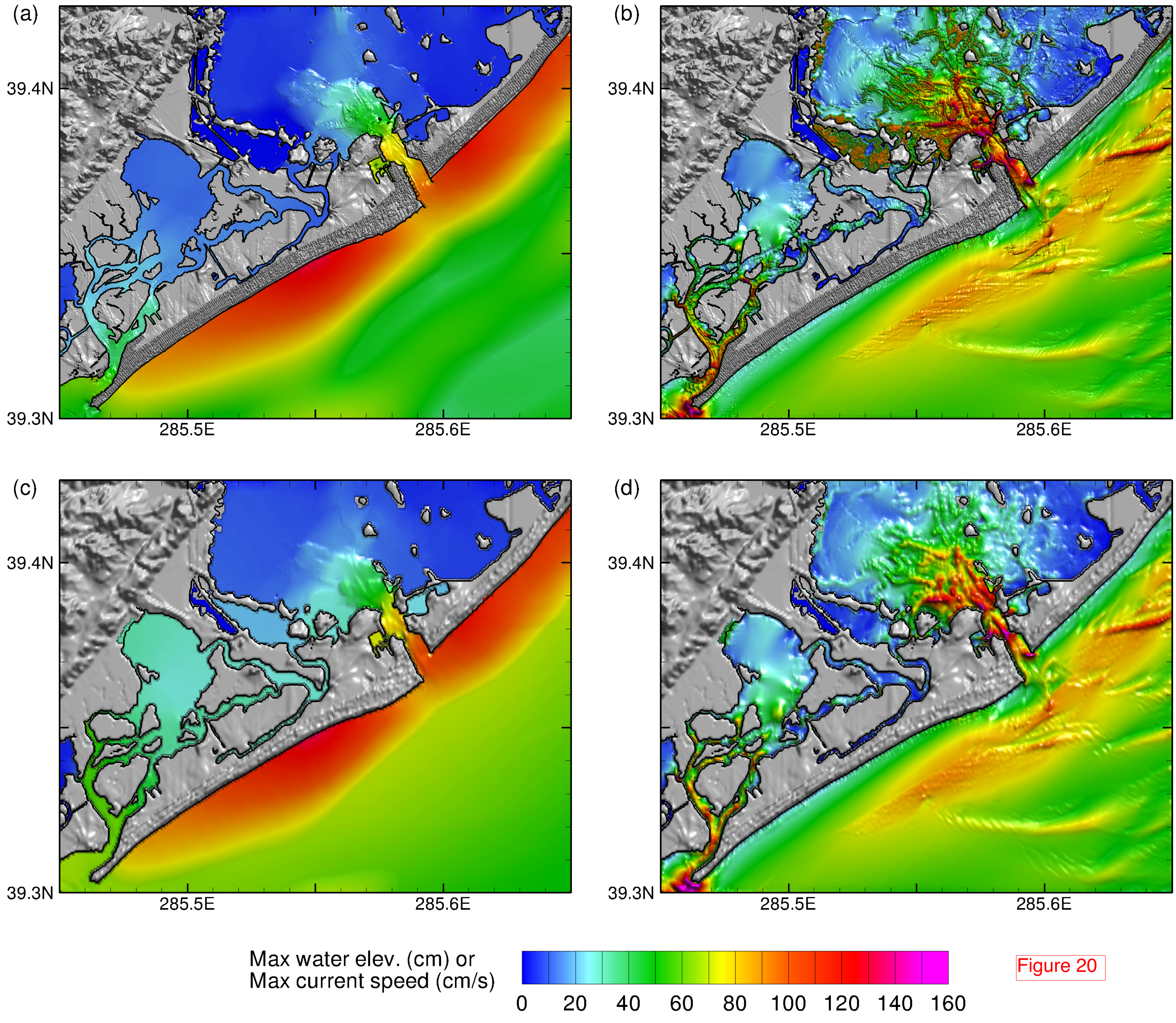

(a)
(b)
(c)
(d)
39.4N
39.3N
285.5E
285.6E
Max water elev. (cm) or
Max current speed (cm/s)
0
20
40
60
80
100
120
140
160

Figure 20

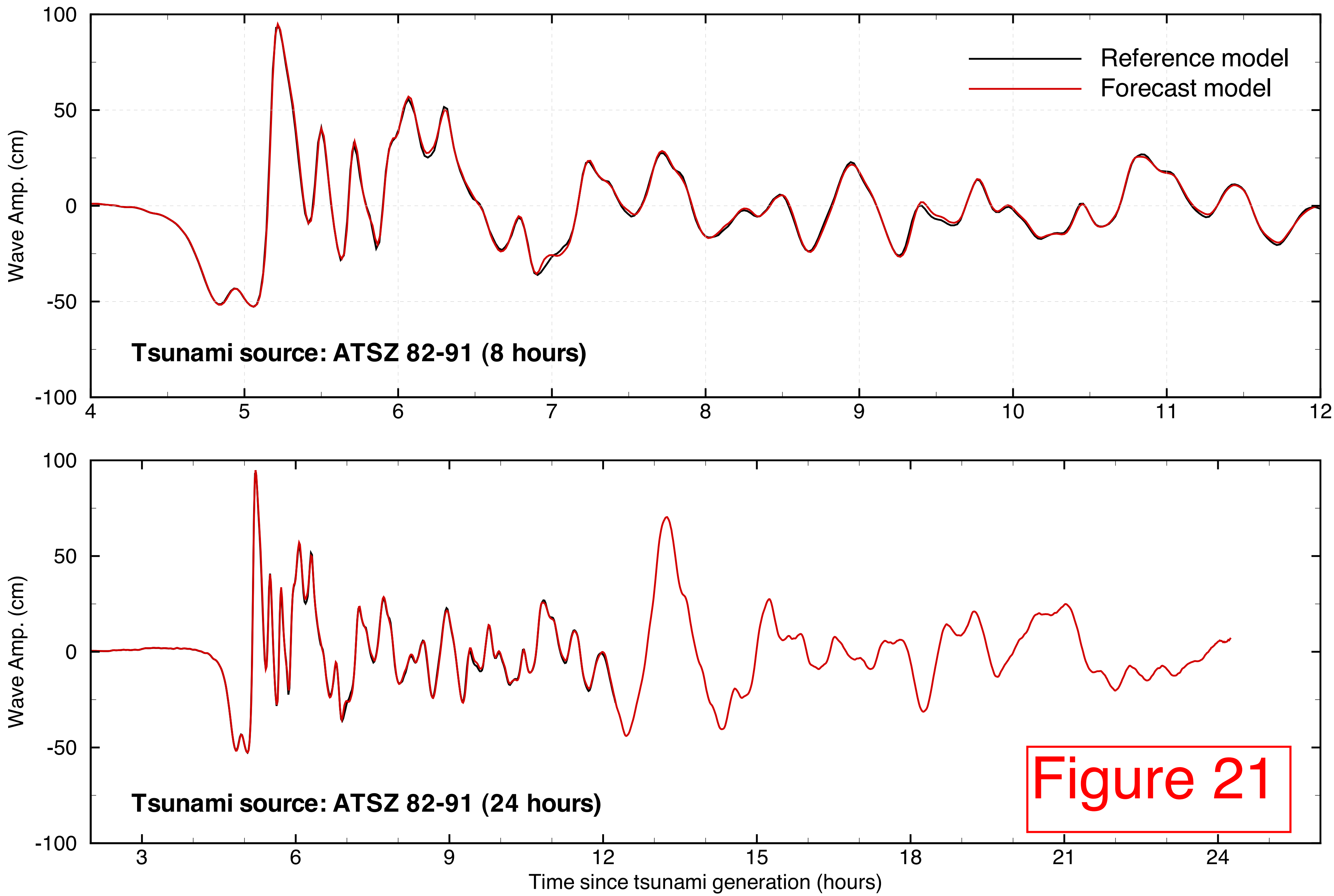

Reference model
Forecast model
Wave Amp. (cm)
Tsunami source: ATSZ 82-91 (8 hours)
Tsunami source: ATSZ 82-91 (24 hours)
Time since tsunami generation (hours)

Figure 21

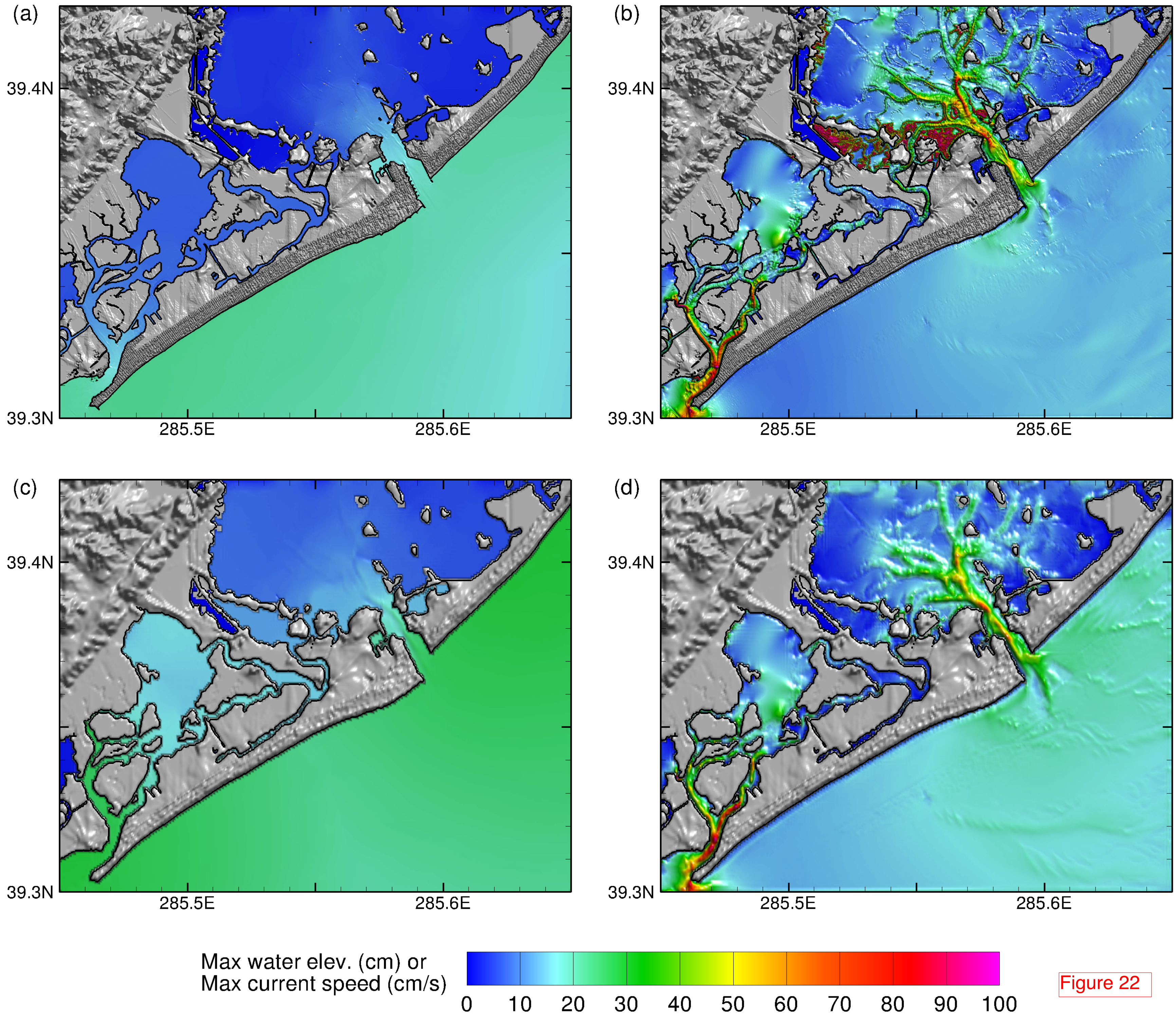
(a)
(b)
(c)
(d)
39.4N
39.3N
285.5E
285.6E
Max water elev. (cm) or
Max current speed (cm/s)
0
10
20
30
40
50
60
70
80
90
100

Figure 22

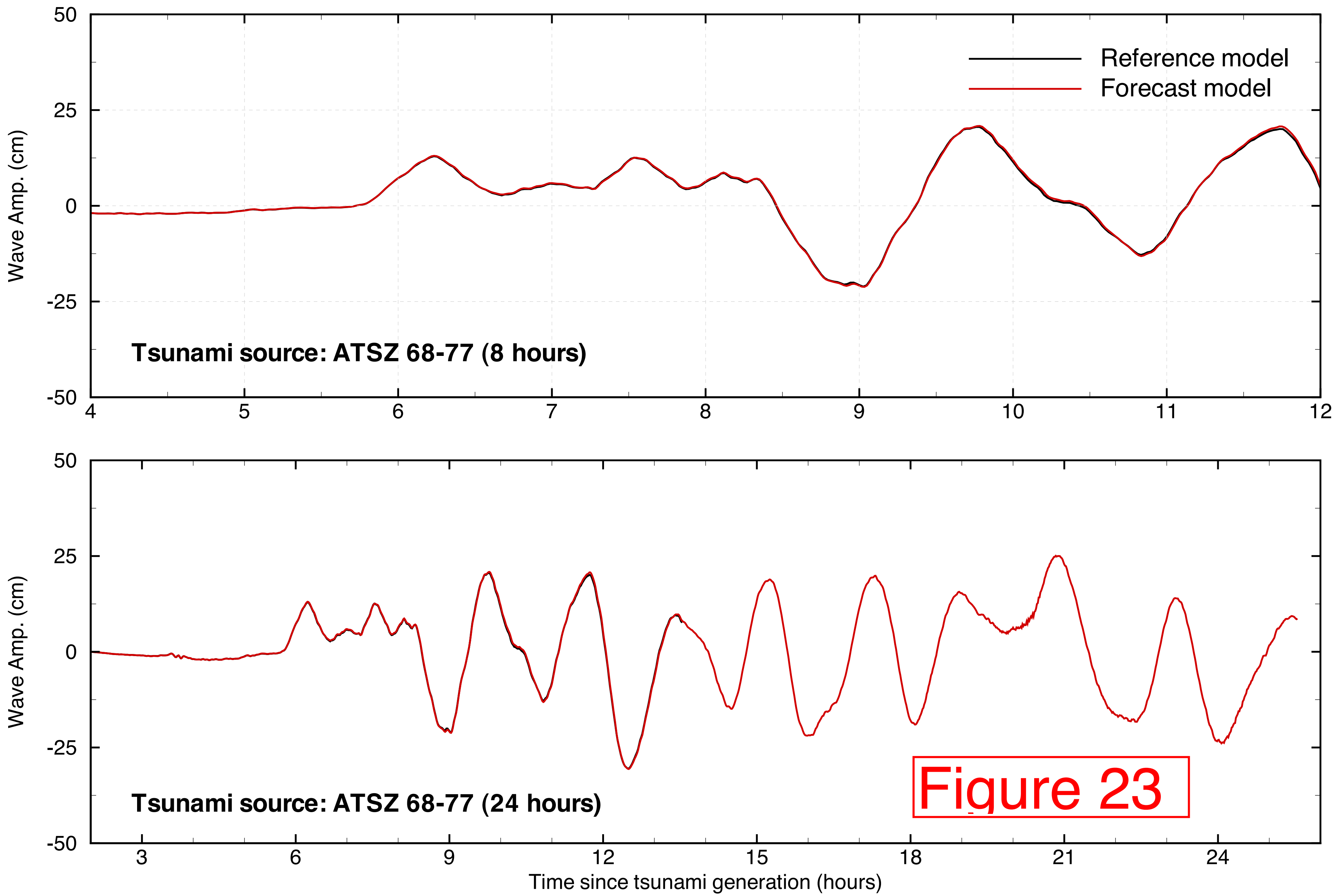
Wave Amp. (cm)
Reference model
Forecast model
Tsunami source: ATSZ 68-77 (8 hours)
Wave Amp. (cm)
Tsunami source: ATSZ 68-77 (24 hours)
Time since tsunami generation (hours)

Figure 23

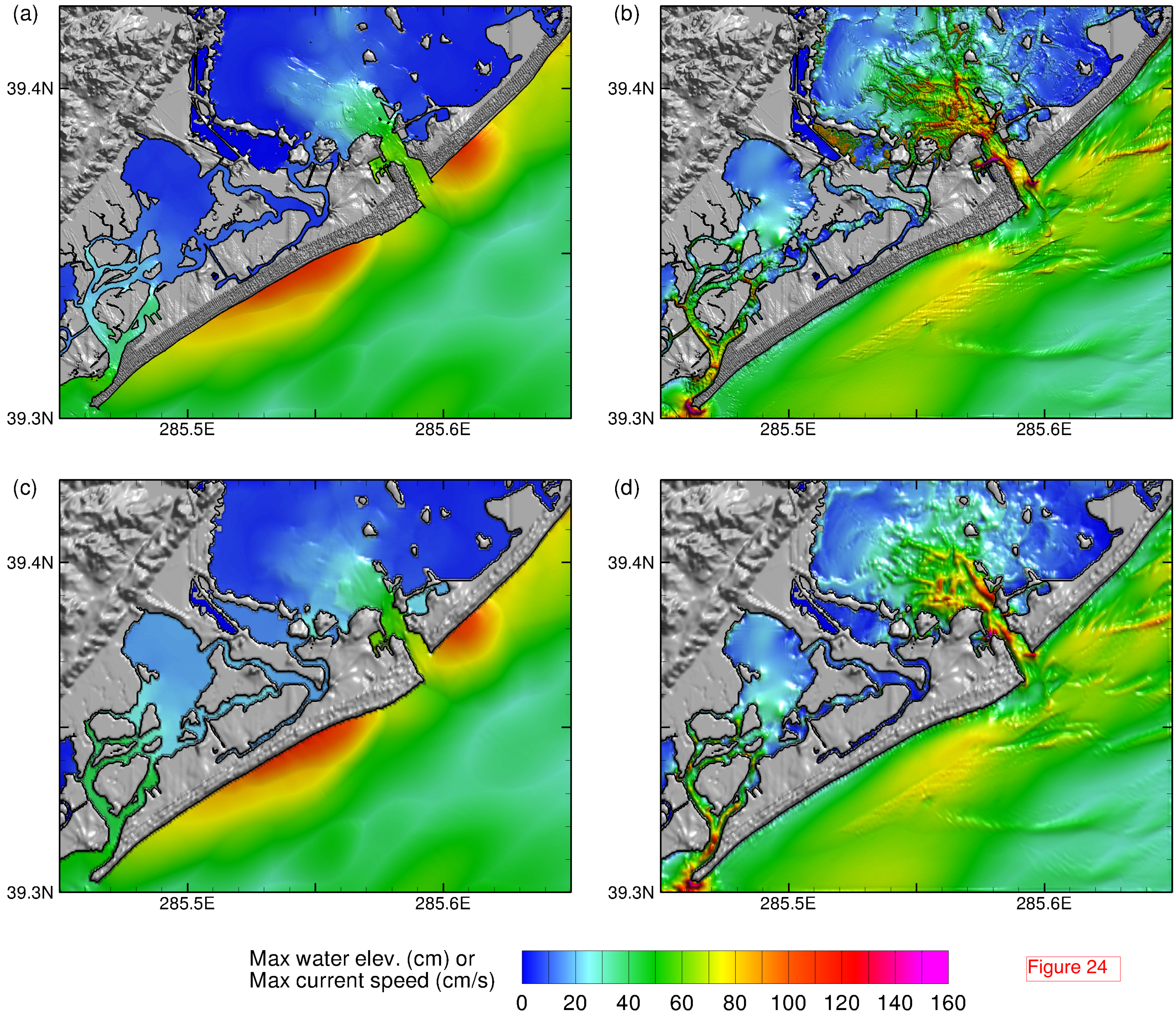
(a)
(b)
(c)
(d)
39.4N
39.3N
285.5E
285.6E
Max water elev. (cm) or
Max current speed (cm/s)
0 20 40 60 80 100 120 140 160

Figure 24

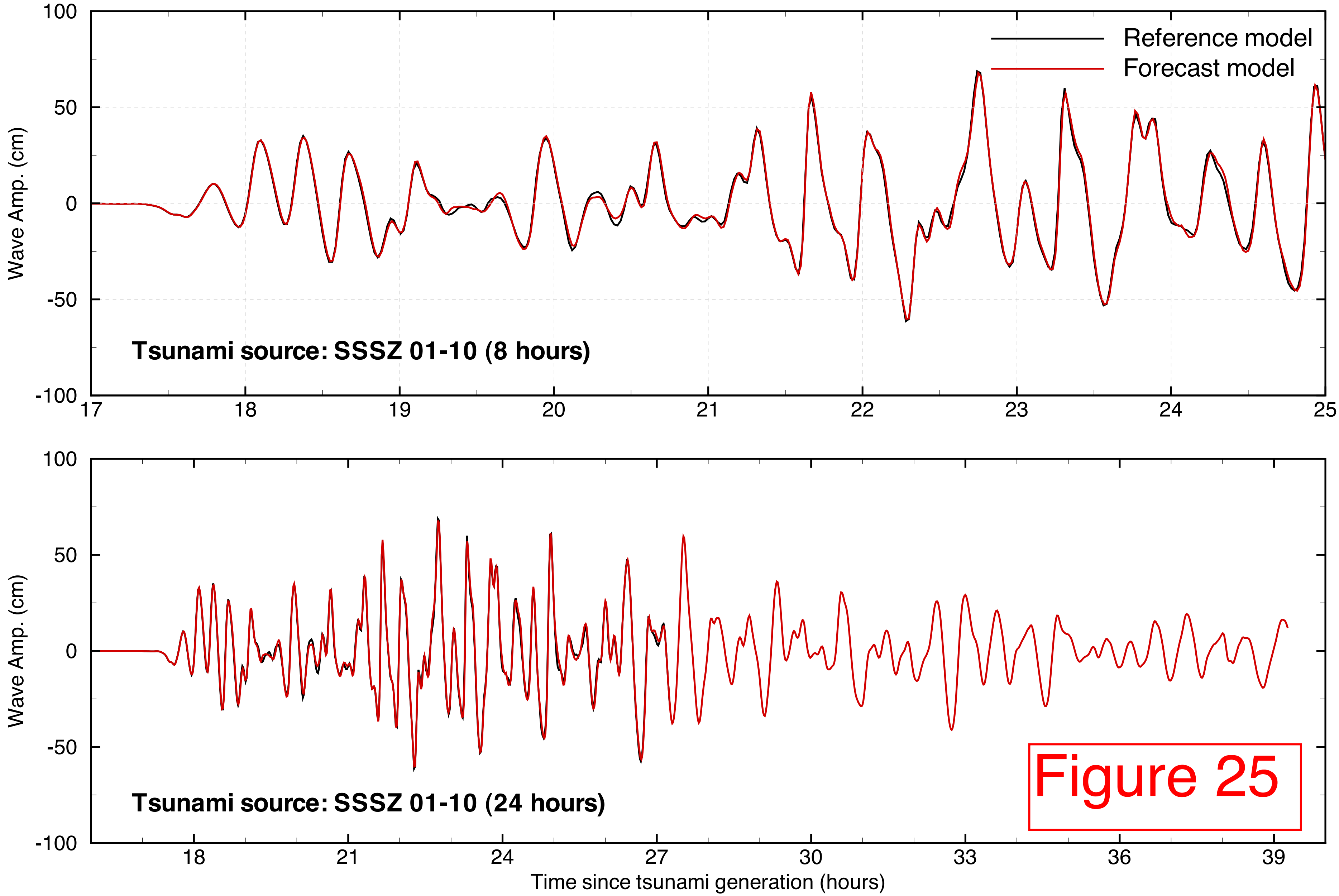
100
50
0
-50
-100
Wave Amp. (cm)
Reference model
Forecast model
Tsunami source: SSSZ 01-10 (8 hours)
17
18
19
20
21
22
23
24
25
Tsunami source: SSSZ 01-10 (24 hours)
18
21
24
27
30
33
36
39
Time since tsunami generation (hours)

Figure 25

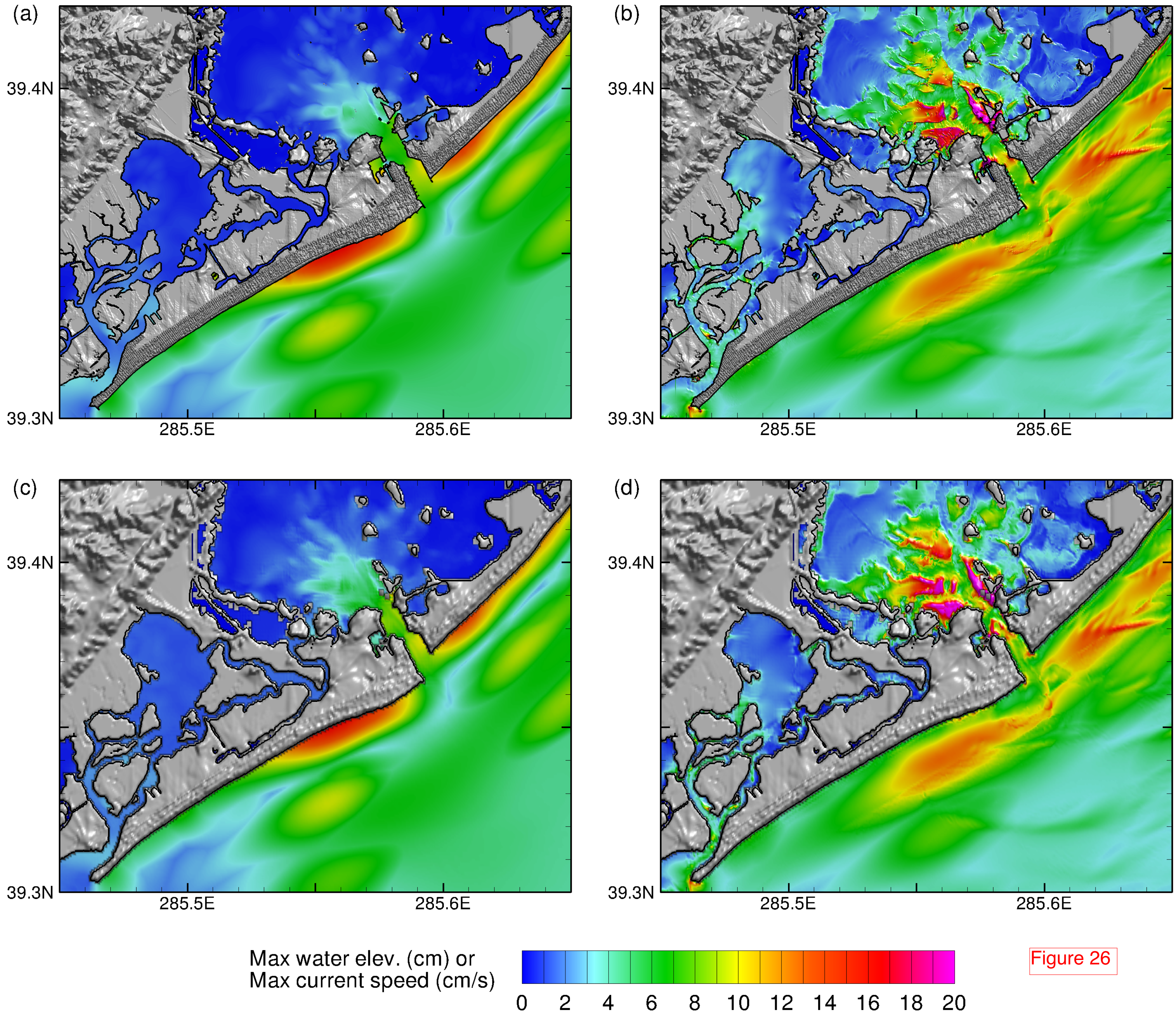
(a)
39.4N
39.3N
285.5E
285.6E
(b)
39.4N
39.3N
285.5E
285.6E
(c)
39.4N
39.3N
285.5E
285.6E
(d)
39.4N
39.3N
285.5E
285.6E
Max water elev. (cm) or
Max current speed (cm/s)
0 2 4 6 8 10 12 14 16 18 20

Figure 26

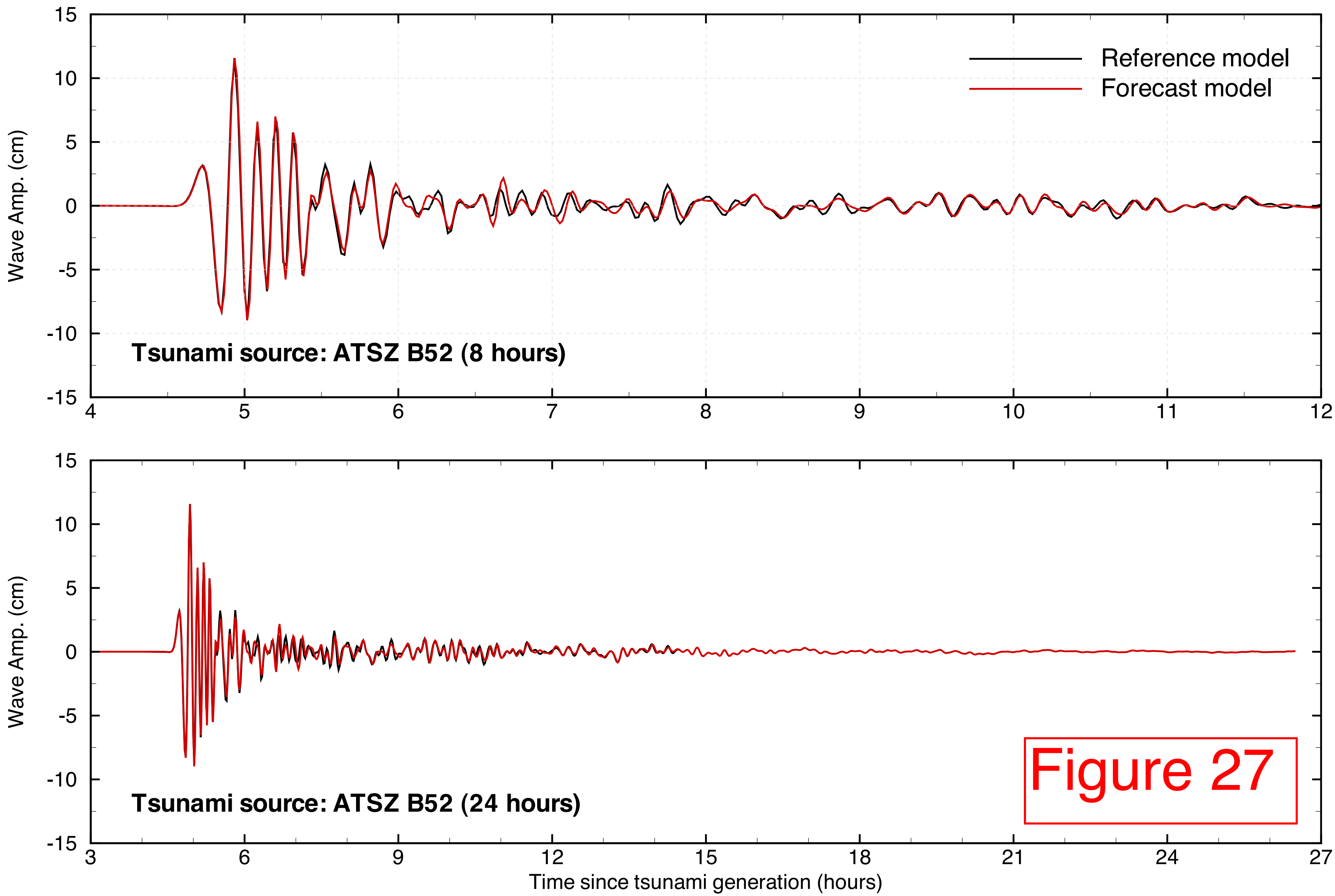
Wave Amp. (cm)
Reference model
Forecast model
Tsunami source: ATSZ B52 (8 hours)
Tsunami source: ATSZ B52 (24 hours)
Time since tsunami generation (hours)

Figure 27

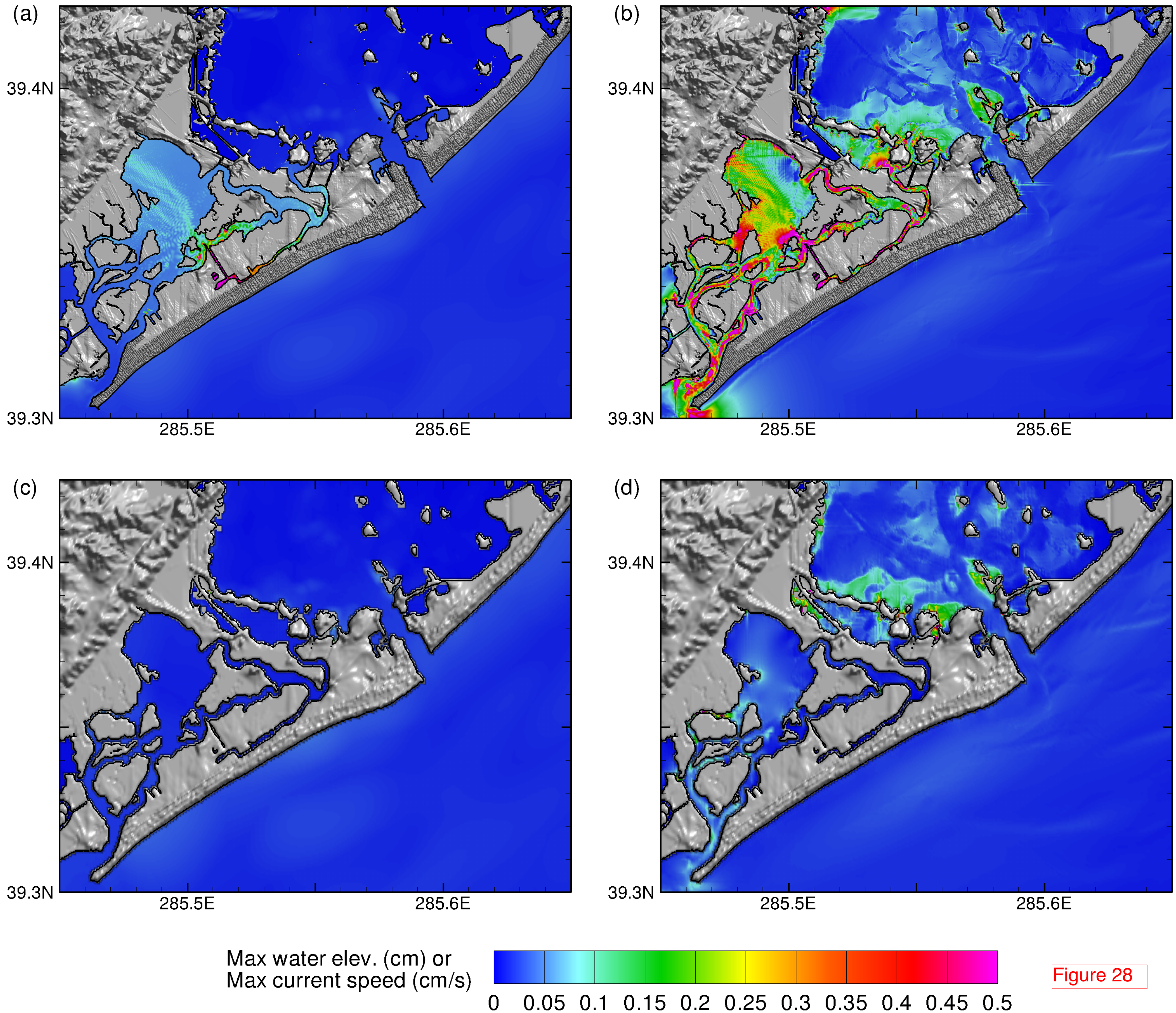
(a)
(b)
(c)
(d)
39.4N
39.3N
285.5E
285.6E
Max water elev. (cm) or
Max current speed (cm/s)
0 0.05 0.1 0.15 0.2 0.25 0.3 0.35 0.4 0.45 0.5

Figure 28

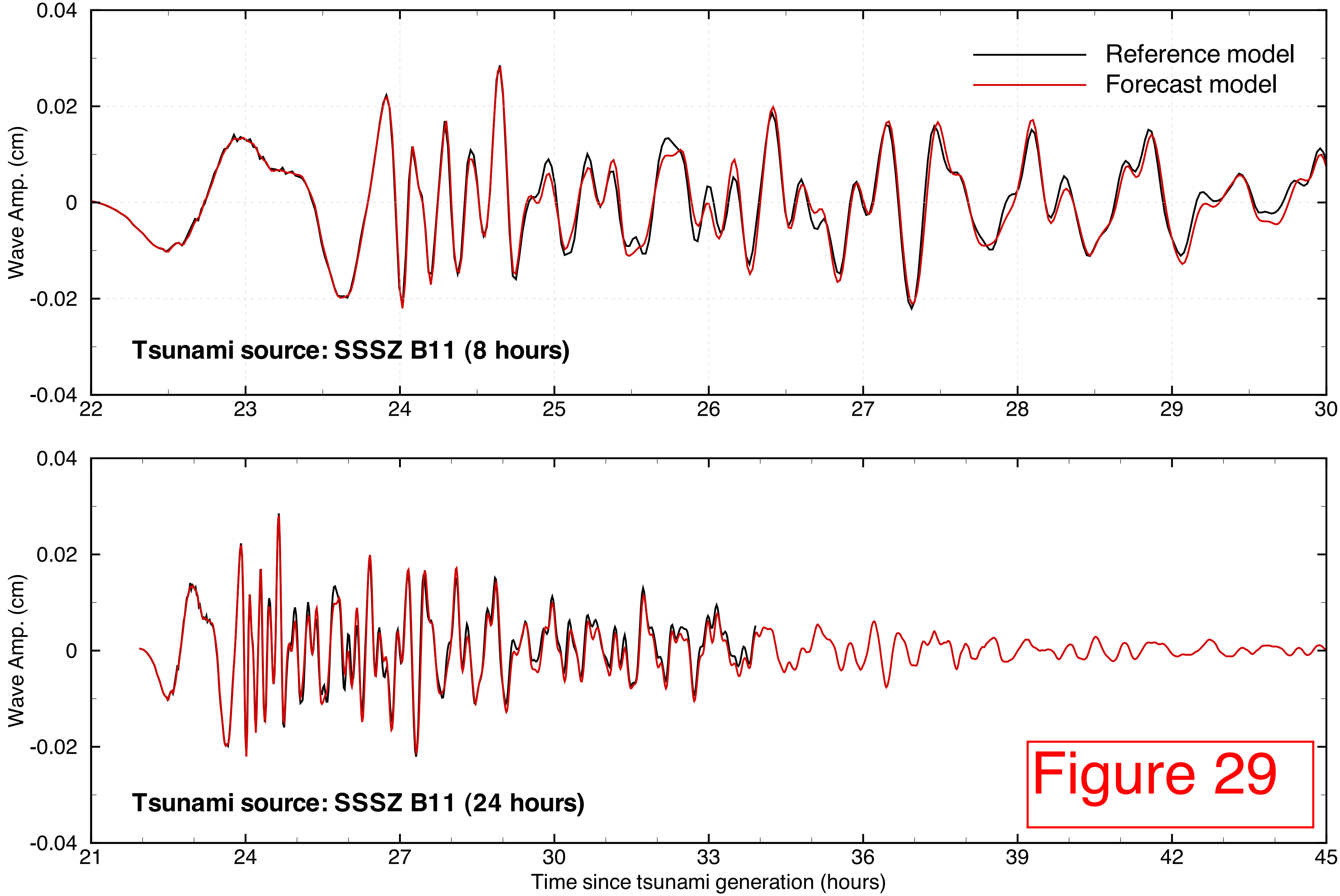

Reference model
Forecast model
Wave Amp. (cm)
0.04
0.02
0
-0.02
-0.04
Tsunami source: SSSZ B11 (8 hours)
22
23
24
25
26
27
28
29
30
Wave Amp. (cm)
Tsunami source: SSSZ B11 (24 hours)
21
24
27
30
33
36
39
42
45
Time since tsunami generation (hours)

Figure 29

Table 1. Historical tsunami events that have affected central north of the U.S. East Coast, including Atlantic City, New Jersey.

Event	Date, Time (UTC), Epicenter	Magnitude	Earthquake source area	Max water elev. at Atlantic City
1755 Lisbon	01 Nov. 10:16:00 36.0°N 11.0°W	8.5 – 9.0	Portugal: Lisbon	-
1817 Philadelphia	08 Jan 39.95°N 75.1°W	?	Philadelphia	-
1821	03 Sep	-	Meteorological	-
1840 Philadelphia	11 Nov 39.8°N 75.2°W	5.2	Philadelphia	-
1871 New York	18 Jun 40.5°N 73.9°W	?	New York	-
1884 New York	10 Aug 10:07:00 40.6°N 73.75°W	5.5	New York	-
1895 New Jersey	1 Sep 11:09:00 40.667°N 74.883°W	4.3	New Jersey	-
1913	9 Jun	-	Unknown	-
1918 Puerto Rico	11 Oct 14:14:00 18.5°N 67.5°W	7.3	Atlantic (ATSZ)	0.06 m
1923	6 Aug	-	Unknown	-
1924	8 Aug	-	Unknown	-
1929 Grand Banks	18 Nov 20:32:00 44.69°N 56.0°W	7.2	Canada: Grand Banks	0.68 m
1931	19 Aug	-	Meteorological	3.0 m
1932	10 Nov	-	Meteorological	-
1938	21 Sep	-	Meteorological	-
1944	14 Sep	-	Meteorological	-
1946 Dominican Republic	4 Aug 17:51:6.0 19.3°N 68.9°W	7.8	Atlantic (ATSZ)	-
1946 Dominican Republic	8 Aug 13:28:0.0 19.71°N 69.51°W	7.4	Atlantic (ATSZ)	-
1964	19 May	-	Possibly a submarine landslide	-
2004 Sumatra	26 Dec 00:58:53 4, 3.295°N 5.982°E	9.0 - 9.3	Indian Ocean (IOSZ)	0.11 m

Table 2: MOST parameters for reference and forecast models for Atlantic City, New Jersey.

		Reference Model				Forecast Model			
Grid	Region	Coverage Lat. [°N] Lon. [°W]	Cell Size [“]	nx x ny	Time Step [sec]	Coverage Lat. [°X] Lon. [°X]	Cell Size [“]	nx x ny	Time Step [sec]
A	Central north of U.S. East Coast	38.0 – 40.5 75.25 – 71.0	30”	511 × 301	3.15	38.0 – 40.5 75.25 – 71.0	30”	511 × 301	3.0
B	East of New Jersey and Delaware	38.85-39.75 75.05 – 74.0	3”	1261 × 1081	2.7	38.85-39.75 75.05 – 74.0	6”	631 × 541	6.0
C	Atlantic City	39.30 -39.425 74.55 – 74.35	1/3”	2161 × 1351	0.45	39.30 -39.425 74.55 – 74.35	2”	361 × 226	3.0
Minimum offshore depth [m]		1.0				1.0			
Water depth for dry land [m]		0.1				0.1			
Friction coefficient [n^2]		0.0009				0.0009			
CPU time for 4-hr simulation		~ 10 hours				~ 12 minutes			
Reference point at tide gage		74.417778W, 39.356667N (row number I = 239, column number J = 124)							

Computations were performed on a single Intel Xeon processor at 3.6 GHz, Dell PowerEdge 1850.

Table 3. Synthetic tsunami scenarios in the Atlantic Ocean used in this study.

Sce. No	Scenario Name	Source Zone	Tsunami Source	α (m)
Mega-tsunami scenario				
1	ATSZ 38-47	Atlantic	A38-A47, A38-A47	25
2	ATSZ 48-57	Atlantic	A48-A57, B48-B57	25
3	ATSZ 58-67	Atlantic	A58-A67, B58-B67	25
4	ATSZ 68-77	Atlantic	A68-A77, B68-B77	25
5	ATSZ 82-91	Atlantic	A82-A91, B82-B91	25
6	SSSZ 1-10	South Sandwich	A1-A10, B1-B10	25
Mw 7.5 Scenario				
7	ATSZ B52	Atlantic	B52	1
Micro-tsunami Scenario				
8	SSSZ B11	South Sandwich	B11	0.01